Dissecting the Intracellular Molecular Mechanisms to Address Pathogenesis of Multifactorial Diseases

January 2020

Kanae GAMO

Dissecting the Intracellular Molecular Mechanisms to Address Pathogenesis of Multifactorial Diseases

A Dissertation Submitted to
the Graduate School of Life and Environmental Sciences,
the University of Tsukuba
in Partial Fulfillment of the Requirements
for the Degree of Doctor of Philosophy in Biological Science
(Doctoral Program in Biological Sciences)

Kanae GAMO

Table of contents

Abstract

Since the introduction of molecular biology to disease research, various molecules have been identified as the cause or trigger of disease and have been studied as targets for therapeutic development. However, such molecular targeted drugs based on identification of one or few mutated genes would produce very little to benefit the patients while causing unexpected life-threatening side-effects. While the isolated specific molecules are parts of the highly heterogeneous biology, they should not be always considered as 'target' for therapy as they may sometime have little or no value on their own for translational purposes for patients. As cellular function is controlled in the context of complex gene regulatory networks, not individual genes, a disease is rarely a consequence of an abnormality in a single gene but reflects the perturbations of the complex intracellular network. Therefore, a disruptive approach for understanding multifactorial diseases by performing inference on the set of intracellular molecular interactions is required in order to bridge the gap between genotype and phenotype, leading to significantly improve the success rate of drug discovery.

To understand the mechanisms of disease systematically, patient stratification by the data-driven matching of patients to the appropriate investigational therapy is critical and important way to enable effective drug discovery and development in the age of precision medicine. Here, I investigate patient segment-specific molecular mechanism in two diseases focused on transcriptome profiling, which has been one of the most utilized approaches to expose expression patterns to define cellular states at the molecular level. First, through the validation of differential gene expression data following treatment with Lysine-specific demethylase (LSD) 1 inhibitor in acute myeloid leukemia cells, prediction of transcriptional regulators involved in mediating the transcriptional response revealed certain acute myeloid leukemia subtypes-specific core regulatory network that are required for their development and maintenance, which could be targeted in personalized therapies. Second, systematic *in silico* screening to analyze the correlation of Crohn's disease patient-derived gene signature and gene expression profile of existing drugs revealed the abnormality of MAPK pathway in even anti-TNFα responders that would be the cause of recurrence of Crohn's disease. Based on these two studies, transcriptome analysis of patient segment-specific gene expressions provides more insights to evaluate biological dysfunctions and helps to explore detailed and underlying molecular changes of human diseases that are emergent properties of biological networks, not the result of changes of single

genes. In addition, systematic *in silico* computational approach offers a versatile platform to explore systematically the molecular complexity of a particular disease, leading to the identification of disease modules and pathways effectively and to better understanding unmet medical needs for precision medicine.

Abbreviations

2-PCPA	tranylcypromine
AEL	acute erythroleukemia
AMKL	acute megakaryoblastic leukemia cells
AML	acute myeloid leukemia
APOA1	apolipoprotein A-1 (APOA1)
AUC	area under the concentration time curve
Af.NR	non-responder after treatment
Af.Res	responder after treatment
BFU-E	burst forming unit-erythroid
Bf.NR	non-responder before treatment
Bf.Res	responder before treatment
CCLE	cancer cell line encyclopedia
CD	Crohn’s disease
CD86	CD86 molecule
CDX2	caudal type homeobox 2
CELLX	cell index database
CFU-E	colony forming unit-erythrocyte
CFU-GM	colony forming unit-granulocyte macrophage
CML	chronic myelogenous leukemia
CMap	connectivity map
CoREST	REST corepressor 1
DEG	differentially expressed gene
DMSO	dimethyl sulfoxide
ERK	mitogen-activated protein kinase
ES	enrichment score
EphB2	EPH receptor B2
FACS	fluorescence-activated cell sorting
FAD	flavin adenine dinucleotide
FC	fold change
FCRLA	Fc receptor like A

FDA	food and drug administration
FITC	fluorescein isothiocyanate
GAPDH	glyceraldehyde-3-phosphate dehydrogenase
GATA1	GATA binding protein 1
GEO	gene expression omnibus
GFI1	growth factor independent 1 transcriptional repressor
GFI1B	growth factor independent 1B transcriptional repressor
GSEA	gene set enrichment analysis
GTEx	the genotype-tissue expression
GYPA	glycophorin A
HDAC1	histone deacetylase 1
IBD	inflammatory bowel disease
IEC	intestinal epithelial cell
ITGAM	integrin subunit alpha M
K4	lysine 4
LGR5	leucine-rich repeat-containing G-protein-coupled receptor 5
LINCS	library of integrated network-based cellular signatures
LSD1	lysine-specific demethylase 1
MAO	monoamine oxidase
MAPK	mitogen-activated protein kinase
MEK1	mitogen-activated protein kinase kinase 1
MEK2	mitogen-activated protein kinase kinase 2
MEP	erythro-megakaryocytic progenitor
MP	microparticle
NCBI	national center for biotechnology information
NIH	national institute of health
PARP	poly (ADP-ribose) polymerase 1
PCA	principal component analysis
PI16	peptidase inhibitor 16
PK	pharmacokinetics
RT-PCR	reverse transcription polymerase chain reaction

SCID	severe combined immunodeficiency
SNP	single nucleotide polymorphism
SPI1	spi-1 proto-oncogene
SRA	sequence read archive
T-ALL	T cell acute lymphocytic leukemia
T/C	the treatment-to-control ratio
TCGA	the cancer genome atlas
TEER	transepithelial electrical resistance
TNFα	tumor necrosis factor-alpha
TTG	anti-TNFα therapy-treatable gene
TUG	anti-TNFα therapy-untreatable gene
UC	ulcerative colitis
mAb	monoclonal antibody
mRNA	messenger ribonucleic acid
pERK	phosphorylated mitogen-activated protein kinase
siRNA	small interfering RNA

General Introduction

Biological pathways play important roles in the development of heterogeneous complex diseases, such as cancers, neurological diseases, metabolic diseases, chronic inflammatory diseases and so on that consist of the dynamic changes of intracellular interactome, where the networks of the various types of molecules that interact each other within a cell [1, 2]. Unlike single gene disorders, thousands to millions of molecular entities comprising multiple molecular interactions in intracellular networks have made it difficult to identify the causal genetic defect in complex diseases. Therefore, it is reasonable to conclude that molecular targeted drugs based on identification of one or a few mutated genes or their expression products tend to produce very little to benefit the patients. Several literatures reported that the outcomes of such drugs have failure rates ranging between 85 and 95% while causing life-threatening side-effects for patients and draining resources [3-5]. This phenomenon is thought to be resulted from complex molecular dynamics, which is known as the "genotype-phenotype gap". To overcome this situation, approach for precision medicine, which offers the possibility of more accurate therapy and better long-term treatment outcomes, is needed to pursue. Precision medicine is an approach which aims to match patients with appropriate molecularly matched treatments based on a person's genes, behaviors and environment. Interventions are tailored to individuals or groups, rather than using the "one-size-fits-all" approach, in which disease treatment is driven with the model of an average person with few considerations for individuals [6]. Applying this precision medicine into mainstream clinical workflow will eventually not only provide more predictive care by bringing better targeted therapies but also generate cost savings in hospitalization, biomedical research and pharmaceutical industry [7].

To understand complex biological dynamics, large-scale biological "omics" technology represents promising strategy for bridging the gap between genotype and phenotype [8-10]. Recent advances in molecular profiling "omics" technologies and development of computational approaches for analyzing these data offer novel systems-oriented approaches towards drug discovery [11]. Unlike the traditional "one-size-fits-all" approach to drug discovery, these systematic approaches identify changes within their larger context and leverage high dimensionality of the molecular data for modeling the broader molecular interactions. The growing number of molecular profiling data and development of sophisticated informatics methods have enabled completely novel approach to drug discovery that attempt to understand

drug activity from a data-driven perspective. In addition to genomics, other omics techniques such as epigenomics, transcriptomics, proteomics and metabolomics have also been used to a broad range of information of human disease [12]. Based on a survey of "-ome" or "-omic"-related publications, there is still increase in the number of transcriptomics articles [13]. Transcriptomics technology has fundamentally changed our ability to explore the molecular mechanisms underlying heterogenic diseases, being used to identify disease-associated changes in gene expression patterns. Gene expression profiles can be analyzed to construct *in silico* systems models of molecular pathology. Such models can be inspected computationally to generate predictions about the molecular network of pharmacologically perturbing one or more biological targets. Moreover, transcriptome profiles can be clustered in order to identify or analyze several sub-populations of patients suffered from the "same" disease by integrating clinical, biological and physiological data from both healthy and disease states in individuals, eventually to characterize a patient's disease progression and to identify predictive biomarkers of drug response [14]. This early patient stratification is critical to enable effective and personalized drug discovery and development, leading to identify patients that most likely respond to the drug allows reducing costs in drug development [15] and maximizing the number of responding patients [16]. Therefore, transcriptome profiling holds the promise to improve a certain segment of patient's treatment in heterogeneous diseases including acute myeloid leukemia (AML) and Crohn's disease (CD), which are targeted in this study, expanding the possibilities of finding the right drug for each patient. One thing to note is that data-driven only unbiased approach is not always perfect; that is, it is not the "optimal" procedure for overcoming the traditional approach because it hardly considers the vast existing biochemical knowledge as this is a very challenging task. In some cases, combining knowledge-driven approach, which heavily depend on literature information to populate a concrete mechanistic model, with data-driven methods can improve the accuracy of clustering to provide more mechanistic understanding [13, 17].

The objective of this study is to identify a robust gene signature that can predict a specific molecular mechanism underlying a specific segment of patients by focusing on transcriptomics as a method for a rational and effective drug discovery to bridge the genotype-phenotype. Here I summarize my findings on underlying patient segment-specific molecular changes of human diseases to shed light on the significance of transcriptome profiling.

In Chapter 1, to dissect the intracellular molecular mechanisms to address pathogenesis

of AML, I elucidated the mode of action of LSD1 inhibitor in AML cells. Despite increasing incidence rates (3.4% per year over the last 10 years) of AML are a growing concern in an aging population [18], few personalized approaches for patients with AML have been established for clinical use due to the increasingly apparent heterogeneity resulted from variability in leukemic cell maturation state. No satisfactory standard treatment exists for a certain segment of AML patients and most of the patients are physically unable to tolerate aggressive chemotherapy showing rapid disease progression in combination with low tolerance of systemic anti-cancer treatments [19]. Thus, emerging approaches in precision medicine is needed to improve AML patient outcomes. I focused on differential gene signature in LSD1 inhibitor sensitive AML cell lines, whose expression level systematically differs between a LSD1 inhibitor treated group and a control group obtained by transcriptome analysis. By combining with gene set enrichment analysis and the observation of morphological changes, I found an interesting phenomenon so-called “transdifferentiation” which convert from erythroid and megakaryocytic lineages into the granulomonocytic lineage. Moreover, by combining data-driven transcriptome data and knowledge-driven information, I revealed a certain AML subtypes-specific regulatory network of transcription factor interactions that are required for leukemogenesis.

In Chapter 2, to dissect the intracellular molecular mechanism to address pathogenesis of CD, I extracted the molecular mechanism of recurrence of CD patients treated with anti-TNFα therapy, matching the treatment to those. Despite increasing available targeted therapies for CD patients, the approved therapies have limited efficacy, and the recurrence rate is still high in post-therapy [20]. Therefore, a large unmet need exists for the treatment of CD. I re-analyzed publicly available CD patient-derived gene signature and identified the abnormality of MAPK pathway by *in silico* screening approach. This systemic computational approach coupled to systematic functional genomic resources is known as a valuable scheme for elucidating small molecule mechanism of action, for generating new therapeutic hypotheses and for increasing repurposing opportunities of druggable targets based on modulation of disease signatures [21]. I experimentally validated this prediction using selective MEK1/2 inhibitor *in vitro* and *in vivo* and provided evidences regarding MEK1/2 inhibitor as a potential treatment against CD to achieve sustainable remission at a molecular level. This novel finding from gene expression profiling of responder to anti-TNFα therapy indicates the abnormalities in anti-TNFα responder's CD colon that would be the cause of recurrence.

An important message of these studies is that transcriptome profiling help pinpoint the molecular processes perturbed in a disease, which in turn can be used as biomarkers for diagnosis and prognosis, patient classification and drug target identification (Fig. 1). This approach can provide an ideal platform, leading to faster drug discovery and safer, more reliable results in an efficient way.

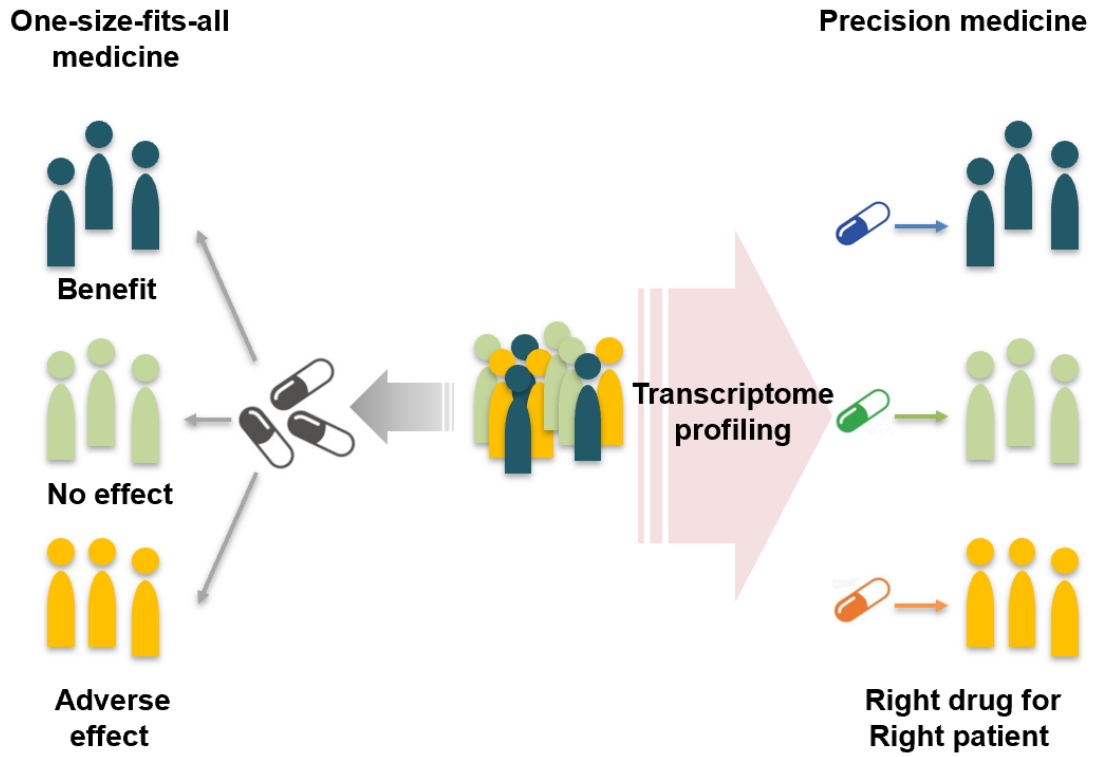

Figure 1. Transitioning from the "one-size-fits-all" approach to "precision medicine" model with patient classification by transcriptome profiling

Chapter 1: A Novel LSD1 Inhibitor T-3775440 Disrupts GFI1B-Containing Complex Leading to Transdifferentiation and Impaired Growth of AML Cells

Abstract

Accumulating evidence suggests that epigenetic regulators play critical roles in normal hematopoiesis and hematologic malignancies. Lysine-specific demethylase (LSD) 1, also known as KDM1A, is a transcriptional co-regulator that specifically demethylates lysine residues, and dysregulation of LSD1 activity has been implicated in the development of diverse cancers, including leukemia. Here, I describe the anti-leukemic activity and mechanism of action of T-3775440, a novel, selective, and potent small molecule inhibitor of LSD1, in acute myeloid leukemia (AML). Cell growth analysis of leukemia cell lines revealed that acute erythroleukemia (AEL, AML-M6) and acute megakaryoblastic leukemia cells (AMKL, AML-M7) are highly sensitive to this compound. T-3775440 induced cell cycle arrest and/or apoptosis in AEL and AMKL cells as well as alterations in the expression patterns of lineage-specific markers, indicate transdifferentiation of erythroid/megakaryocytic cells into granulomonocytic cells. Flow cytometric analysis demonstrated that transdifferentiation led to impaired cell growth. Conversely, blockade of transdifferentiation attenuated T-3775440-mediated cell growth inhibition. Mechanistically, T-3775440 blocked the interaction between LSD1 and Growth factor-independent 1B (GFI1B), which is critical for transcription repression in the differentiation processes of erythroid and megakaryocytic lineage cells. GFI1B knockdown recapitulated T-3775440-induced transdifferentiation and cell growth suppression, highlighting the importance of GFI1B inhibition in the pharmacological effects of T-3775440. Moreover, T-3775440 exhibited significant antitumor efficacy in tumor xenograft models of AEL and AMKL. My findings provide the rationale for testing T-3775440 as a potential treatment with a novel mechanism of action for AML, particularly AEL and AMKL.

Introduction

The hematopoietic system is maintained by stem cell self-renewal and a continuous hierarchical differentiation process as well as lineage commitment [22]. Many transcriptional machineries function as key regulators of terminal differentiation. Dysregulation of hematopoietic cell differentiation and improper stem cell maintenance are frequently associated with acute myeloid leukemia (AML) [23, 24]. Although developments in chemotherapeutics and bone marrow transplantation have led to significant progress in the treatment of leukemia, the prognosis of patients with relapsed AML remains a significant problem. In particular, research and development aimed at the identification of novel targeted anti-AML compounds are needed.

Lysine-specific demethylase 1 (LSD1; KDM1A) is a flavin adenine dinucleotide (FAD)-dependent histone demethylase that demethylates di- and mono-methylated lysine 4 (K4) on histone H3 [25]. Histone markers are often associated with the activation or repression of adjacent gene transcription. To augment its gene repressor activity, LSD1 is known to form a complex with corepressor proteins, namely CoREST and HDAC1 [26]. In hematopoietic cells, LSD1 also physically interacts with GFI1 or GFI1B, which are transcriptional repressors and critical regulators of hematopoietic cell lineage development and differentiation [27, 28]. Hematopoietic lineage-specific conditional LSD1 knockdown and knockout models have shown that loss of LSD1 results in hematopoietic stem cell expansion and inhibited terminal differentiation in the granulomonocytic, erythroid, and megakaryocytic lineages, highlighting the importance of LSD1 in normal hematopoiesis [29, 30].

LSD1 is significantly overexpressed in a number of hematologic malignancies, including AML, and has gained attention as a potential therapeutic target in AML. Small interfering RNA (siRNA)- or small molecule-mediated inhibition of LSD1 activity has been shown to induce differentiation of AML cells [31, 32]. Synergistic growth suppression effects with a combination of all-trans retinoic acid (ATRA) were observed in acute promyelocytic leukemia [33]. A reversible LSD1 small molecule inhibitor, SP2509, sensitized AML cells to the pan-HDAC inhibitor panobinostat [34]. However, the molecular mechanism underlying the mode of action of LSD1 inhibitors in the AML subclass remains to be fully elucidated.

In this study, I describe the anti-leukemic activities and mechanism of action of a novel, selective and potent LSD1 inhibitor in AML cell subsets. LSD1 inhibitor disrupted the LSD1-GFI1B interaction, thus inducing transcriptional de-repression of downstream-target genes of

GFI1B and consequent transdifferentiation, exhibiting antitumor efficacy in GFI1B-expressing acute erythroleukemia (AEL) and acute megakaryoblastic leukemia (AMKL) cell lines. My results suggest the potential of LSD1 inhibition with small molecule inhibitors as a novel strategy for the treatment of certain types of AML with a poor prognosis.

Materials & Methods

Cells and reagents

Human leukemia cell lines TF-1a and HEL92.1.7 were obtained from ATCC (Manassas, VA, USA). CMK11-5 and M07e were obtained from JCRB Cell Bank (Osaka, Japan) and DSMZ (Braunschweig, Germany), respectively. All cells were grown in RPMI1640 plus 10% fetal bovine serum (FBS) and maintained in a humidified incubator at 37ºC and 5% CO_2. T-3775440 was synthesized by the Oncology Drug Discovery Unit of Takeda Pharmaceutical Company (Osaka, Japan).

Cell proliferation assay

To assess cell proliferation and viability in human leukemia cell lines, exponentially growing cells were plated in duplicate or triplicate. Compounds were added at 24 hours post-cell seeding. After the incubation period, cells were lysed with CellTiter-Glo (Promega, Madison, WI, USA) and chemiluminescent signals were detected using an ARVO MX1420 microplate reader (PerkinElmer, Wellesley, MA, USA). IC_{50} values were calculated using a four-parameter logistic model with XLfit (ID Business Solutions, Alameda, CA, USA).

Cell cycle analysis

For cell cycle analysis, cells were fixed overnight with 70% ethanol. Fixed cells were stained with propidium iodide (PI) and analyzed on a FACSCalibur or FACSVerse flow cytometer (Becton-Dickinson, Franklin Lakes, NJ, USA)

Quantitative RT-PCR analysis and microarray

Following the designated treatment, total RNA was isolated from cells and purified with an RNeasy Mini Kit (Qiagen, Valencia, CA, USA). Complementary DNA was synthesized using the Verso cDNA Synthesis Kit (ThermoFisher Scientific). Quantitative real-time PCR analysis was performed on a ViiA7 (Applied Biosystems, Foster City, CA, USA), using TaqMan Fast Advanced Master Mix with TaqMan probes against the indicated genes (Applied Biosystems). Data were analyzed according to the $2^{-\Delta\Delta Ct}$ method and normalized relative to the amount of *GAPDH* mRNA. The normalized abundances of target mRNAs were expressed relative to the corresponding values for cells treated with DMSO or negative control siRNAs. The following TaqMan probes were used for quantitative RT-PCR analysis: *CD86* (Hs01567026_m1), *FCRLA* (Hs00893173_m1), *GAPDH* (Hs02758991_g1), *GATA1* (Hs01085823_m1), *GFI1B* (Hs01062469_m1), *GYPA* (Hs00266777_m1), *ITGAM* (Hs00355885_m1), *LSD1*

(Hs01002741_m1), and *PI16* (Hs00542137_m1).

For the microarray analysis, total RNA was purified as described, and quality was verified on an Agilent 2100 Bioanalyzer (Agilent Technologies, Santa Clara, CA, USA). RNA was labeled and hybridized to Agilent SurePrint G3 Human Gene Expression 8 x 60K arrays at the Macrogen Company (Seoul, South Korea). Microarray data have been deposited in NCBI GEO (accession number: GSE87580).

Bioinformatics

To determine differentially expressed genes (DEGs) between T-3775440-treated and control treated cells, microarray data were subjected to a two-sample comparison. DEGs with a *t*-test *P* value <0.01 and fold change of 2 were extracted. The extracted genes were evaluated in a pathway enrichment analysis on NextBio (www.nextbio.com).

To check the expression levels of gene signatures for each cell linage, microarray data were subjected to a gene set enrichment analysis [35]. The reference signatures used in the analysis was generated from data published by the Immunological Genome Project, which are available in the NCBI GEO database (GSE15907). The methods for extracting cell-type-specific signatures were described elsewhere [36]. Signature data were originally generated for mouse genes and mapped onto human gene symbols for this analysis.

Immunoprecipitation

The chromatin fraction was used for immunoprecipitation. Cells were harvested and lysed in lysis buffer (20 mM HEPES [pH 7.5], 25% glycerol, 0.2 mM EDTA, 150 mM KCl, 1.5 mM $MgCl_2$, 0.5% NP-40, 1 mM PMSF) containing a protease inhibitor. After centrifugation, the insoluble fraction was resuspended in micrococcal nuclease (MNase) buffer (20 mM HEPES (pH7.5), 0.3 M sucrose, 100 mM KCl, 2 mM $MgCl_2$, 1 mM $CaCl_2$, 0.1% Triton X-100, 1 x protease inhibitor cocktail) containing MNase and incubated for 10 minutes. After centrifugation, the supernatant was harvested as the chromatin fraction. For immunoprecipitation, lysates were incubated with protein G (GE Healthcare, Waukesha, WI, USA) to exclude non-specific protein binding. Subsequently, antibodies against LSD1 or GFI1B were added to the lysates for a 4-hour incubation, followed by further incubation with protein G for 2 hours. Finally, protein G was removed using Wash buffer 1 (20 mM HEPES [pH 7.5], 100 mM KCl, 5 mM $MgCl_2$, 0.2 mM EDTA, 10% glycerol, 0.1% Tween 20), Wash buffer 2 (20 mM HEPES [pH 7.5], 300 mM KCl, 5 mM $MgCl_2$, 0.2 mM EDTA, 10% glycerol, 0.1% Tween2 0) twice each, followed by heating

for 10 minutes at 70°C with 4 x SDS loading buffer (Wako).

Western blotting

Whole cell extracts were prepared with 1 × Laemmli sample buffer (Tris-HCl 125 mM pH 7.5, 1% SDS, 20% Glycerol). Whole cell extracts or immunoprecipitates were fractionated by SDS-PAGE, and the separated proteins were transferred using an iBlot Transfer Stack (Nitrocellulose) and iBlot Gel Transfer Device (Invitrogen/Thermo Fisher Scientific, Waltham, MA, USA). After incubation with StartingBlock™ T20 (PBS) Blocking Buffer (Pierce Biotechnology, Rockford, IL, USA), the membranes were labeled overnight with primary antibodies, followed by incubation with horseradish peroxidase-conjugated secondary antibodies (Cell Signaling Technology, Beverly, MA, USA). Membranes were incubated with ImmunoStar Zeta (Wako) and scanned using an ImageQuant LAS-3000 (Fujifilm, Tokyo, Japan).

The following antibodies were used for immunoprecipitation or western blot analysis: LSD1 (pAb-067-050; Diagenode s.a., Liège, Belgium), GFI1B (immunoprecipitation: 5849; Cell Signaling Technology; western blotting: sc28356; Santa Cruz Biotechnology, Dallas, TX, USA), CoREST (07-455; Millipore, Billerica, MA, USA), cleaved PARP (9541; Cell Signaling Technology), p27 (616242; BD Biosciences, San Diego, CA, USA), and β-actin (A3854; Sigma-Aldrich, St. Louis, MO, USA).

May-Grünwald Giemsa staining

For a morphological analysis of human leukemia cell lines, we prepared cytospin slides via centrifugation at 700 rpm for 3 min on Cytospin 4 positively charged glass slides (Thermo Fisher Scientific, San Jose, CA, USA). The slides were stained with May-Grünwald solution (Wako, Osaka, Japan) in PBS (pH 6.4) for 3 min at room temperature and washed briefly. Giemsa solution (Wako) was added to each slide, followed by a 15-min incubation. Cellular morphology was evaluated on the stained slides using an Axiokop 2 plus microscope with NanoZoomer Digital Pathology (Hamamatsu Photonics, Shizuoka, Japan).

Surface marker array

TF-1a and HEL92.1.7 cells were incubated with 50 nM and 100 nM T-3775440 for 72 hours, respectively. Treated cells were stained with BD Lyoplate™ (560747; BD Biosciences, San Diego, CA, USA) according to the manufacturer's instructions, and analyzed on an LSRFortessa™ (Becton-Dickinson). Mean fluorescent intensities (MFI) were calculated according to the BD Lyoplate™ Human Screen Analysis Instructions for BD FACSDiva, available as an Excel file on

the manufacturer's web site.

siRNA transfection

For each targeted gene, siRNA was obtained from Dharmacon (Chicago, IL, USA) or Ambion (Austin, TX, USA) as described in the table below. siRNA was formulated into lipid-based nanoparticles. Nanoparticulated siRNA was mixed with cells at a final concentration of 10 nM. For drug treatment experiments, cells were reseeded into tissue culture plates at 48 h post-siRNA transduction and treated with DMSO or drugs. The following siRNAs were used in this study:

siRNA	ID	Format	Vendor
siCTRL	D-001810-10	ON-TARGETplus Non-targeting pool	Dharmacon
siKDM1A #1	L-009223-00	SMARTpool: ON-TARGETplus KDM1A siRNA	Dharmacon
siKDM1A #2	118783	Silencer Validated siRNA	Ambion
siGFI1B #1	s15850	Silencer Select Pre-Designed siRNA	Ambion
siGFI1B #2	s15851	Silencer Select Pre-Designed siRNA	Ambion
siSPI1 #1	s13351	Silencer Select Pre-Designed siRNA	Ambion
siSPI1 #2	s13352	Silencer Select Pre-Designed siRNA	Ambion

Tumor xenograft models

Female C.B17/Icr-scid/scid Jcl mice (CLEA Japan, Inc., Tokyo, Japan) were maintained under specific pathogen-free conditions and used in compliance with the guidelines of the Takeda Institutional Animal Care and Use Committee in a facility accredited by the American Association for Accreditation of Laboratory Animal Care (AAALAC). AML cells (2×10^6 cells) in Matrigel were inoculated subcutaneously (s.c.) into the left flanks of 6- to 7-week-old mice (day 0). Mice were randomized when the mean tumor volume reached approximately 140–230 mm^3. Subsequently, mice were treated with vehicle or T-3775440 once daily on a 5 days on/2 days off schedule for 2 or 3 weeks. Tumor volume was measured twice weekly with Vernier calipers and calculated as (length × $width^2$) × 0.5. The percentage treated/control ratio (T/C %) was calculated by dividing the change in tumor volumes in T-3775440-treated mice by the change in volumes vehicle-treated mice. Statistical comparisons were conducted using the Dunnett-type test, one-tailed Williams test, and Aspin-Welch *t*-test to calculate *P* values with EXSUS version 8.0.0 software (CAC Croit). *P* values of <0.05 were considered statistically significant.

Results

Erythroleukemia and megakaryoblastic leukemia cells are highly sensitive to T-3775440

LSD1 demethylase activity has been reported to be inhibited by monoamine oxidase (MAO) inhibitor tranylcypromine (2-PCPA). Therefore, I selected 2-PCPA as the starting entity for the medicinal chemistry effort and developed T-3775440 (Fig. 2A), which contains a cyclopropylamine moiety. Cyclopropylamine derivatives have been reported to irreversibly bind to FAD within the catalytic core of the enzyme [37]. T-3775440 demonstrated irreversible inhibition with k_{inact}/ K_I value of $1.7\times10^5 \pm 2.6\times10^4$ ($sec^{-1} M^{-1}$) for recombinant human LSD1 (Fig. 2B). T-3775440 was highly selective for LSD1 with a half-maximal inhibitory concentrations (IC_{50}) value of 2.1 nM when compared with other monoamine oxidases, namely MAO-A and MAO-B (Fig. 2B). To take advantage of this novel, potent, and selective inhibitor, I first determined its anti-cancer activity *in vitro*. Previously, LSD1 inhibitors were reported to be effective against AML cell lines and primary AML cells. To elucidate which leukemic subtypes are sensitive to T-3775440, I conducted a cell line panel analysis of 27 leukemia cell lines, including 22 AML cell lines, a CML cell line and 4 T-ALL cell lines. Although small molecule inhibitors for epigenetic enzymes generally tend to require sustained incubation to induce phenotypic changes, I realized that T-3775440 blocked the proliferation of several cell lines at day 3 of treatment (Fig. 2C). Of interest, four of five AEL cell lines and three of four AMKL cell lines exhibited clear responses to T-3775440 following a 3-day treatment. In contrast, T-ALL cell lines were insensitive to T-3775440 (Fig. 2C). A western blot analysis of p27 and PARP cleavage revealed that 48-hour T-3775440 treatment showed cell-cycle arrest and apoptosis in AEL (TF-1a, HEL92.1.7; Fig. 2D) and AMKL cell lines (CMK11-5, M07e; Fig. 2E). Consistent with changes in protein levels, a flow cytometric cell-cycle analysis revealed that T-3775440 treatment increased the G1 and sub-G1 phase populations in TF-1a and CMK11-5 cells (Fig. 2F and G). These results indicate that T-3775440 exhibits rapid antiproliferative and proapoptotic activities against AEL and AMKL cells.

Treatment with T-3775440 induces transdifferentiation in AML cells

Previous reports have demonstrated that the pharmacological inhibition or knockdown of LSD1 induces myeloid differentiation associated with altered marker expression and morphological change in AML cells [31, 33, 34]. Consistent with this observation, T-3775440

treatment resulted in the presence of lobular nuclei and granulocytic cytoplasm, both are characteristics of differentiated myeloid cells, in TF-1a and HEL92.1.7 cells (Fig. 3A). To investigate the genetic program regulated by LSD1 in AML cells, I compared the transcriptomes of control and T-3775440-treated HEL92.1.7 AEL cells and CMK11-5 AMKL cells in a microarray analysis. T-3775440 treatment increased the signal intensities of 1,277 probes (≥2-fold) in HEL92.1.7 and 793 probes in CMK11-5. In contrast, significantly fewer downregulated probe sets (≤ 2-fold) were detected: 282 probes in HEL92.1.7 and 289 probes in CMK11-5. To interpret the biological significance of these post-treatment gene expression changes, I employed a NextBio data-mining framework (www.nextbio.com). Interestingly, commonly upregulated genes in both HEL92.1.7 and CMK11-5 cells were significantly enriched in SPI1 binding site gene sets (Table 1). SPI1, also known as PU.1, is a DNA-binding transcription factor that plays a critical role in myeloid development and activates lineage-specific gene expression [38]; my finding suggests that T-3775440 induces the ectopic upregulation of myeloid lineage genes, which are normally repressed in erythroid and megakaryocytic lineage cells. A gene set enrichment analysis was also conducted using the same microarray data. In HEL92.1.7 cells, the monocytic lineage gene signature was significantly upregulated, whereas the erythroid gene signature was downregulated by treatment with T-3775440 (Figs. 3B and C). Similarly, upon treatment with T-3775440, CMK11-5 tended to lose its original features indicative of a megakaryocytic gene signature and acquired both natural killer cell and monocytic lineage gene signatures (Figs. 3D-F). To further address whether morphological changes were associated with immunophenotypic changes or not, I determined the expression levels of 242 surface molecules on AML cell lines. Notably, the granulocyte/macrophage marker CD86 was upregulated by treatment with T-3775440 in TF-1a and HEL92.1.7 cells (Fig. 3G), whereas the erythroid marker CD235a was downregulated by treatment (Fig. 3H). Consistent with the observation that T-3775440 induced elevation of cell surface CD86 expression, CD86 mRNA expression was clearly upregulated in a dose-dependent manner in HEL92.1.7 and CMK11-5 cells, as well as TF-1a cells (Figs. 3I-K). Taken together, these results suggest that T-3775440 converts these AML cell lineages from the original erythroid or megakaryocytic lineage to myeloid-like lineages.

Growth inhibition induced by T-3775440 is attributed to transdifferentiation to a myeloid-like lineage

The results from morphological, transcriptomics and immunophenotyping analyses implicated that T-3775440 induces cell transdifferentiation in the erythroid and megakaryocytic lineages. To test whether lineage conversion was involved in T-3775440-induced growth inhibition in AML cell lines, I applied TF-1a cells to flow cytometric sorting and washout analysis to test whether CD86 expression affect cell growth. After a 3-day T-3775440 treatment, cells were sorted according to CD86 expression levels and cultured without T-3775440 (Figs. 4A and B). Cell population expressing moderate or high levels of CD86 grew more slowly than did cells expressing low levels of CD86 (Fig. 4B). This growth suppression was sustained for up to 7 days after compound removal, suggesting profound effects of transdifferentiation on TF-1a cell growth. Because T-3775440 upregulated a substantial number of genes under the control of the myeloid master regulator transcription factor SPI1 (Table 1), I knocked down SPI1 to further address whether T-3775440-dependent transdifferentiation was associated with growth inhibition. In control cells, T-3775440 treatment increased *CD86*, *ITGAM*, *FCRLA* and *SPI1* expression and decreased *GYPA* (encodes CD235a) and *GATA1* gene expression, whereas such T-3775440-dependent increases or decreases in gene expression were attenuated in SPI1 knockdown cells (Figs. 4C-H). Furthermore, SPI1 depletion partially rescued cells from T-3775440-mediated apoptosis (Fig. 4I) and growth suppression (Fig. 4J). These data suggest that T-3775440 suppresses AEL cell growth through a transdifferentiation-dependent mechanism in which SPI1-regulated genes play at least some key roles.

T-3775440 treatment inhibits the association of LSD1 with GFI1B, and knockdown of GFI1B or LSD1 phenocopies the anti-leukemic activity of T-3775440

To gain further insight into the molecular mechanism underlying T-3775440-mediated growth suppression, I tested how this inhibitor affected protein complexes containing LSD1. LSD1 is known to form complexes with the corepressor proteins CoREST and GFI1B in GFI1B-expressing cells [28]. As shown in Figure 5A, T-3775440 treatment disrupted the association of LSD1 with GFI1B in a concentration-dependent manner, although the association of LSD1 with CoREST was retained when immunoprecipitated by anti-LSD1 antibody. On the other hand, when immunoprecipitated by anti-GFI1B antibody, T-3775440 treatment disrupted the association of GFI1B with LSD1-CoREST complex. Because CoREST is known to interact through LSD1 not through GFI1B [39], it is reasonable to assume that T-3775440 disrupt GFI1B and LSD1-CoREST

complex to induce terminal differentiation of leukemia cells. To evaluate whether the effect of T-3775440 on AML cells was mediated through the disruption of this complex, I examined the effects of siRNA-mediated knockdown of either LSD1 or GFI1B in TF-1a cells (Figs. 5B and C). Single knockdown of either LSD1 or GFI1B led to increased *CD86* expression and reduced *GYPA* expression (Figs. 5D and E); however, the effects on cell proliferation were modest (Fig. 5G). Because the LSD1-GFI1B complex represses the *GFI1B* promoter [40], LSD1 knockdown led to an increase in *GFI1B* expression (Fig. 5C). Therefore, I speculated that dual gene knockdown would more closely recapitulate the effect of T-3775440 and induce more robust effects on cell differentiation and proliferation. Indeed, depletion of both LSD1 and GFI1B additively augmented CD86 upregulation (Fig. 5D), induced nuclear segmentation (Fig. 5F), and significantly reduced proliferative capacity relative to either single-siRNA treatment (Fig. 5G), thus confirming the phenotypic interaction between transdifferentiation and growth suppression in TF-1a cells. These results suggest that the effects of T-3775440 are mediated mainly through the inhibition of GFI1B and LSD1-CoREST complex formation.

T-3775440 affects the later stages of hematopoiesis

The effect of T-3775440 on human erythroid and myeloid progenitor proliferation was evaluated in MethoCult™ GF H84434 using bone marrow from three healthy volunteers. T-3775440 had no significant observable effect on myeloid progenitor numbers (Figs. 6A-C). In contrast, significant inhibition of erythroid progenitor proliferation was observed at IC_{50} values ranging between 0.1 μM and 0.14 μM (Figs. 6D-F). These results suggest that T-3775440 exerts more specific effects at the stages of erythroid progenitors, including CFU-E and BFU-E.

T-3775440 exerts tumor growth suppression *in vivo* mouse xenograft models of AML

I next conducted an *in vivo* efficacy study of T-3775440 using mouse subcutaneous xenograft models of AML cell lines. Corroborating my *in vitro* observation, T-3775440 upregulated *CD86* mRNA expression in tumor xenografts of HEL92.1.7 cells in a dose-dependent manner following the oral administration of single doses ranging from 3 to 30 mg/kg (Fig. 7A). To investigate the target engagement of this compound in tumors, I tested the expression levels of *PI16*, which is reported to be directly regulated by LSD1 in AML cells [41]. As expected, *PI16* expression was dramatically derepressed by T-3775440 treatment *in vivo*, which serves as a

downstream marker for T-3775440 mediated LSD1 inhibition (Fig. 7B).

In a TF-1a (AEL) tumor xenograft model, T-3775440 exhibited significant antitumor effects in a dose-dependent manner, with 15-day T/C values of 15.6% and <0% at doses of 20 and 40 mg/kg, respectively (Fig. 7C). T-3775440 also exhibited significantly potent antitumor effects in an additional AEL model of HEL 92.1.7 and an AMKL model of CMK11-5 (Figs 7D and E), leading to nearly complete tumor growth suppression during the dosing period. In accordance with a previous report in which conditional LSD1 knockdown was tested in mice[30], I found that in mice, T-3775440 treatment resulted in a transient reduction in platelets followed by a significant rebound (Fig. 7F), which was considered a mechanism-based side effect of LSD1 inhibition. The mechanism by which LSD1 depletion causes a decrease in platelet production is only incompletely understood, but the recruitment of LSD1 to chromatin by the transcription factor GFI1B is essential for megakaryocyte maturation and platelet production [42]. On the other hand, there was no obvious effect on red blood cell (RBC) counts following the single administration, likely because of the longer half-lives of matured RBCs (Fig. 7G). On a dosing schedule comprising 5 days on/2 days off, a statistically significant difference in body weight was observed between vehicle- and T-3775440-treated tumor xenograft model mice at higher doses. However, efficacious doses of T-3775440 were tolerated in all these AEL and AMKL subcutaneous tumor xenograft models. These results demonstrate that T-3775440 possesses profound anti-AEL and anti-AMKL activity in *in vivo* xenograft models, as well as *in vitro* models.

Discussion

AEL and AMKL are rare subtypes of AML that account for approximately 3% and 1% of adult AML cases, respectively [43, 44]. However, both subtypes are aggressive and refractory to conventional therapies. Both subtypes have very poor prognosis, with reported median survival durations of 36 and 23 weeks for AEL and AMKL patients, respectively [45, 46]. In addition, no recurrent cytogenetic abnormalities are specific to these diseases, and therefore it is challenging to develop molecular-targeting therapeutics such as all-trans retinoic acid, which was discovered for acute promyelocytic leukemias harboring the PML-RARA fusion [47, 48]. Therefore, dissecting AEL and AMKL patients-specific molecular mechanism to develop novel therapeutics that are different from conventional therapeutics with respect to the modes of action is urgently needed for these AML subtypes.

Here, I found that T-3775440, a potent and selective inhibitor of LSD1, showed a sensitivity of erythroid and megakaryocytic leukemic cell lines. This lineage selectivity clearly distinguishes T-3775440 from conventional chemotherapeutics used for AML treatment, such as cytarabine or anthracyclines. Based on analyses of morphological, gene expression and immnunophenotyping changes, I demonstrated that T-3775440 treatment directed erythroleukemia and megakaryoblastic leukemia cells towards transdifferentiation into granulomonocytic lineage cells, as evidenced by nuclear segmentation and CD86 induction in TF-1a cells. Of note, after compound treatment, cells that expressed higher levels of CD86 exhibited more severely impaired proliferation than did cells with lower levels of CD86, suggesting a close linkage of transdifferentiation to cell growth inhibition by T-3775440. Furthermore, knockdown of *SPI1*, which encodes the critical hematopoietic transcription factor for myeloid differentiation PU.1, reversed not only T-377540-dependent transdifferentiation, but also partially reversed the related growth suppression and apoptosis. These results also indicate that the transdifferentiation plays a critical role in cell growth inhibition and apoptosis by T-3775440 in these cells.

Furthermore, I found that T-3775440 disrupted the interaction between LSD1 and GFI1B in AEL cells. GFI1B is a zinc finger protein that functions as a transcriptional repressor and is essential for the generation of definitive erythroid and megakaryocytic lineages [49]. Saleque and colleagues described that the epigenetic regulation of hematopoietic differentiation by GFI1B is dependent on the cofactors CoREST and LSD1 [28]. LSD1 and CoREST are

recruited to the promoter regions of downstream target genes of GFI1B in a process mediated by the interaction between the SNAG domain of GFI1B and LSD1, and inhibition of this process perturbs erythroid and megakaryocytic differentiation [27]. Notably, GFI1B overexpression is observed in erythroid and megakaryocytic leukemia [50]. These lines of evidence strongly suggest that GFI1B and its interaction with LSD1 participate in the pharmacological effects of T-3775440 in AEL and AMKL. Indeed, analogous to my observations in T-3775440-treated cells, GFI1B knockdown derepressed SPI1 target genes, including *CD86*, and cell growth suppression in TF-1a cells. In addition, double knockdown of GFI1B and LSD1 led to greater effects on *CD86* induction and cell growth, compared with each single knockdown. These results support the hypothesis that the effects of T-3775440 are mediated through a disrupted protein-protein interaction of GFI1B and LSD1. Recently, GFI1B was reported to directly regulate SPI1 [51]. Indeed, T-3775440 resulted in the upregulation of SPI1 in AEL cells. Therefore, the LSD1-GFI1B-SPI1 axis might be involved in T-3775440 mediated transdifferentiation and growth suppression. Although the molecular mechanism by which T-3775440 affects the LSD1-GFI1B interaction remains to be elucidated, it is assumed that T-3775440, a derivative of tranylcypromine (TCP), covalently binds to FAD in a manner similar to other TCP analogous inhibitors [52] and that the resultant FAD adduct might hinder the interaction between LSD1 and the SNAG domain of GFI1B.

In recent years, several inhibitors of LSD1 have been generated with various scaffolds and subjected to efficacy evaluation [32, 53, 54]. Among them, two LSD1 inhibitors, ORY-1001 and GSK2879552, have entered clinical trials for the treatment of patients with AML (EudraCT Number: 2013-002447-29, ClinicalTrials.gov identifier: NCT02177812). Like T-3775440, both inhibitors harbor a cyclopropylamine moiety that is responsible for the covalent interaction between the inhibitor and FAD within the catalytic domain of LSD1 [53, 55]. GSK2879552 and some other cyclopropylamine derivatives with LSD1 inhibitory activities have been reported to suppress the growth of a diverse range of AML cell lines, irrespective of subtype, following a 6- or 12-day treatment course [41, 55]. Similarly, I found that T-3775440 was more profoundly efficacious and exhibited a broader anti-AML spectrum after prolonged treatment. However, I also observed a characteristic rapid response to T-3775440 (with 3-day treatment) in GFI1B-expressing AEL and AKML cell lines. The relatively quick effects of T-3775440 might also underscore the significant impact of LSD1-GFI1B complex disruption and subsequent

transdifferentiation in GFI1B-dependent AML cells. It would be highly interesting to investigate the clinical efficacies of other cyclopropylamine derivatives, especially ORY-1001 and GSK2879552 (currently under clinical trials), in patients with AEL and AKML.

During the course of my *in vivo* evaluation, I observed a considerable reduction in the number of platelets in T-3775440-treated mice. This inhibitor effect on erythroid and megakaryocytic progenitors could be related to the capacity of T3775440 to disrupt GFI1B-containing transcriptional complexes. This observation is consistent with a previous report in which conditional LSD1 knockdown in adult mice led to severe thrombocytopenia [29, 30]; a colony forming cell (CFC) assay using normal human bone marrow cells revealed the selective activity of T-3775440 at the stage from CFU-GEMM toward BFU-E, which was also consistent with the previously reported effects of 2-PCPA on erythroid progenitor cells [31]. These results suggest that during hematopoiesis, T-3775440 targets the common erythro-megakaryocytic progenitor (MEP) population, which is known to express high levels of GFI1B [56]. Prominent thrombocytopenia is likely due to the relatively short half-life of platelets, compared with red blood cells. Importantly, the effect of T-3775440 on platelets was reversible and is expected to be manageable by platelet transfusion in clinical settings.

Although numerous attempts have been made to identify novel oncogenic driver mutations and possible mutation-related cancer vulnerabilities in AMLs, the available therapeutic option and the number of actionable oncogenic drivers have still been limited. AEL and AMKL have not been reported to possess such driver mutations and therefore remain as diseases with a major unmet medical need. In this study, I revealed AEL and AMKL subtypes-specific regulatory network driven by LSD1-GFI1B complex that are required for leukemogenesis using T-3775440, a novel inhibitor of LSD1. Moreover, I found that this compound disrupted the LSD1-GFI1B interaction, inducing transcriptional de-repression of downstream-target genes of GFI1B, leading to cell transdifferentiation and consequent cell growth inhibition and/or apoptosis induction. My findings provide a rationale for the testing of T-3775440 as a potential treatment with a novel mechanism of action for AML, especially AEL and AMKL, and also suggest the possibility of transdifferentiation induction as a novel therapeutic strategy to override the differentiation block and self-renewal capability of AML.

Table and Figures

TABLE 1. List of enriched pathways from commonly upregulated genes in both HEL92.1.7 and CMK11-5 cells by the treatment of T-3775440.

Biogroup	Source	*P* value
Immunoglobulin-like fold	InterPro	6.70E-11
Immunoglobulin-like	InterPro	7.40E-11
Cell periphery	GO	1.50E-09
Immune response	GO	2.00E-08
SPI1 binding site geneset 2	Broad MSigDB-Regulatory Motifs	6.90E-08
Single-organism process	GO	1.00E-07
ETS2 binding site geneset 2	Broad MSigDB-Regulatory Motifs	1.20E-07
Immunoglobulin subtype	InterPro	1.70E-07
Response to stress	GO	9.30E-07
Immunoglobulin V-set	InterPro	1.90E-06
Cellular response to stimulus	GO	2.40E-06
SPI1 binding site geneset 1	Broad MSigDB-Regulatory Motifs	2.60E-06
SOX9 binding site geneset 1	Broad MSigDB-Regulatory Motifs	3.10E-06
Single organism signaling	GO	3.90E-06
Leukocyte migration	GO	4.10E-06
Response to bacterium	GO	4.90E-06
ELF1 binding site geneset 1	Broad MSigDB-Regulatory Motifs	4.90E-06
ETV4 binding site geneset 1	Broad MSigDB-Regulatory Motifs	8.80E-06
Response to other organism	GO	1.80E-05
FOXD1 binding site geneset 1	Broad MSigDB-Regulatory Motifs	1.70E-05
Regulation of immune response	GO	2.70E-05
Response to wounding	GO	2.80E-05
HMGA1 binding site geneset 1	Broad MSigDB-Regulatory Motifs	2.90E-05
NFATNFATC binding site geneset 1	Broad MSigDB-Regulatory Motifs	3.60E-05
FOXF2 binding site geneset 3	Broad MSigDB-Regulatory Motifs	4.20E-05
Immunoglobulin protein family	InterPro	4.40E-05
MYOD1 binding site geneset 4	Broad MSigDB-Regulatory Motifs	5.20E-05
Beta-microsemin protein	InterPro	6.20E-05
Signaling receptor activity	GO	9.80E-05

A

T-3775440

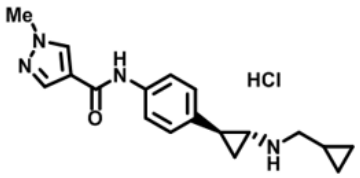

B

IC_{50} (nM)	T-3775440
LSD1	2.1
MAO-A/B	>100,000/>100,000

C

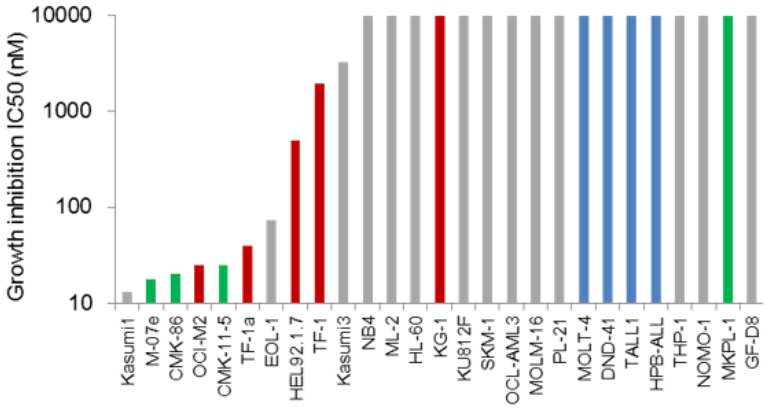

D

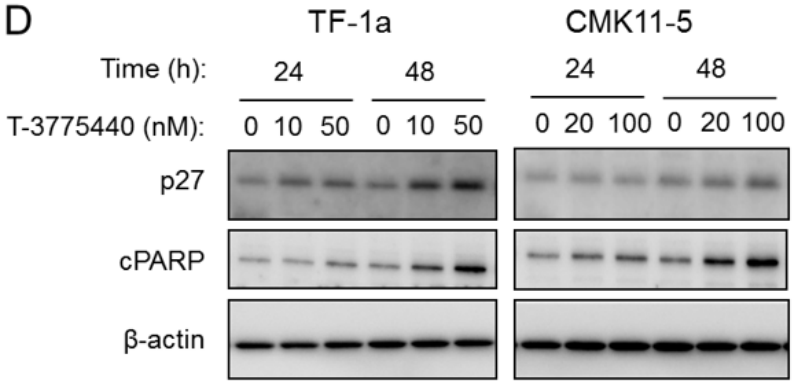

E

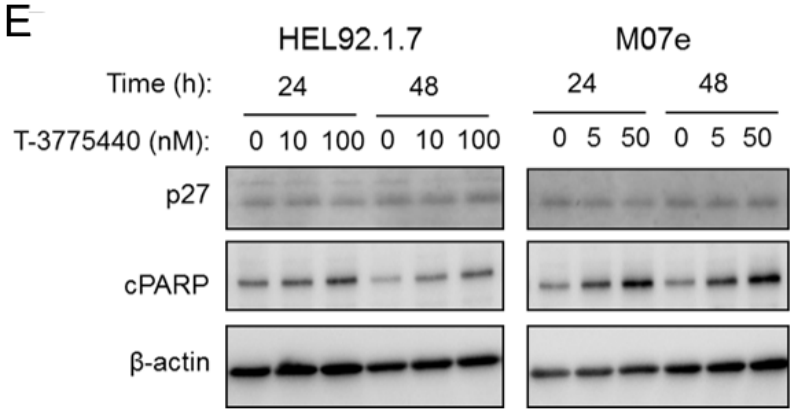

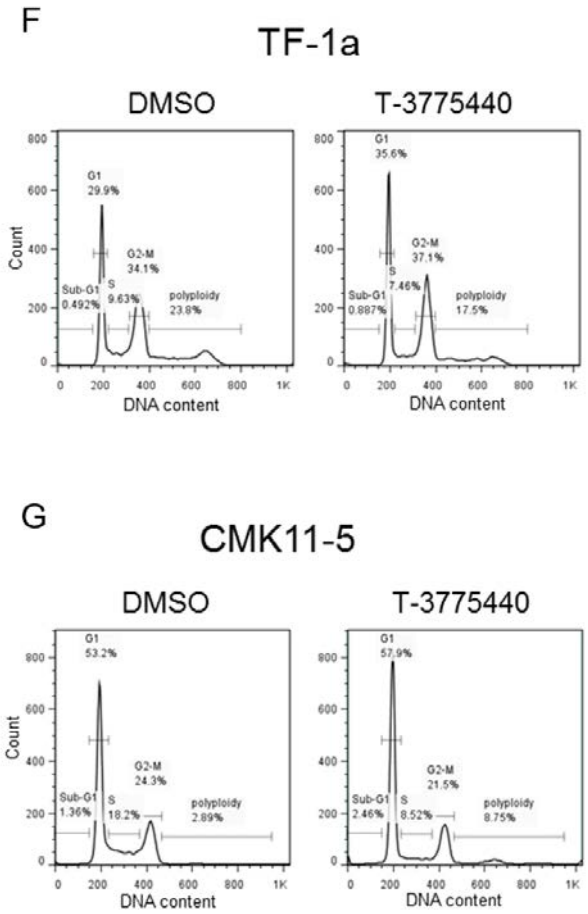

Figure 2. T-3775440 leads to cell growth inhibition in acute myeloid leukemia cell lines.

(A) Chemical structure of T-3775440. (B) *In vitro* enzymatic activity and selectivity of T-3775440. (C) *In vitro* proliferation assay of 27 leukemia cell lines. Cells were treated with T-3775440 for 3 days. Red bars indicate acute erythroleukemia cell lines, green bars indicate acute megakaryoblastic leukemia cell lines, and blue bars indicate acute T cell lymphoblastic leukemia cell lines. (D and E) acute erythroleukemia (AEL) TF-1a and CMK11-5 cells (D), and acute megakaryoblastic leukemia (AMKL) HEL92.1.7 and M07e cells (E) were treated with the indicated concentration of T-3775440 for 24 or 48 hours. Treated cells were subsequently harvested and lysed, and total lysates were prepared. Immunoblotting analyses were performed to determine the expression levels of p27, cleaved PARP, and β-actin in the cell lysates. (F and G) TF-1a (F) and CMK11-5 (G) cells were treated with T-3775440 or DMSO control at concentrations of 50 nM and 100 nM, respectively. Forty-eight hours later, cells were harvested, and cell cycle profiles were analyzed using flow cytometry.

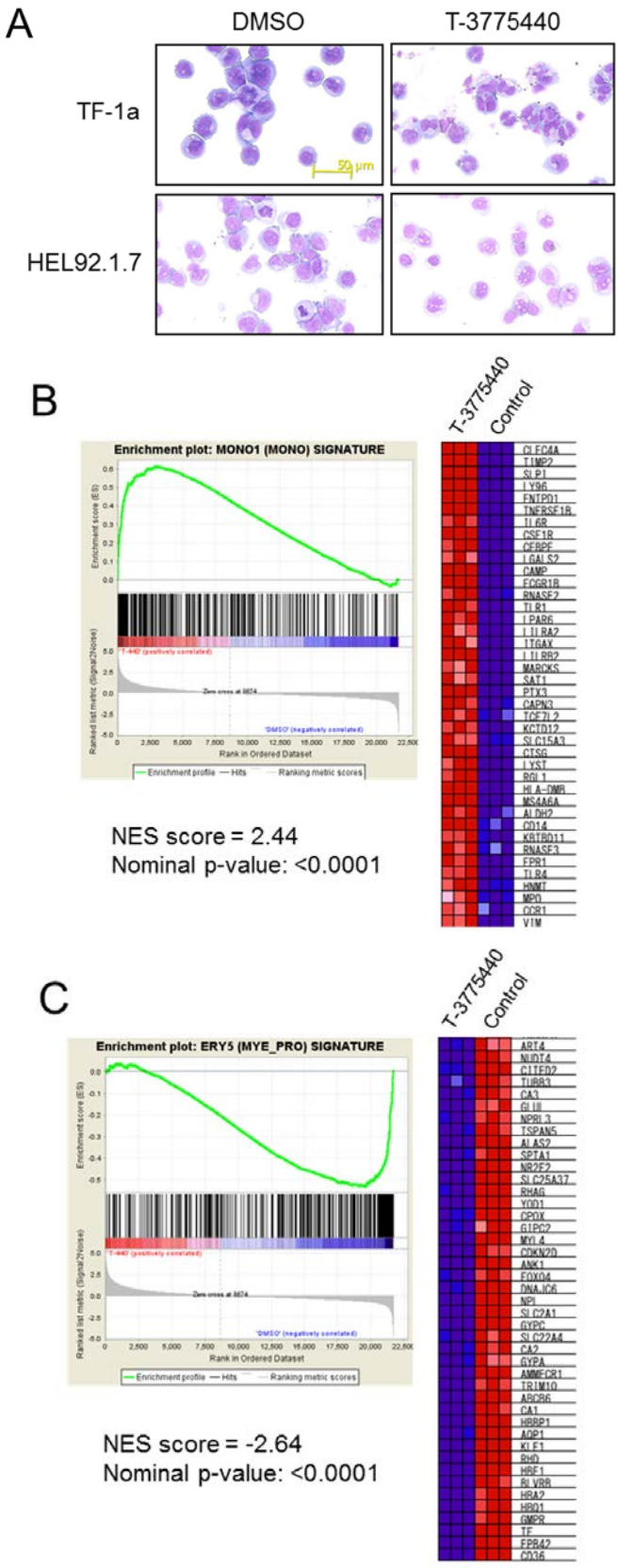
A
DMSO
T-3775440
TF-1a
HEL92.1.7
50 µm
B
T-3775440
Control
Enrichment plot: MONO1 (MONO) SIGNATURE
Enrichment score (ES)
Ranked list metric (Signal2Noise)
Rank in Ordered Dataset
Enrichment profile
Hits
Ranking metric scores
NES score = 2.44
Nominal p-value: <0.0001
C
T-3775440
Control
Enrichment plot: ERY5 (MYE_PRO) SIGNATURE
Enrichment score (ES)
Ranked list metric (Signal2Noise)
Rank in Ordered Dataset
Enrichment profile
Hits
Ranking metric scores
NES score = -2.64
Nominal p-value: <0.0001

D

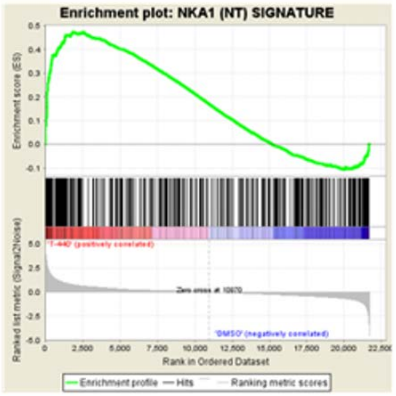

NES score = 1.64
Nominal p-value: <0.0001

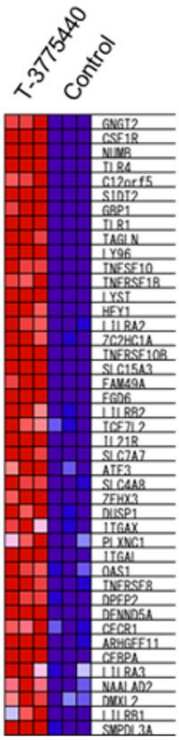

E

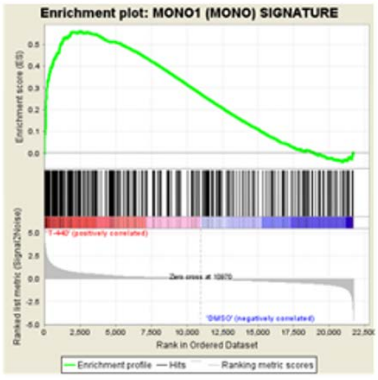

NES score = 1.52
Nominal p-value: <0.0001

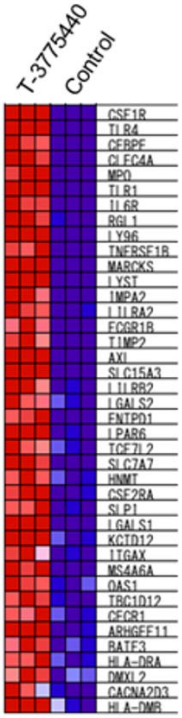

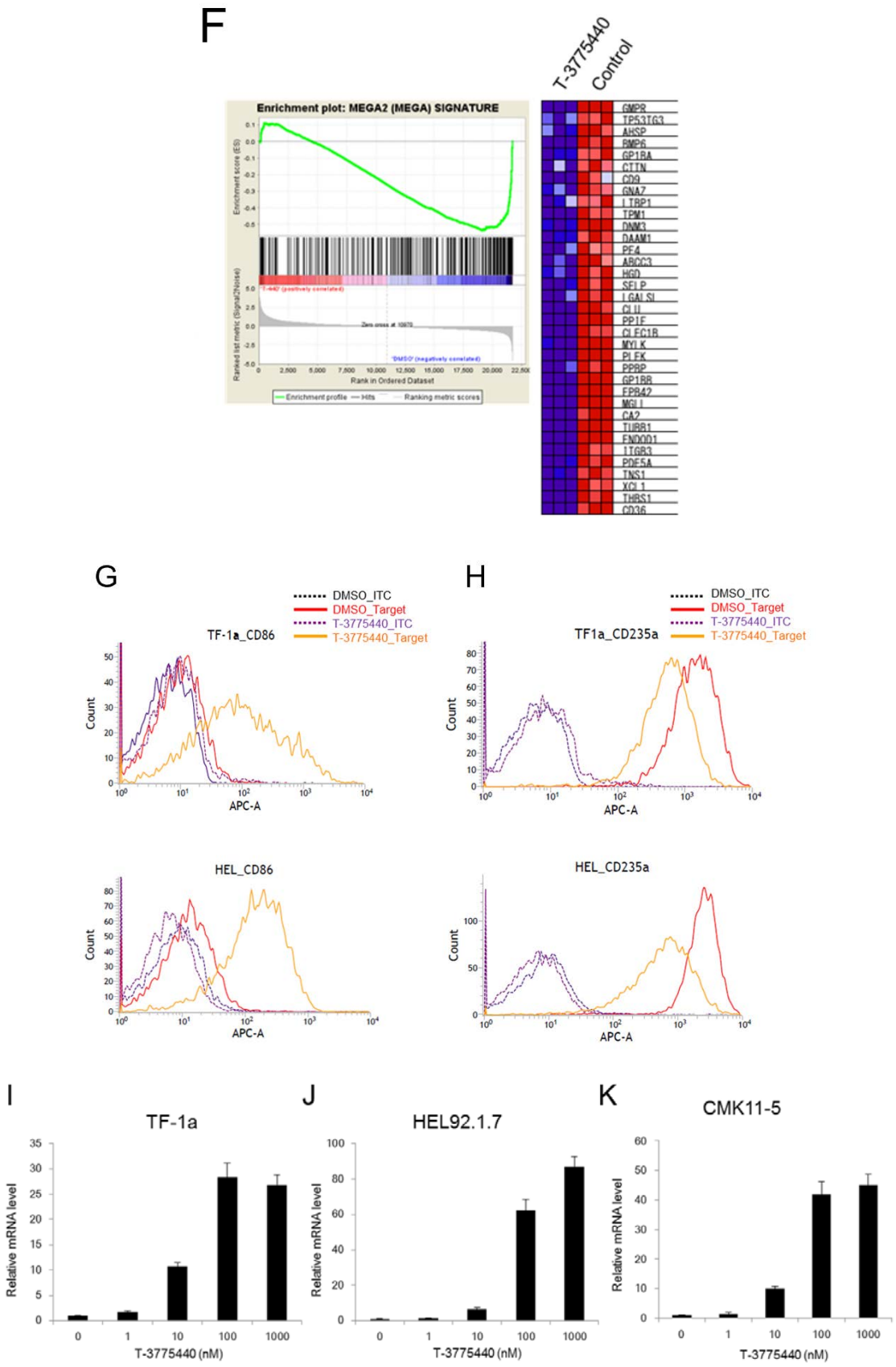
F
T-3775440
Control
Enrichment plot: MEGA2 (MEGA) SIGNATURE
Enrichment score (ES)
Ranked list metric (Signal2Noise)
Rank in Ordered Dataset
Enrichment profile
Hits
Ranking metric scores
GMPR
TP53TG3
AHSP
BMP6
GP1BA
CTTN
CD9
GNAZ
ITRP1
TPM1
DNM3
DAAM1
PF4
ABCC3
HGD
SELP
LGALS1
CLU
PPIF
CLEC1B
MYLK
PLEK
PPBP
GP1BB
EPB42
MGLL
CA2
TUBB1
ENDOD1
ITGB3
PDE5A
TNS1
XCL1
THBS1
CD36
G
DMSO_ITC
DMSO_Target
T-3775440_ITC
T-3775440_Target
TF-1a_CD86
Count
APC-A
HEL_CD86
H
TF1a_CD235a
HEL_CD235a
I
TF-1a
Relative mRNA level
T-3775440 (nM)
J
HEL92.1.7
K
CMK11-5

Figure 3. Treatment with T-3775440 induced features of morphological differentiation in cultured AML cells.

(A) TF-1a and HEL92.1.7 cells were treated with T-3775440 for 72 hours. Representative images of cytospin preparations are shown. (B, C) Gene set enrichment analysis plots demonstrate the upregulation of monocytic gene signature genes (B) and downregulation of erythroid gene signature genes (C) in HEL92.1.7 cells following T-3775440 treatment versus control treatment. (D, E) A gene set enrichment analysis (GSEA) plot shows the upregulation of natural killer signature genes (D) and monocytic signature genes (E) in CMK11-5 cells following treatment with T-3775440 versus a control. (F) A GSEA plot illustrates downregulation of the megakaryocytic signature genes in CMK11-5 cells following treatment with T-3775440 versus a control. (G, H) TF-1a (upper) and HEL92.1.7 (lower) cells were treated with or without 100 nM of T-3775440 for 72 hours, after which the expression 242 surface molecules were analyzed using flow cytometry. Representative surface marker expression levels are described for CD86 (G) and CD235a (H). (I-K) Cells were treated with DMSO or T-3775440 for 24 h. CD86 gene expression changes were measured by qRT-PCR in TF-1a (I), HEL92.1.7 (J) and CMK11-5 cells (K). Values represent the means of triplicate samples ± standard deviations.

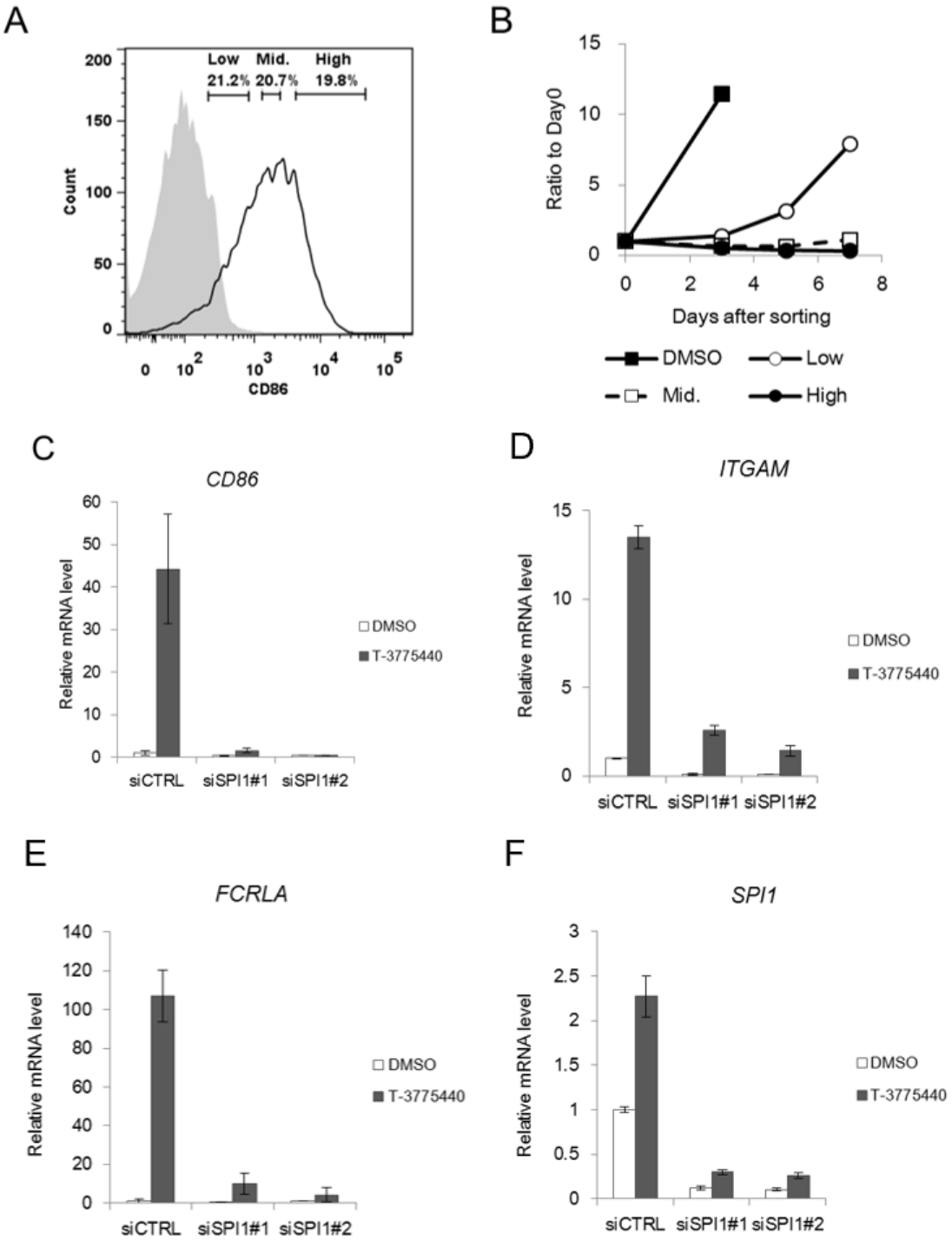
A
Low Mid. High
21.2% 20.7% 19.8%
Count
CD86
B
Ratio to Day0
Days after sorting
DMSO
Low
Mid.
High
C
CD86
Relative mRNA level
DMSO
T-3775440
siCTRL
siSPI1#1
siSPI1#2
D
ITGAM
Relative mRNA level
DMSO
T-3775440
siCTRL
siSPI1#1
siSPI1#2
E
FCRLA
Relative mRNA level
DMSO
T-3775440
siCTRL
siSPI1#1
siSPI1#2
F
SPI1
Relative mRNA level
DMSO
T-3775440
siCTRL
siSPI1#1
siSPI1#2

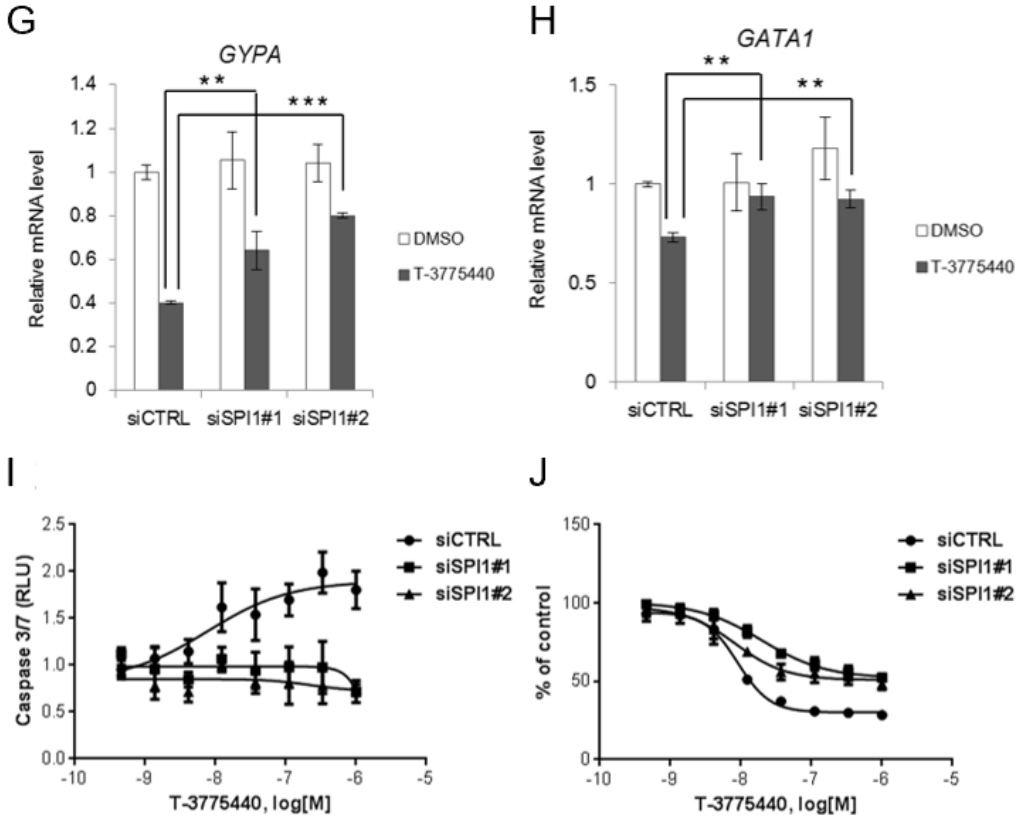

Figure 4. Myeloid gene expression correlates with and is required for the growth inhibitory activity of T-3775440.

(A, B) TF-1a cells were treated with T-3775440 for 72 hours. Cells were sorted based on CD86 expression intensity (A) and further cultivated without T-3775440. Proliferation rates were measured at the indicated time points (B). DMSO indicates cells treated with DMSO only and subsequently cultivated further. (C-H) *SPI1* was knocked down by siRNA treatment in TF-1a cells, which were subsequently reseeded in the presence or absence of 100 nM T-3775440. Twenty-four hours after treatment with the compound or vehicle control, cells were harvested for RNA purification. Changes in *CD86* (C), *ITGAM* (D), *FCRLA* (E), *SPI1* (F), *GYPA* (G) and *GATA1* (H) expression were measured by qRT-PCR. Values represent the means of triplicate samples ± standard deviations. Asterisks denote P <0.01 (**) and P <0.001 (***) as determined by a Dunnett-type test. (I) Apoptosis induction in a dose-response manner was measured with Caspase 3/7 Glo in TF-1a cells treated with T-3775440 for 24 hours. (J) Knockdown of SPI1 using siRNA-attenuated, T-3775440-induced growth inhibition in TF-1a cells.

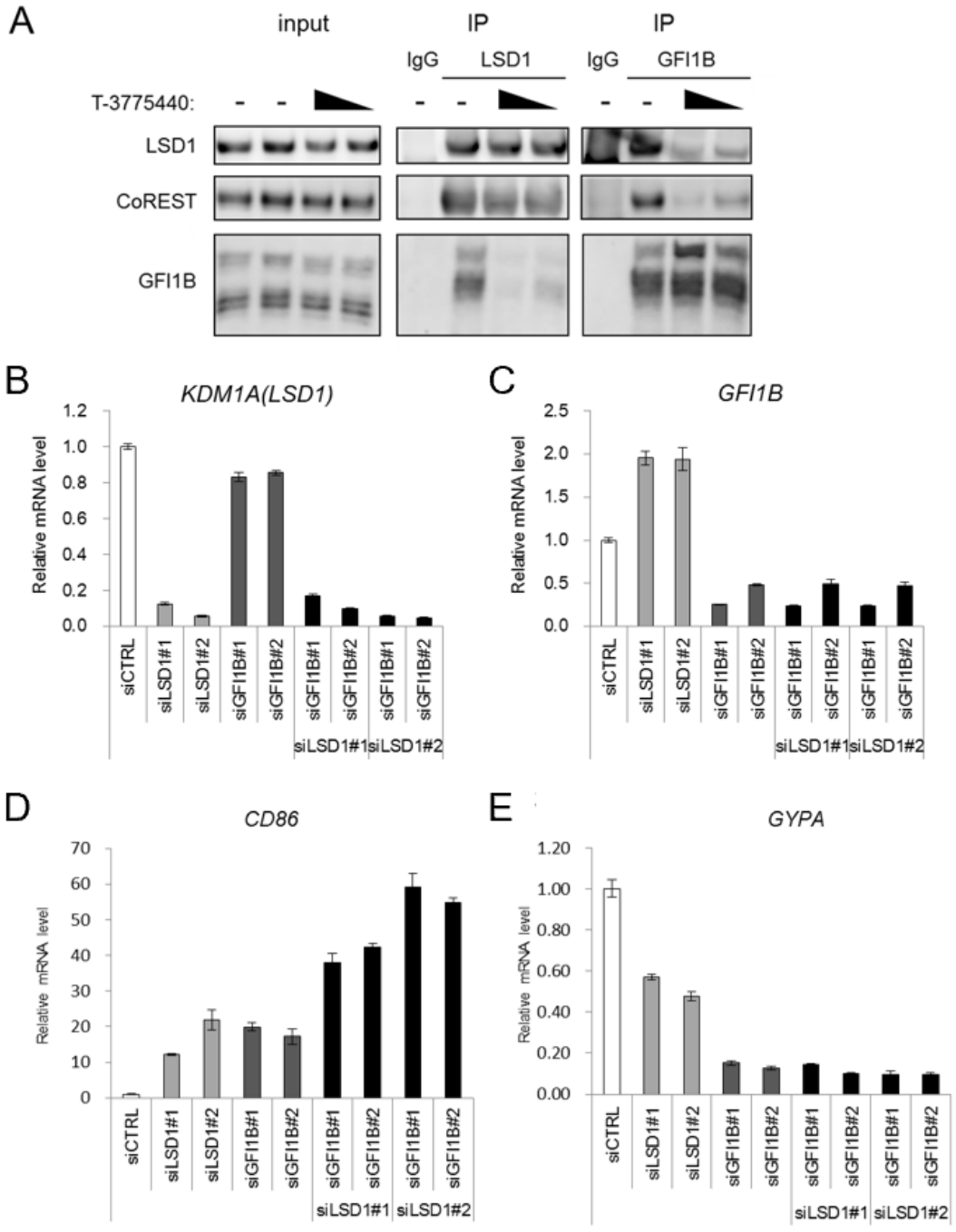
A
input
IP
IP
IgG
LSD1
IgG
GFI1B
T-3775440:
LSD1
CoREST
GFI1B
B
KDM1A(LSD1)
Relative mRNA level
siCTRL
siLSD1#1
siLSD1#2
siGFI1B#1
siGFI1B#2
siLSD1#1
siLSD1#2
C
GFI1B
Relative mRNA level
D
CD86
Relative mRNA level
E
GYPA
Relative mRNA level

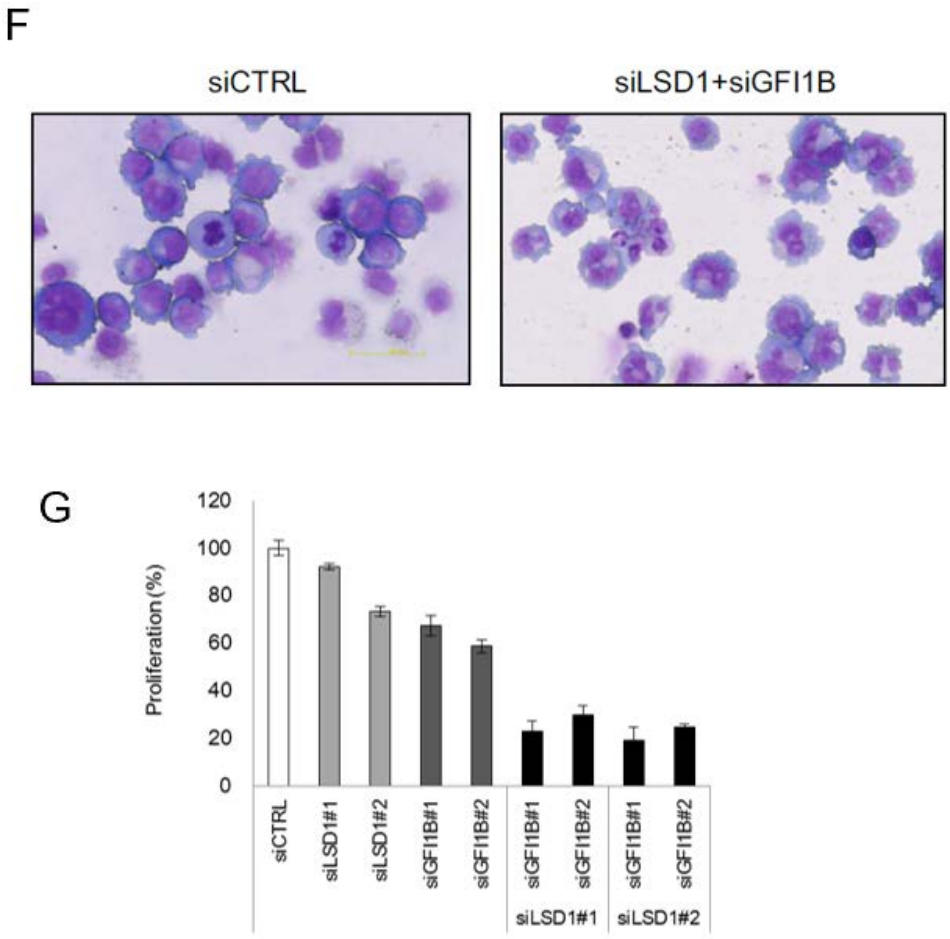

Figure 5. T-3775440 disrupts the LSD1-GFI1B-CoREST complex, and GFI1B knockdown phenocopies T-3775440 treatment.

(A) TF-1a cells were incubated in the presence or absence of T-3775440. A chromatin fraction was prepared, and GFI1B-containing complexes were immunoprecipitated. An immunoblotting analysis was conducted for the indicated proteins. (B-E) TF-1a cells were treated with the indicated siRNAs, and *LSD1* (B), *GFI1B* (C), *CD86* (D) and *GYPA* (F) expression levels were measured by qRT-PCR after a 48-hour treatment. Values represent the mean of triplicate samples ± standard deviations (SDs). (F) TF-1a cells were treated with the indicated siRNAs, and cells were harvested after a 72-hour treatment. Representative images of cytospin preparations are shown. Cells were observed at 40x magnification using a light microscope. (G) The proliferation rate was measured 6 days after treatment with T-3775440. The values represent means ± SDs of three independent experiments.

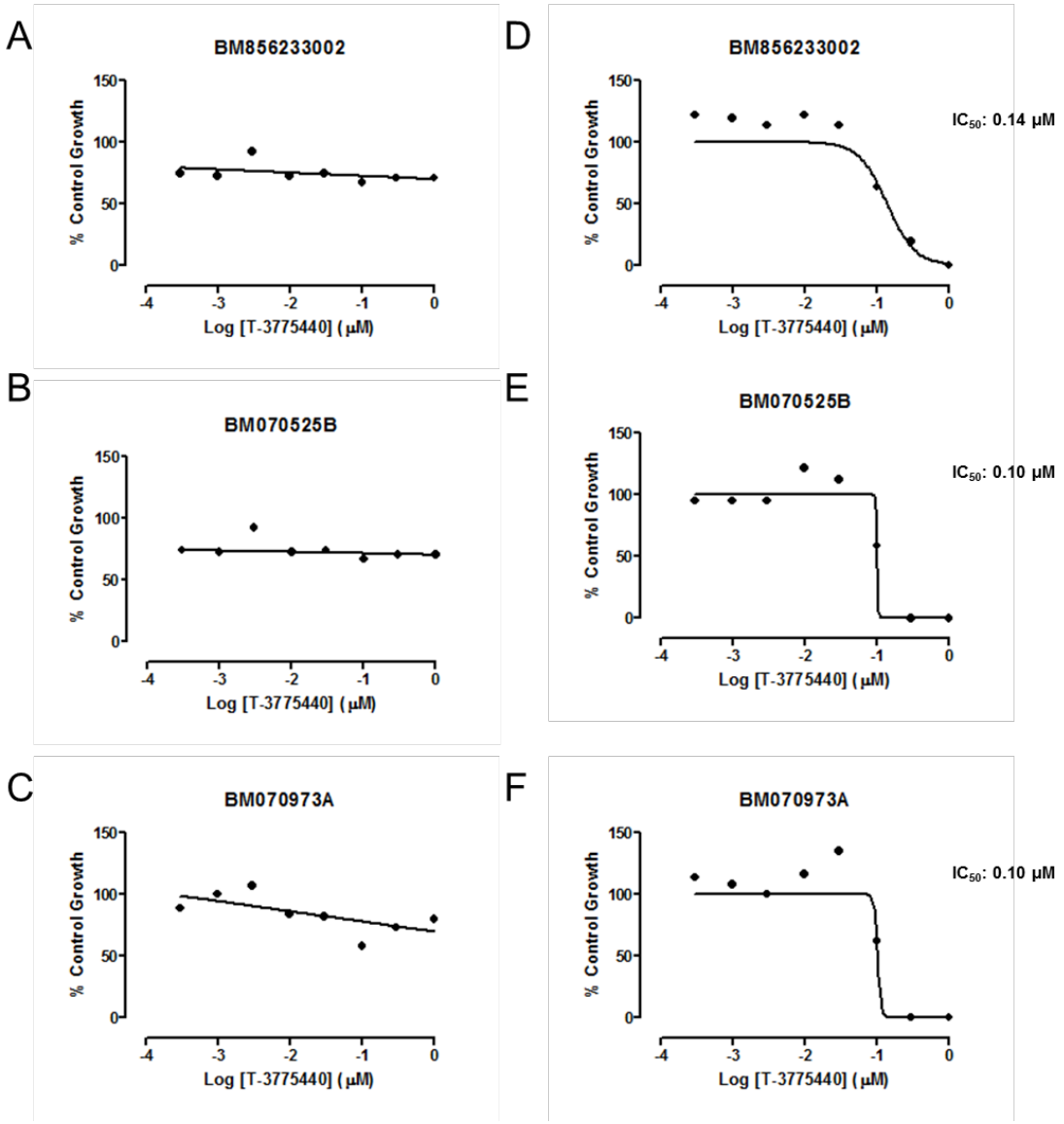

Figure 6. Dose-response curves of the effects of T-3775440 on erythroid and myeloid progenitor proliferation

The average colony counts per dish were obtained from cultures of each bone marrow lot (A and D, BM856233002; B and E, BM070525B; C and F, BM070973A). (A–C) Myeloid progenitors: CFU-GM. (D–F) Erythroid progenitors: CFU-E and BFU-E. Values are expressed as percentages of the numbers of colonies in DMSO-treated controls. IC_{50} values are also presented for D, E and F.

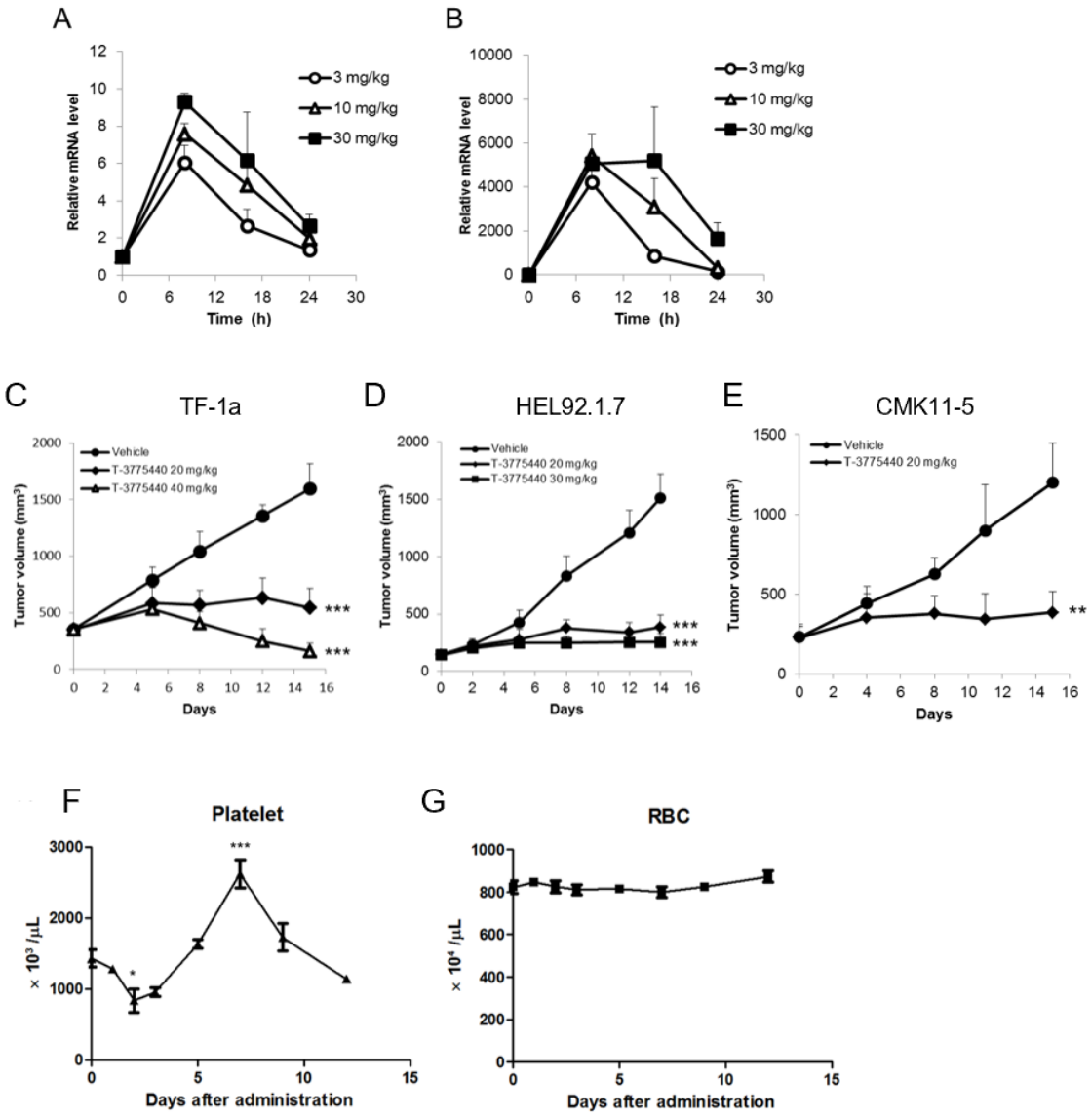

Figure 7. T-3775440 exhibited significant anti-leukemic effects *in vivo*.

(A, B) *In vivo* pharmacodynamics marker responses were analyzed by measuring mRNA expression levels. *CD86* (A) and *PI16* (B) expression levels were measured by qRT-PCR. The values represent the means ± standard deviations (SDs; $n = 3$). (C–F) *In vivo* anti-tumor efficacy following once-daily oral T-3775440 treatment was evaluated in TF-1a (C), HEL92.1.7 (D), and CMK-11-5 (E) tumors. The values represent the mean tumor volumes ± SDs ($n = 5$). (F, G) Peripheral platelet (F) and red blood cell (RBC) (G) counts in ICR mice were analyzed using a Sysmex XT-1800i Automated Hematology Analyzer (Sysmex, Kobe, Japan) before and after a single oral administration of T-3775440. *$P < 0.05$, ***$P < 0.001$ by Dunnett's multiple comparison test.

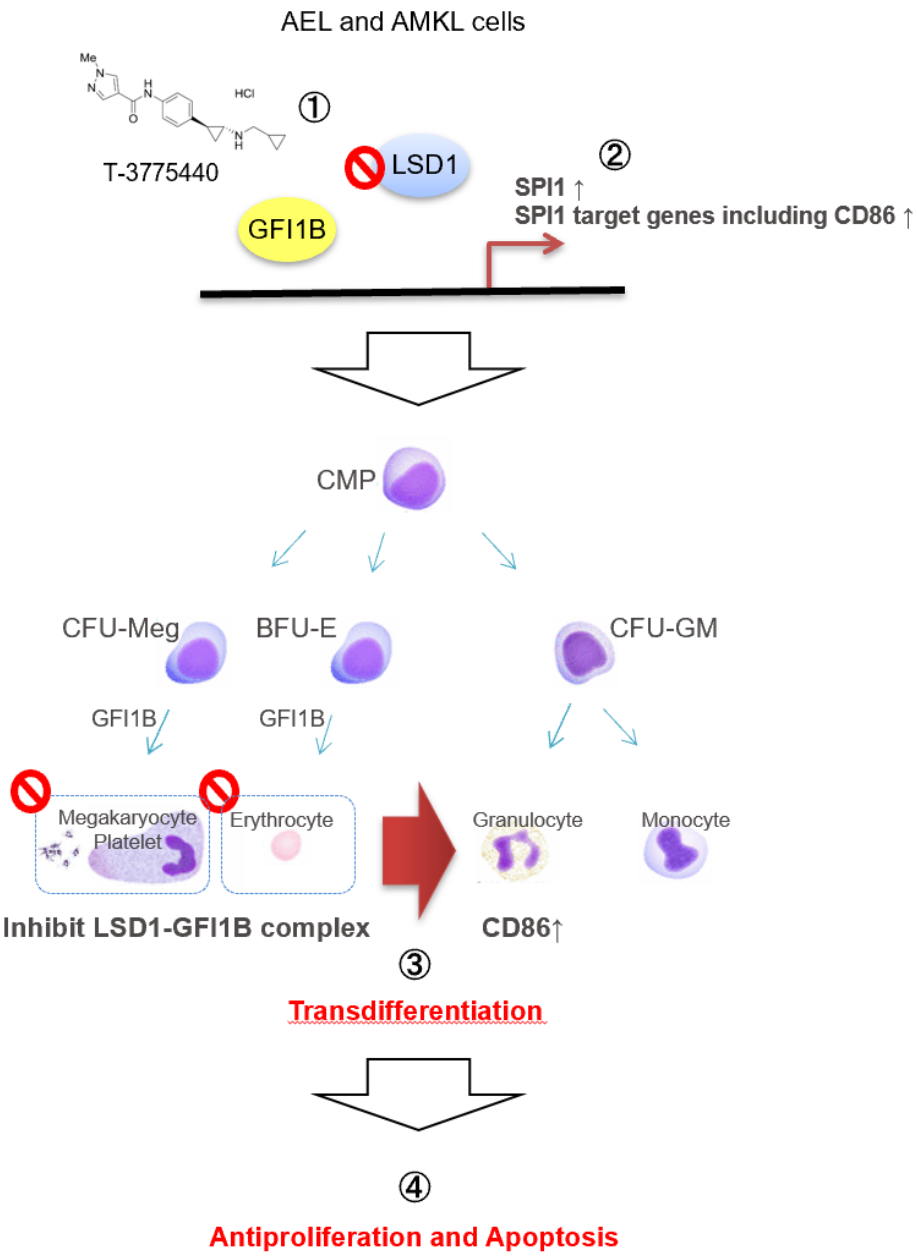

Figure 8. Schematic representation of possible mechanism of action of T-3775440 in AEL and AMKL cells

LSD1 inhibitor, T-3775440 1) disrupts the LSD1-GFI1B interaction, thus 2) inducing transcriptional de-repression of downstream-target genes of GFI1B, and consequently, 3) lead transdifferentiation from erythroid/megakaryocytic lineages into the granulomonocytic lineage, 4) eventually exhibits antiproliferative and proapoptotic activities against GFI1B-expressing acute erythroleukemia (AEL) and acute megakaryoblastic leukemia (AMKL) cells.

Chapter 2: Gene Signature–Based Approach Identified MEK1/2 as a Potential Target Associated with Relapse After Anti-TNFα Treatment for Crohn's Disease

Abstract

Biologic anti-tumor necrosis factor alpha monoclonal antibodies (anti-TNFα mAb), such as infliximab and adalimumab, have transformed the treatment of immune-mediated inflammatory conditions such as Crohn's disease (CD) and Ulcerative colitis (UC), collectively known as inflammatory bowel disease (IBD), thereby rapidly becoming a mainstay of therapy. However, over 50% patients of CD patients are estimated to undergo surgery during their lifetime even with the therapy, and novel therapeutic options are needed. To dissect the general mechanism of response to anti-TNFα therapy, I analyzed colonic gene expression data of CD patients at the time of pre- and post-infliximab treatment therapy. I found that a series of gene expression signature which is abnormally expressed in pre-treatment colon tissue remains unresolved even after patients achieved clinical remission after treatment. Pathway enrichment analysis clearly showed excessive growth state and suppressed terminal differentiation in post-infliximab treatment CD colon whereas immune components are clearly resolved by infliximab therapy. I took connectivity map (CMap) approach based on colon signature of CD patients to discover novel therapeutic concept/target for untreatable mechanism of anti-TNFα mAb therapy, and found that mitogen-activated protein kinase (MAPK) pathway inhibitors (EGFR, RAF and MEK inhibitors) were negatively correlated with reference signature match infliximab therapy untreatable signature. *In vitro* transcriptome analysis demonstrated that a selective MEK1/2 inhibitor significantly normalized reference residual CD signature. In addition, validation study using Caco-2, human colon epithelial cells, revealed that MEK1/2 inhibitor facilitated intestinal epithelial differentiation and enhanced barrier function. Finally, administration of enteric microparticles of MEK1/2 inhibitor significantly improved diarrhea and histological score of colitis in murine colitis model. These findings suggested that abnormalities in CD colon are not completely resolved by infliximab therapy even after achieving clinical remission, and MEK1/2 would be a potential target for CD patients to address the untreatable mechanism of anti-TNFα mAb therapy, which may lead to sustainable remission.

Introduction

Crohn's disease (CD) is a chronic and progressive inflammatory disease of the gastrointestinal tract [57]. The management of CD has evolved dramatically over the last decade with the emergence of biological therapies. Infliximab, an anti-tumor necrosis factor alpha monoclonal antibody (anti-TNFα mAb), is effective in managing the symptoms of CD and induces remission even in patients not responding to conventional treatment including mesalamine, antibiotics, corticosteroids, and immunomodulators [58, 59]. Despite these advances, still over 50% of CD patients are estimated to undergo recurrence surgery during their lifetime due to stricturing and penetrating complications [60, 61]. Furthermore, the meta-analysis study showed that the risk of relapse remained significant in CD patients when discontinuation of anti-TNFα treatment was based on clinical and endoscopic remission [62]. Therefore, treatments that achieve sustainable remission in CD are needed.

While it is largely unknown what etiology is involved in the disease, recent genetic advances have revealed that CD is presumably driven by both immune and non-immune pathophysiology [63]. However, most conventional CD therapies currently target only the immune components [64]. Recently, the so-called "deep remission" defined as complete mucosal healing has become the ultimate endpoint of the therapeutic advances for CD [65]. Therefore, there is a great promise in new therapeutic approaches that integrate both immune and non-immune pathophysiological components and potentially induce greater and sustainable deep remission as a single agent or in combination with established immunosuppressants. A previous report has demonstrated that loss of barrier function identified by confocal laser endomicroscopy would be a sensitive predictor of relapse of inflammatory bowel disease (IBD) patients in remission states [66]. It has also been reported that the histology of CD patient’s ileum in remission with anti-TNFα therapy showed complete clearance of inflammation and immune cell infiltration, whereas crypt architecture remained disturbed [67]. Based on these evidences, I hypothesized that there may be some structural and functional abnormalities in patients who achieve clinical remission after anti-TNFα therapy that might predispose to recurrence.

Integrating disease analysis into drug discovery based on molecular states is critical to find effective therapeutics for complex diseases. At the mRNA level, gene expression signature has been used in a wide range of disease characterization, drug discovery process, or as a pharmacodynamic marker with the dose-dependent cellular response [68]. Recent advances in

methods for gathering and analyzing transcriptome data across many technology platforms serve as the groundwork for enabling data-driven drug discovery [69]. Connectivity map (CMap) has recently been applied for the repurposing of drugs [70]. The approach is to look for inverse drug-disease relationships by comparing disease molecular features with drug molecular features. Notably, Cheng J et al. [71] reported a systematic approach to quantitatively evaluate CMap methodology and showed that it can significantly enrich true positive drug-indication pairs using an effective matching algorithm. Thus, analyzing clinically relevant molecular signatures allowed me to identify potential therapeutic targets as well as to understand the etiology of complex diseases.

In this study, I focused on mucosal gene signatures before and after first infliximab therapy on CD patients [72] and found that a series of gene signature remained unresolved even after patients achieved clinical remission with the therapy. Analysis of the gene signature provided me not only insights into non-immune abnormalities but also a rational strategy to address this mechanism. By using a systematic computational approach, I predicted therapeutic benefit of inhibition of MAPK pathway. I demonstrated that both treating CD and preventing the disease recurrence would be deliverable by a selective MEK1/2 inhibitor. My results suggested that targeting MEK is a novel strategy that could induce a sustainable remission via normalizing molecular alterations to baseline, which in part, leads to the promotion of reconstitution of intestinal epithelium.

Materials & Methods

Microarray data and differential gene expression analysis

In order to reanalyze publicly available transcriptome data from Arijs I et al. [72], I obtained the gene expression data set GSE16879 from GEO, the NCBI Gene Expression Omnibus, which was run on the Affymetrix platform Human Genome U133 Plus 2.0. In this study, mucosal gene expression profiles were obtained from the colonic biopsies of 19 CD patients and 24 UC patients, refractory to corticosteroids and/or immunosuppression, before and 4 - 6 weeks after their first infliximab infusion and from 6 healthy controls. The response to infliximab was defined as mucosal healing with a decrease of at least 3 points on the histological score for CD [73], and as a decrease to a Mayo endoscopic subscore of 0 or 1 with a decrease to grade 0 or 1 on the histological score for UC [74, 75]. Probe set expression values were estimated with the frozen RMA algorithm using R/Bioconductor, the frma package, and their presence call was calculated with the MAS5 algorithm using R/Bioconductor, the affyPLM package. Probes that were called absent in > 90% samples were filtered out. Lastly, less variable probes whose interquartile ranges were in the bottom 10% of all probes were filtered out. Identification of differentially expressed genes (DEGs) was conducted based on the empirical Bayes method using R/Bioconductor, the limma package. Human crypt signature generated from GSE6894 [76] was downloaded from Nextbio database (http://www.nextbio.com/). For statistical test, paired *t*-test was performed to detect the DEGs with an adjusted *P* value < 0.05, absolute fold change > 1.2 in the Nextbio platform. Mouse crypt signature was obtained from GSE27605 on GEO datasets [77], which was run on the Affymetrix-platform Mouse Genome 430 2.0 Array. Data processing and statistical analysis were performed applying the same methods as GSE16879.

Principal component analysis

Principal component analysis (PCA) was performed by "prcomp" function of the R/CRAN stats package. To determine whether the patient groups were significantly different from healthy group, Dunnett's tests were conducted to examine the patient vs. healthy control in PC1 by "SimTestDiff" function of R/CRAN SimComp package. Visualization of scatter plot and boxplot was done using R/CRAN ggplot2 package.

Pathway enrichment analysis

The extracted genes were evaluated in a pathway enrichment analysis on NextBio using the Gene Ontology (GO) database.

Hierarchical clustering and Heatmap visualization

Clustering using cosine distance and Ward linkage method was performed by "Heatmap" function of the ComplexHeatmap package which is available on R/Bioconductor.

For calculation of Enrichment Scores (ES), the association of DEGs and a gene set (Signature) was assessed with a contingency table and the *P* value was calculated using Fisher's exact test. Then all the *P* values are transformed by a formula (-Log10(*P* value)) into ES calculated as follows:

$$ES = (-Log10(P1)) + (-Log10(P2)) – (-Log10(N1)) – (-Log10(N2))$$

P1 and P2 mean positive correlation between DEGs and Signature, both Log FC of DEGs and Signature, Log FC > 0 or < 0. N1 and N2 means negative correlation between DEGs and Signature, DEGs Log FC > 0 and Signature Log FC < 0, or DEGs Log FC > 0 and Signature Log FC < 0.

Computational prediction

I modified the CMap database build 02 [70] by integrating it with the drug signatures obtained from internal microarray transcriptome data (data source is shown as "Internal") to compute Enrichment Scores of gene set against drugs. For microarray analysis, total RNAs were extracted using the RNeasy Miniprep kit (Qiagen, Valencia, CA, USA) according to the manufacturer's protocol. Preparation of cDNAs and cRNAs, hybridization, and microarray scanning were performed according to the manufacturer's protocols (Affymetrix Inc., Santa Clara, CA, USA). Biotinylated cRNAs were hybridized to Affymetrix Human Genome U133A Array or U133 Plus 2.0 Array. The data were analyzed with Microarray Suite version 5.0 (MAS5) using Affymetrix default analysis settings and global scaling as normalization method. A list of negative permuted Enrichment Scores associated with each of the small molecules in the CMap and internal dataset as calculated by Kolmogorov-Smirnov statistics was generated against signatures of anti-TNFα therapy-untreatable genes (TUGs) and anti-TNFα therapy-treatable genes (TTGs). For computational prediction, TUG and TTG signatures are extracted from GSE16879 as per the following criteria: significant value referred to false discovery rate (FDR) adjusted *P* value < 0.05 and absolute fold change > 1.2, and not significant value referred to FDR adjusted *P* value > 0.05.

Cell culture and reagent

Human colorectal cancer cell lines LoVo and Caco-2 cells were obtained from ATCC (Manassas, VA, USA). LoVo cells were grown in F-12K with 10% FBS, and Caco-2 cells were grown in Dulbecco's modified Eagle's medium (DMEM) with 10% FBS. Both cells were maintained in a

humidified incubator at 37 °C and 5% CO_2. Compound A was synthesized at laboratories in Takeda California as a selective and potent MEK allosteric site inhibitor (IC_{50} of 38 nM against purified MEK1) which was orally bioavailable and efficacious in tumor xenograft models as previously reported [78]. PD0325901 was obtained from SelleckChem (Houston, TX, USA), Gemcitabine (GEMZAR®) was obtained from Eli Lilly (Indianapolis, IN, USA) and Bicalutamide (Casodex® tablets) was obtained from AstraZeneca (London, UK).

Amplicon sequencing and DEG analysis

AmpliSeq™ human-transcriptome libraries were constructed and sequenced in technical triplicates using the Ion Proton™ platform (Thermo Fisher Scientific, Waltham, MA, USA), according to the manufacturer's instructions. Briefly, 10 ng of total RNA was reverse transcribed using the SuperScript® VILO™ cDNA Synthesis Kit (Thermo Fisher Scientific) followed by library generation using the Ion AmpliSeq™ Transcriptome Human Gene Expression Kit. Libraries were diluted to 100 pM and pooled equally, with 18 individual samples per pool. The pooled libraries were multiplexed and clonally amplified by using the Ion OneTouch 2 System, and then sequenced on Ion PI™ chips using an Ion Proton™ sequencing system. Data were first analyzed by Torrent Suite and ampliSeqRNA analysis plugin to generate count data. Read count normalization was performed using voom method, and the extraction of DEGs was conducted based on the empirical Bayes method using R/Bioconductor, the limma package.

pERK inhibition assay

Total and p-ERK1/2 contents were measured using an ERK1/2 (pT202/Y204 + Total) ELISA Kit (ab176660, Abcam, Cambridge, UK) following the manufacturer's protocol. LoVo cells (5×10^4) were incubated in 96-well plate treated with Compound A at indicated concentrations for 1 hour. The cells were then washed with PBS and lysed in lysis buffer. Standards for ERK1/2 and p-ERK1/2 were run simultaneously in parallel. Samples were incubated in antibody solution for 1 hour with gentle shaking at room temperature. After washing, TMB substrate was added to each well and incubated for 15 minutes. Optical density was recorded at 450 nm using a plate reader.

Transepithelial electrical resistance assay

To measure the effects of Compound A on the Caco-2 monolayer barrier function, Caco-2 cells were seeded at 1×10^5 cells/ml on 24 well Transwell inserts with 0.45 μm pore size (Corning Costar, USA). After 1 day of cell culture, the cells were treated with Compound A at indicated concentrations and cultured for 7 days. Culture medium with Compound A was changed every 2

- 3 days. To assess the integrity of the monolayer, transepithelial electrical resistance (TEER) was monitored by measuring the transmembrane resistance using an epithelial voltohmmeter EVOM2™ (LMS). The TEER value was corrected for surface area and expressed as Ohms cm^2.

Caco-2 differentiation assay

Cells were plated in a 96 well plate at the density of 1.6×10^4 cells/well. 1 day after plating, the cells were treated with compounds and allowed to grow at confluence. The entire time course was performed twice, and total RNA from cells were obtained at 1, 3 and 6 days from plating. The *APOA1* and *LGR5* mRNA expression levels at day 3 and 6 relative to *GAPDH* mRNA level at day 1 were measured by RT-PCR.

Quantitative RT-PCR analysis

Total RNA was isolated from cells and purified using RNeasy 96 kit (Qiagen, Valencia, CA, USA). Quantitative real-time PCR analysis was performed on an Applied Biosystems 7900HT Fast Real Time PCR System (Applied Biosystems, Foster City, CA, USA), using QuantiTect Probe RT-PCR Kit (Qiagen) with TaqMan probes against the target genes (Applied Biosystems). Data were analyzed according to the $2^{-\Delta\Delta Ct}$ method and normalized relative to the amount of *GAPDH* mRNA. The normalized abundances of target mRNAs were expressed relative to the corresponding values for cells treated with DMSO. The following TaqMan probes were used: *GAPDH* (4310884E), *APOA1* (Hs00163641_m1), and *LGR5* (Hs00969422_m1).

Preparation of enteric Compound A microparticles (MPs)

Microparticles (MPs) were fabricated using oil-in-oil emulsion solvent evaporation method [79, 80]. 0.25 g of Compound A and 1.5 g of polymer mixture of Eudragit S100 and Eudragit RS (1:2 (w/w)) were suspended in 15 mL of ethanol and acetone mixture (1:1). The solution was emulsified into 83 g of liquid paraffin containing sorbitan sesquioleate (Span 83) (1%, w/w) as a dispersing agent. The stirring speed was set at 1,000 rpm using a magnetic stirrer. After an over-night stirring, solidified enteric Compound A MPs were collected by centrifugation (1,000 rpm, 3 min) and washed three times with 50 ml of n-hexane and dried at room temperature. The drug concentration was determined by HPLC at a wavelength of 285 nm.

Animals

Studies were performed in accordance with the standards for humane care, and treatment of research animal was approved by Institutional Animal Care and Use Committee (IACUC) in Takeda Pharmaceutical Company, Ltd (Approval No. 10797). Female BALB/c mice (7 weeks of

age) and C.B-17/Icr-scid/scid mice (SCID, 7 weeks of age) were purchased from Charles River Japan and CLEA Japan, respectively. They were housed in plastic cages with free access to food and water. All animals were kept under constant temperature (23 ± 3°C) and humidity (55 ± 15%) conditions with a 12 hours light/dark cycle.

Activated T cell transfer colitis model

Total lymphoid cells were recovered from splenocytes of BALB/c mice by lympholyte-M (Cedarlane Lab., Ontario, Canada). Then, the cell suspension was treated with HLB solution (IBL) for hemolysis. Total lymphoid cells (2×10^6 cells/mL) were cultured in RPMI-1640 (WAKO, Japan) supplemented with 10% FBS (Gibco Life Technologies), Concanavalin A (4 μg/mL), and recombinant human IL-2 (10 ng/mL, R&D systems, Minneapolis, MN, USA) for 3 days. After the incubation, $CD4^+$ T cells were isolated by MACS separation systems with CD4 (L3T4) MicroBeads (Miltenyi Biotec, Bergisch Gladbach, Germany). Activated $CD4^+$ T cells (2×10^5 cells) from BALB/c mice were intravenously injected into SCID mice (day 0). At day 17, diarrhea score for stool consistency was graded on a scale of 1 - 4 (1, normal: 2, pasty and formed: 3, pasty and unformed: 4, diarrhea).

Therapeutic treatment of enteric Compound A MPs and anti-TNFα mAb in the experimental colitis

A total of 35 mice graded for 2 and 3 were equally divided into 5 groups as follows: vehicle control, enteric Compound A MPs at 0.3 mg/kg and at 1 mg/kg, isotype mAb (HRPN; Bio X Cell) and anti-TNFα mAb (XT3.11; Bio X Cell, West Lebanon, NH, USA). Enteric Compound A MPs were suspended in 0.5% methylcellulose (WAKO) and orally administered once a day from day 17 to 27. Isotype mAb and anti-TNFα mAb were intraperitoneally injected every 4 days from day 17 at 0.1 mg/mouse, based on preliminary studies in which maximum efficacy of anti-TNFα treatment was observed at 0.1 mg/mouse. At day 27, diarrhea score for stool consistency was graded on a scale of 1 - 4. Colon of each mouse was surgically removed, rinsed with saline, and the weight was measured at day 28.

Pharmacokinetic studies

Pharmacokinetic studies were performed using female C57BL/6J mice and activated T cell transfer colitis mice after oral administration of enteric Compound A MPs at a dose of 1 mg/kg. Quantification of drug concentration by LC-MS/MS: Aliquots 5 μL of the plasma or 30 μL of the colon homogenate were mixed with acetonitrile containing the internal standards. The mixtures

were centrifuged at 4,283 × g and 4°C for 5 min. The supernatants were diluted with solvents for LC-MS/MS. The diluted solutions (5 or 7 μL) were injected into an LC-MS/MS instrument (API5000 or QTRAP5500, AB Sciex, Framingham, MA, USA) equipped with Shimadzu Shim-pack XR-ODS (2.2 μm, 2.0 × 30 mm) maintained at 50°C. Mobile phase condition consisted of 10 mM ammonium formate/formic acid (100/0.2, v/v) (mobile phase A) and acetonitrile/formic acid (100/0.2, v/v) (mobile phase B). The chromatographic separation was performed with a gradient elution at a flow rate of 0.7 mL/min. Mobile phase B was held at 5% for 0.2 min, and increased linearly to 99% for 1.1 min. After mobile phase B was held at 99% for another 0.7 min, it was brought back to 5% for mobile phase B followed by re-equilibration for 0.6 min. The total cycle time for one injection was 2.6 min. Compounds were detected using a multiple reaction monitoring mode. Analyst software TM (version 1.6.2, AB Sciex) was used for data acquisition and processing.

Histopathological analysis

After euthanasia, the colon was collected from just below the cecum to the rectal site from each mouse and the lumen was washed with PBS. The distal part of the colon was placed in 4 vol% neutral buffered formalin for 24 hours, which was replaced with PBS. All tissues were embedded in paraffin, sectioned in a cross-sectional manner and stained with hematoxylin and eosin (H&E) stain. Histopathological evaluation was performed independently by two pathologists using scoring criteria (Table 2). The score of colitis from the distal section was calculated by combining the scores of all two findings (maximum score: 8) for each animal.

***In vivo* intestinal permeability assay**

All mice were gavaged with FITC-dextran (40 mg/100g body weight, MW 4,000; Sigma-Aldrich, St Louis, MO, USA) 4 h before sacrifice. Whole blood was collected by cardiac puncture and plasma was fractionated from the collected blood samples via centrifugation at 5,000×g for 10 min at 4°C. Fluorescence intensity in plasma was analyzed using a plate reader (excitation, 485 nm; emission, 535 nm). The concentration of FITC-dextran was determined from FITC-dextran standard curve generated by serial dilution. Permeability was calculated by linear regression of sample fluorescence.

Statistical analysis of *in vivo* data

Values were expressed as the mean ± SEM. To evaluate the data, either Student's *t*-test or the Wilcoxon test was performed for comparisons between two groups. P value < 0.05 was considered

as the level of significance. For comparisons of mean values among the three groups, one-tailed Williams test or Shirley-Williams test was used, and *P* value < 0.025 was considered significant. All data were analyzed using The SAS System for Windows (Release 9.3, SAS Institute Inc., Cary, NC, USA).

RNA sequencing of mouse colon and differential gene expression analysis

The distal part of the colon was stored in RNAlater (Qiagen) at 4°C. Total RNA was prepared using Isogen II (Nippongene, Japan) and further purified by the aid of RNeasy Mini Kit column (Qiagen) and DNaseI (Qiagen) to avoid genomic DNA contamination, according to the manufacturer's instructions. PolyA-RNA was isolated from 2 μg of total RNA using the Dynabeads mRNA Direct Purification Kit (Thermo Fisher Scientific). The polyA-RNA was then processed for library preparation following standard procedures for Ion Proton™ sequencing using the Ion Total RNA-Seq Kit v2 (#4476286, Thermo Fisher Scientific). Libraries were sequenced as barcoded-pooled samples on Ion PI™ chips using an Ion Proton™ sequencing system. Normalization and DEG analysis were performed applying the same methods as amplicon sequencing.

Data availability

Raw sequence data of my study are deposited in the Gene Expression Omnibus database (http://www.ncbi.nlm.nih.gov/geo/). The Ampli-seq data of LoVo cell line have been deposited under accession number GSE108050, and the RNA-seq data of murine colitis model have been deposited under accession number GSE108052.

Results

Mucosal abnormal gene expression remains even after achieving clinical remission with infliximab treatment

To compare the mucosal transcriptional profiles between IBD patients and healthy controls, I analyzed publicly available Leuven cohort (GSE16879) in which data were obtained from control and CD patients at the time of pre- and post-infliximab treatment [72]. A clear differentiation among the samples, depending on their disease activity, was observed when applying PCA using the given Log2 microarray expression data (Fig. 9A). In case of CD patients, 9,872 gene expressions were found to be statistically different from those in healthy controls (Table 3). Importantly, transcriptome data of post-therapy samples from responders was clustered together and significantly away from the healthy controls (Fig. 9A). These results suggest that the CD intestinal mucosa in responder is molecularly different from that of healthy controls in terms of gene expression.

Indeed, I identified a set of 3,545 genes whose expression in CD patients with remission is significantly different from healthy controls (Table 3). I designated this residual genomic expression that did not return to healthy controls as anti-TNFα therapy-untreatable genes (TUGs). On the other hand, I also identified a set of 2,061 genes whose expression was differently expressed from healthy controls before treatment and normalized to healthy controls in post-treatment (Table 3). I designated these recovered genes as anti-TNFα therapy-treatable genes (TTGs). To examine which tissue type is potentially responsible for TUGs and TTGs gene expression of CD patients, I compared the expression levels of TUGs and TTGs using the RNA sequence-based Nextbio body atlas application. The application allows the aggregated analysis of gene expression across >50 normal tissues of the human body system [81]. I found that TUGs were highly expressed in the lower gastrointestinal tract while TTGs were highly expressed in immune systems such as spleen and whole blood cells (Fig. 9B).

Next, I performed pathway enrichment analysis of TUGs and TTGs on NextBio using the Gene Ontology database. The results showed that TUGs were enriched in genes associated with cell cycle pathways while TTGs were enriched in inflammation and immune pathways (Fig. 9C). These results suggested that abnormal growth state in intestinal epithelial cells (IECs) persisted after achieving remission in CD colonic mucosa, whereas inflammation and immune reactions were largely resolved by infliximab therapy. To investigate whether TUGs of CD

patients represent dysregulated proliferation/differentiation properties in IECs, I analyzed the association between each crypt cell gene expression signature and TUGs [76]. Of interest, TUGs showed significant positive correlation with intestinal stem cells ($EphB2^{high}$) vs. differentiating cells ($EphB2^{low}$) immature signature, thereby, demonstrating imbalance of self-renewal and differentiation of IECs that persists after clinical remission by anti-TNFα therapy (Fig. 10E). These results indicate that structural and functional abnormalities may be due to unregulated self-renewal and differentiation of IECs in CD patients in remission state.

***In silico* screening identifies MAPK pathway inhibitors as potential drugs targeting CD**

Given that TUGs remained unresolved in remission state, I hypothesized that normalization of residual TUGs to healthy control could be effective in preventing recurrence of CD through correction of imbalance of IECs proliferation and differentiation. To find novel therapeutic concept/target, I performed *in silico* screening strategy to modulate TUG signature. I used the CMap system, a systematic computational approach for drug repositioning, which is based on the integration of public gene expression signatures of drugs and diseases [82]. For *in silico* screening, I modified CMap database [70] by integrating with the drug signatures obtained from internal transcriptome data with the aim of investigating drug repositioning opportunities of internal compounds for CD treatment. For this computational prediction, I extracted TUGs and TTGs for CD by applying FDR that adjusts the *P* value to account for multiple hypothesis testing. It is to obtain more robust signature and to safeguard the findings of DEGs against too many false positives creeping in. As I could identify optimal number of TUGs for CD by filtering with the criteria, I inputted extracted signatures of CD patients and statistically compared to each of the reference drug expression signature from the system. As a result, I observed that MAPK pathway inhibitors (EGFR, Raf and MEK inhibitors) were enriched and had strong negative scores with both TUGs and TTGs (Table 4). Indeed, the expression of MEK signature genes (e.g. DUSP4/6, PHLDA1, SPRY2, ETV5, etc.), which has been reported previously [83], were up-regulated even in responders to infliximab treatment in CD (Fig. 10B, left). This indicates that MAPK pathway, especially MEK, is strongly activated in CD patients even in remission state. To further investigate whether MAPK pathway is involved in the regulation of TUGs, I used Compound A [78] (Fig. 10A), a highly selective allosteric site binder of MEK1/2, among inhibitors of Raf-MEK-ERK pathway for experimental validation.

MEK1/2 inhibitor normalizes reference CD signature *in vitro*

To examine whether Compound A modulates TUGs and TTGs expression *in vitro*, I used Compound A-treated LoVo, a human colorectal cancer cell line, to compare the transcriptomes with DMSO control. I first looked at the expression of MEK signature genes and confirmed that most of these genes were down-regulated in response to Compound A treatment (Fig. 10B, right). Importantly, TUGs showed a significant negative correlation with DEGs between Compound A-treated and DMSO-treated cells in a dose-dependent manner (Figs. 10C and D). This reversible effect against TUGs was almost equivalent to the value for pharmacodynamic inhibitory effect against ERK1/2 phosphorylation in LoVo cells (Fig. 10D). On the other hand, negative correlation rate between TTGs and the DEGs was lower than that of TUGs (Fig. 10D). Moreover, a significant negative correlation was observed between human $EphB2^{high}$ vs. $EphB2^{low}$ immature crypt signature and the DEGs in a dose-dependent manner while TUGs was significantly positively correlated (Fig. 10E). My important finding from this transcriptome analysis is that MEK inhibitor significantly induced an opposite effect on the TUG signature, and the result also provided an important insight into the effect of MEK inhibitor on pathophysiological function on IECs.

MEK1/2 inhibitor promotes *in vitro* Caco-2 cell differentiation and barrier function

Next, I investigated whether TUG modulation by Compound A has a significant effect on pathophysiological function of intestinal permeability resembling enterocytes. Caco-2, a human colorectal cancer cell line, was reported to acquire “matureness” such as tight junction assembly and cell-cell adhesion initiated polarization during 21 days in culture, and the regulation of transcription underlying Caco-2 cell polarization is similar to that of *in vivo* enterocyte differentiation [84]. First, I evaluated the effect of Compound A on transepithelial electrical resistance (TEER) assay, which is commonly used to assess the barrier function of IECs. As shown in Fig. 11A, Compound A exhibits a significant increase in TEER over a Caco-2 monolayer in a dose-dependent manner. Next, I examined the expression of apolipoprotein A-1 (*APOA1*) and leucine-rich repeat-containing G-protein-coupled receptor 5 (*LGR5),* which are enterocyte and stem cell markers, respectively. Consistent with the results in TEER measurement, Compound A treatment increased the expression of *APOA1* and decreased the expression of *LGR5* (Figs. 11B

and C). These results indicate that inhibition of MEK enhances IECs differentiation and maturation as well as epithelial barrier function.

MEK1/2 inhibitor shows significant therapeutic effect on histology and diarrhea in activated T cell transfer colitis model

To determine whether my *in silico* target prediction model would be translated into therapeutic efficacy *in vivo*, I performed efficacy study using Compound A by means of an activated T cell transfer colitis model [85]. The adoptive transfer of activated $CD4^+$ T cell to SCID mice promoted diarrhea within 2 - 3 weeks, and histological changes correlated well with the disease parameters of colitis such as colon weight gain, stool consistency score and the increase in the colonic inflammatory cytokines. Although highly selective and potent oral MEK inhibitors have been developed and assessed in numerous clinical studies for cancer treatment, a number of mechanism-based toxicities have emerged [86]. In particular, acneiform dermatitis, a serious skin rash, is a frequent side effect of MEK inhibitors including Compound A. Thus, to minimize systemic exposure leading to systemic toxicities, I developed colon specific drug delivery system for Compound A by conducting several formulation approaches. This also aims to enhance local therapeutic efficacy [87]. Importantly, Compound A has superior characteristics for design colon targeted formulation such as higher solubility and lower permeability which can limit systemic absorption to prevent drug distribution into normal tissues despite its long-term retention in the colon, compared to other MEK inhibitors (e.g. trametinib, selumetinib and binimetinib). Based on a preliminary pharmacokinetic study using C57BL/6J normal mice, the area under the plasma concentration time curve (AUC) of Compound A MPs decreased 97.32% as compared to the suspensions, whereas the concentrations in colon of both groups were almost the same level. This demonstrated that the amount of Compound A absorbed into plasma was obviously decreased when encapsulated in the enteric MPs, thus reducing the side effects caused by systemic absorption. Moreover, *in vivo* colonic pharmacodynamics study using enteric Compound A MPs in LPS-treated mice demonstrated that the level of colon $AUC_{0\text{-}24h}$ (1206.6 ng·h/g) showed target engagement defined as pERK inhibition at the dose level where plasma $AUC_{0\text{-}24h}$ (7.2 ng·h/ml) was within safe range. Likewise, in colitis mice, Compound A MPs showed safe systemic exposure at the dose levels where therapeutic effect was observed in spite of repeated dosing. Further, since the colon AUC level was also almost the same as LPS-treated normal mice that was

enough to inhibit MEK enzymatic function, I concluded that enteric Compound A MPs were efficiently delivered to colon.

When enteric Compound A MPs were orally administrated therapeutically at the dose of 0.3 and 1 mg/kg, q.d., diarrhea score and the increase in colon weight were significantly inhibited compared to vehicle treatment (Figs. 12A and B). On the other hand, only a partial inhibition of diarrhea score and colon weight gain was observed in the mice treated with anti-TNFα mAb at the dose of 0.1 mg/mouse compared to isotype control treatment (Figs. 12A and B). Importantly, enteric Compound A MPs substantially ameliorated extensive injury of the colon mucosal layer, which was observed in the vehicle mice with histopathological analysis (Fig. 12C). Quantitative evaluation demonstrated that histology score of colitis was significantly reduced with mucosal regeneration (Fig. 12D and Table 5). Also, immune cell infiltration was reduced in mice treated with Compound A at the dose of 1 mg/kg compared to vehicle control group significantly (Table 5). On the other hand, histology score of colitis was not significantly reduced in the mice treated with anti-TNFα mAb compared to isotype control treatment. I also performed *in vivo* permeability assay using a fluorescein isothiocyanate (FITC)-labeled dextran method. This experiment revealed that activated T cell transfer colitis model mice receiving oral treatment with Compound A had tended to decrease intestinal permeability compared with untreated colitis mice (0.3 mg/kg and 1 mg/kg vs. vehicle control; 72.2% and 75.0%, *P* value = 0.055, 0.049 by one-tailed Shirley-Williams test, respectively), whereas treatment of anti-TNFα mAb had no effect on it (vs. isotype control; 133.0%, not significant). Together, these data provided an *in vivo* evidence that enteric Compound A MPs exhibit therapeutic efficacy and improve the histological changes in the colitis model.

MEK1/2 inhibitor-treated colitis mice down-regulates gene expression that associates with both dysregulated growth in IECs and pro-inflammatory response in immune cells

To compare transcriptome differences between Compound A-treated and anti-TNFα mAb-treated colitis mice, I examined the global gene expression profile by RNA-sequencing. The Venn diagram summarizes the overlapping transcripts detected in each sample (Fig. 13A). As a result, 5,157 genes were identified as DEGs of Compound A, which was subsequently compared with colitis signature (vehicle vs. normal mice). Of interest, 46.1% of Compound A regulated genes were negatively correlated with colitis signature, whereas only 11.1% of anti-TNFα mAb

DEGs (1,668 genes) were negatively correlated with it, which reflects the superior efficacy of Compound A to anti-TNFα mAb (Fig. 13C). I hypothesized that the dynamic molecular and signaling changes might occur specifically in activated T cell transfer colitis model treated with Compound A. To obtain new insights, I conducted a tissue-type enrichment analysis using mouse Body Atlas database of each Compound A specific, anti-TNFα mAb specific and common DEGs between Compound A and anti-TNFα mAb. I found nearly four-fifth of Compound A DEGs, which were different from anti-TNFα mAb DEGs that were significantly enriched in the lower gastrointestinal tract. In contrast, immune systems such as bone marrow, mesenteric lymph node and spleen were enriched in common DEGs (Fig. 13D). Pathway enrichment analysis was also performed for each DEGs. The results demonstrated that genes associated with cell-cycle and DNA replication were significantly down-regulated in Compound A specifically treatable genes (Fig. 13E). On the other hand, common DEGs between Compound A and anti-TNFα mAb showed significantly positive correlation (Fig. 13B). The pathway analysis of common signature revealed that inflammation and immune pathways were significantly down-regulated (Fig. 13E). These results indicate that Compound A can attenuate abnormal growth state in colonic mucosa by targeting IECs as well as exhibit anti-inflammatory effect by targeting immune cells. Moreover, compared to mouse crypt gene expression, colitis signature was significantly positively correlated with mouse immature signature, which was extracted from publicly available mouse $EphB2^{high}$ vs. $EphB2^{low}$ transcriptome data [77] (Fig. 13F). Interestingly, the immature signature was significantly negatively correlated with DEGs of Compound A (ES: -163) while negative correlation with anti-TNFα mAb DEGs was not so significant (ES: -5.4). These results suggest that Compound A could restitute of dysregulated IECs more effectively than anti-TNFα mAb. These findings corroborated the expected mechanism of efficacy of Compound A in the colitis model, which was computationally predicted by using CD patients derived gene signature.

Discussion

In the current study, I present evidence that may help to resolve the relapse of CD and obtain sustainable remission. CD has periods of relapse and remission, but there is no long-term cure. Surgeries are still required in some patients. For CD patients in remission, relapse rates at one, two, five, and ten years are estimated to be 20%, 40%, 67%, and 76%, respectively [88]. As for infliximab, Chauvin et al. reported a recurrence rate of 68% among CD patients with its treatment in a 12-years retrospective study [89]. These evidences suggest that there are unmet medical needs in the management of CD. For assessing the possible mechanism of relapse, an unresolved issue is whether colonic lesions of CD patients in remission state continue to express abnormal transcripts or not as compared to healthy controls. I present a method to dissect the physiological response with anti-TNFα therapy by exploiting several bioinformatics analysis with CD patients-relevant mucosal gene signature. I have defined a unique gene signature "TUGs," which did not return to "healthy" state even after achieving clinical remission. Importantly, TUGs are positively correlated with immature signature of IECs, suggesting that the residual transcripts are involved in expansion of undifferentiated cells as well as decrease or loss of mature functional IECs in infliximab responders. Recently, it has been proposed that dysregulation within differentiation system for correct IEC formation perpetuates impaired epithelial homeostasis and has a crucial role in IBD pathogenesis by increasing intestinal permeability [90-93]. Furthermore, in case of CD patients, an increase in intestinal permeability has been reported to precede episodes of disease relapse and the onset of symptoms by up to one year [94, 95]. However, it is not yet clear what molecular events are responsible for dysregulated homeostasis of IECs that predispose to relapse in patients with quiescent CD. Considering that perturbations of IECs homeostasis can lead to intestinal disorders [96], I hypothesized that TUGs might lead to increased intestinal permeability and distorted intestinal mucosal barrier function, ultimately causing recurrence. Similar strategies to extract unresolved gene signature have been previously tried in patients with psoriasis [97] and UC [98], but gene signature associated with CD remission was not studied.

In this study, I inferred that the MEK1/2 inhibitor would be a potential new therapeutic agent for CD based on the results of *in silico* computational approach using TUGs. Previous reports have demonstrated that ERK1/2 activation may have importance for diarrhea in CD patients [99]. It has also been reported that constitutive activation of the MEK/ERK cascade inhibits enterocyte differentiation, in part through inhibition of transcriptional activity of CDX2,

a master transcription factor regulating the differentiation, cell-cell adhesion, and polarity of IECs [100-102]. Conditional homozygotes *Cdx2* knockout mice have been previously shown to exhibit loss of intestinal morphology and cause a serious disruption in the mucosal architecture [103]. Interestingly, I observed that transcripts linked to intestinal differentiation including several CDX2 target genes [100] were up-regulated following MEK1/2 inhibition *in vitro*. This finding is consistent with the role of CDX2 as a master regulator of intestinal morphogenesis and suggests that genes controlling epithelial differentiation is suppressed by constitutive activation of the MEK/ERK pathway. Although I cannot conclude what the physiological consequences of reversing TUGs to normal state are, it could be speculated that MEK1/2 inhibitor partly enhances CDX2 transcriptional activity, which in turn enhances epithelial differentiation and finally leads to restitution of dysregulated IECs.

Indeed, MEK1/2 inhibitor exhibited a significant increase of the TEER using Caco-2 cell line which is a widely used intestinal cellular model that retains very similar morphologic properties to enterocytes. However, use of transformed cell lines have some limitations [104]. A major limitation is that intestinal cells growing in 2D monoculture lack the physiological extracellular matrix microenvironment that is necessary to maintain *in situ* phenotypes. To overcome this limitation, the utility of *in vitro* 3D organoids that effectively mimic IECs structure and functional features has been well confirmed for testing epithelial differentiation with the capacity to model heterogeneous cell fates [105]. Therefore, further studies will be necessary to clarify the effect of MEK1/2 inhibitor on intestinal differentiation using organoid model for drug validation. Nevertheless, although animal models also incompletely recapitulate the complex pathophysiology of intestinal diseases of humans, histology score was significantly reduced in response to MEK inhibitor treatment in the *in vivo* colitis model in this study. These results provide important insight into beneficial effect of MEK1/2 inhibitor on promoting intestinal barrier function.

In addition, interestingly, *in silico* computational screening revealed that several MEK1/2 inhibitors scored high in not only TUG but also TTG signatures. From this result, MEK1/2 inhibitor would have a potential therapeutic effect to reverse both TNFα-untreatable and treatable gene expression. MEK1/2 inhibitor would be a great promise in new therapeutic approaches that integrate both immune and non-immune pathophysiological components and potentially induce greater and sustainable remission as a single agent. Indeed, transcriptome

analysis showed that Compound A reverses a set of genes that are not only cell-cycle related genes, which are highly expressed in IECs, but also inflammation related genes, which were overlapped with DEGs of anti-TNFα mAb *in vivo* model. Moreover, a previous report has demonstrated that selective MEK1/2 inhibitor, trametinib, has potential inhibitory effect on LPS-mediated inflammation in macrophages [106]. These results suggest that MEK1/2 inhibitor can target not only histological abnormalities of IECs but also aberrant intestinal inflammation.

Here, I present a rational strategy for CD based on a systematic drug repositioning bioinformatics approach using publicly available patient derived gene signature to explore connections with existing drugs. One might assume that effective clinical treatments serve not only to reverse the clinical course of the disease but also to restore disease-affected molecular-level phenotypes to their normal level. Notably, several recent studies have made this assumption by directly searching for drug therapies whose molecular effects anti-correlate with disease molecular signatures using CMap-based computational approach [82, 107-110]. Although drugs were validated in preclinical models, it remains unknown whether the disease gene expression was reversed in disease models or not. It is important to note the limitations of this study. The gene signature, which was extracted from patients, can provide a "snapshot" in remission state. Therefore, the interpretation of the "snapshot" requires careful thought about the result without excessive speculation. Moreover, some genomic effects might be agent specific, thus further studies will be needed to compare clinical outcomes with different anti-inflammatory therapeutic agents.

Nevertheless, here I showed that MEK1/2 inhibitor could significantly reverse residual TUG signature to normal state in gene expression *in vitro* (Fig. 14). Also, colon targeted delivery of MEK1/2 inhibitor was associated with both the successful improvement of diarrhea and restoration of histological abnormalities *in vivo* (Fig. 14). These results suggest that additional clinical investigation using MEK1/2 inhibitor could be beneficial, especially contributing to accelerate restitution of dysregulated IECs and to prevent recurrence as a solution to unmet medical needs in CD therapy. In practice, however, there is no direct evidence showing how sustainable the clinical and endoscopic effectiveness of biological therapies for CD are. Hence, a close study focusing not only on effectiveness but also on large-scale long-term safety in a clinical setting is necessary for my purpose. In addition, colon targeting approach could ensure direct treatment at the inflamed site with lower dosing, and hopefully lead to more optimal and less toxic

promising therapeutic strategies in the future. Finally, my study provides a sound rationale for predicting a drug's potential therapeutic effect, which is based on its ability to induce molecular remission. It would exert the most favorable clinical outcomes rather than modulating only a certain subset of disease phenotypes.

Table and Figures

TABLE 2. Histopathological scoring system

	Score	Grade	Criteria
Mucosal regeneration/ hyperplasia	0	None	Not remarkable
	1	Minimal	Regeneration/hyperplasia of mucosa without goblet cells are observed in focal area.
	2	Mild	Regeneration/hyperplasia of mucosa are observed diffusely with 2-fold mucosal thickness. Goblet cells are observed diffusely and occasionally crypt abscesses and cell debris in lumen are observed.
	3	Moderate	Regeneration/hyperplasia of mucosa are observed diffusely with 2- to 3-fold mucosal thickness. Goblet cells are observed focally and often crypt abscesses and cell debris in lumen are observed.
	4	Marked	Regeneration/hyperplasia of mucosa are observed diffusely with 4- to 5-fold mucosal thickness. Goblet cells are scant and crypt abscesses and cell debris in lumen are observed diffusely.
Mononuclear cell infiltration	0	None	Not remarkable
	1	Minimal	Focal or multifocal infiltration of mononuclear cells (mainly lymphocytes) in mucosa and/or submucosa
	2	Mild	Diffuse infiltration of mononuclear cells (mainly lymphocytes) in mucosa and/or submucosa with focally extended area of lamina propria.
	3	Moderate	Diffuse infiltration of mononuclear cells (mainly lymphocytes and some neutrophils) in mucosa and/or submucosa with focally and/or diffusely extended area of lamina propria.
	4	Marked	Diffuse infiltration of mononuclear cells (mainly lymphocytes and some neutrophils) in mucosa and/or submucosa with more diffusely extended area of lamina propria.

TABLE 3. Gene number of treatment response in CD patients

Comparisons	Significant genes	TUGs	TTGs
Before treatment vs. Healthy control	9,872	Significant	Significant
After treatment vs. Healthy control	5,514	Significant	Not significant
After treatment vs. Before treatment	3,602	Not significant	Significant
Gene number		3,545	2,061

TUGs, anti-TNFα therapy-untreatable genes; TTGs, anti-TNFα therapy-treatable genes

Significant = *P* value < 0.05 and Absolute Fold Change > 1.2, Not significant = *P* value > 0.05

TABLE 4. Results of Gene Expression Correlation Analysis of TUGs and TTGs

Top 20 compounds with negative enrichment score across TUGs

Rank	Data source	Compound	Classification	Enrichment Score	Cell source
1	Internal	Example C25 [111]	Raf/VEGFR inhibitor	-0.62	COLO205
2	Internal	Example 114 [112]	EGFR inhibitor	-0.56	BT-474
3	Internal	Compound 2cb [113]	HER2/EGFR inhibitor	-0.55	BT-474
4	Internal	Compound 5 [114]	Raf/VEGFR inhibitor	-0.54	A375
5	Internal	PD0325901 [115]	MEK inhibitor	-0.51	COLO205
6	CMap	Urapidil	α1-adrenoceptor antagonist	-0.5	PC3
7	Internal	Gemcitabine [116]	Ribonucleotide reductase inhibitor	-0.47	Su.86.86
8	Internal	Example 27 [117]	MEK inhibitor	-0.47	A375
9	Internal	PD0325901	MEK inhibitor	-0.47	A375
10	Internal	Example 74 [112]	EGFR inhibitor	-0.47	TGBC2TKB
11	Internal	Compound 33 [78]	MEK inhibitor	-0.46	A375
12	Internal	Compound 27 [78]	MEK inhibitor	-0.46	A375
13	Internal	TAK-285 [118]	HER2/EGFR inhibitor	-0.45	BT-474
14	CMap	Metergoline	5-HT antagonist	-0.44	PC3
15	CMap	Flunixin	NSAID	-0.43	PC3
16	CMap	Alprenolol	Adrenergic beta-Antagonists	-0.43	MCF7
17	CMap	Tiabendazole	Anthelmintic	-0.43	MCF7
18	Internal	TAK-733 [119]	MEK inhibitor	-0.43	A375
19	CMap	Benzamil	ENaC channel blocker	-0.42	PC3
20	CMap	Dicloxacillin	Anti-bacterial agent	-0.42	MCF7

Top 20 compounds with negative enrichment score across TTGs

Rank	Data source	Compound	Classification	Enrichment Score	Cell source
1	Internal	PD0325901	MEK inhibitor	-0.55	COLO205
2	Internal	TAK-733	MEK inhibitor	-0.4	A375
3	Internal	Bicalutamide [120]	Androgen antagonist	-0.38	LNCaP

4	CMap	Carbenoxolone	11β-hydroxysteroid dehydrogenase inhibitor	-0.34	PC3
5	CMap	Sitosterol	Inhibit cholesterol's absorption	-0.33	MCF7
6	CMap	Betahistine	H1 receptor agonist	-0.33	PC3
7	CMap	Iohexol	Contrast agents	-0.33	MCF7
8	CMap	Cinchonine	Antimalarial drug	-0.32	PC3
9	CMap	Dicloxacillin	Penicillin-like antibiotic	-0.32	MCF7
10	CMap	Methylergometrine	Oxytocics	-0.31	PC3
11	CMap	Co-dergocrine mesilate	Antimigraine	-0.31	PC3
12	CMap	Prestwick-1083	-	-0.31	PC3
13	CMap	Nadolol	Adrenergic beta antagonist	-0.3	MCF7
14	CMap	Sulmazole	A1 adenosine receptor antagonist	-0.3	PC3
15	CMap	Triamterene	Sodium channel blocker	-0.29	MCF7
16	CMap	Ajmaline	Sodium channel blocker	-0.29	MCF7
17	CMap	Furosemide	Sodium potassium chloride symporter inhibitor	-0.29	PC3
18	CMap	Midodrine	Adrenergic alpha agonist	-0.29	PC3
19	CMap	4-hydroxyphenazone	-	-0.29	MCF7
20	CMap	Amiprilose	Anti-inflammatory agent	-0.29	MCF7

Note: TUGs, anti-TNFα therapy-untreatable genes; TTGs, anti-TNFα therapy-treatable genes

TABLE 5. Histopathological findings of the colon

Treatment	Normal																				
Test article	-																				
Dose (mg/kg/day)	-																				
Animal No.	1-1	1-2	1-3	1-4																	
Mucosal regeneration/hyperplasia	0	0	0	0																	
Mononuclear cell infiltration	0	0	0	0																	
Histology score of colitis	0	0	0	0																	
mean ± SE	0.0	±	0.0																		
Treatment	Con A-activated CD4+ T-cell transfer																				
Test article	Vehicle (0.5% MC)							Enteric Compound A MPs							Enteric Compound A MPs						
Dose (mg/kg/day)	0 QD							0.3 QD							1 QD						
Animal No.	2-1	2-2	2-3	2-4	2-5	2-6	2-7	3-1	3-2	3-3	3-4	3-5	3-6	3-7	4-1	4-2	4-3	4-4	4-5	4-6	4-7
Mucosal regeneration/hyperplasia	4	3	3	4	1	1	3	1	0	1	3	3	3	0	0	2	0	1	0	4	0
Mononuclear cell infiltration	4	3	2	3	2	1	2	1	0	1	3	3	3	1	1	2	1	1	0	3	0
Histology score of colitis	8	6	5	7	3	2	5	2	0	2	6	6	6	1	1	4	1	2	0	7	0
mean ± SE	5.1	±	0.8					3.3	±	1.0					2.1	±	1.0				
Treatment	Con A-activated CD4+ T-cell transfer																				
Test article	Isotype mAb							anti-TNFα mAb													
Dose (mg/kg/day)	5 Q4D							5 Q4D													
Animal No.	5-1	5-2	5-3	5-4	5-5	5-6	5-7	6-1	6-2	6-3	6-4	6-5	6-6	6-7							
Mucosal regeneration/hyperplasia	3	2	3	2	3	4	2	3	2	3	0	0	3	2							
Mononuclear cell infiltration	3	2	3	2	3	3	3	2	2	2	0	1	2	2							
Histology score of colitis	6	4	6	4	6	7	5	5	4	5	0	1	5	4							
mean ± SE	5.4	±	0.4					3.4	±	0.8											

0: Not remarkable, 1: Minimal, 2: Mild, 3: Moderate, 4: Marked

MC: methylcellulose solution

Histology score of colitis for each animal represents the sum of grades of all findings in the colon.

A

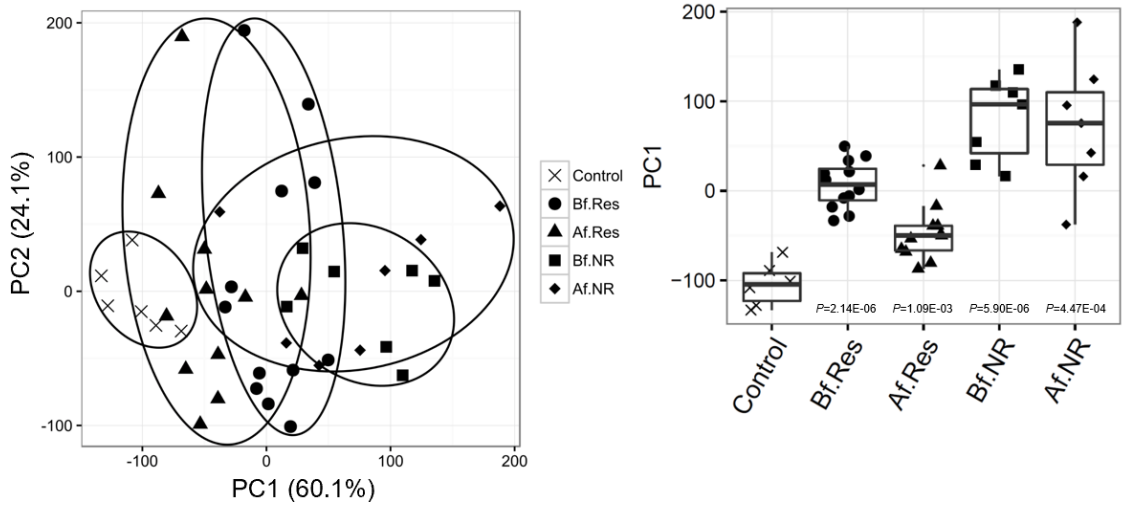
PC2 (24.1%)
PC1 (60.1%)
Control
Bf.Res
Af.Res
Bf.NR
Af.NR
PC1
P=2.14E-06
P=1.09E-03
P=5.90E-06
P=4.47E-04
Control
Bf.Res
Af.Res
Bf.NR
Af.NR

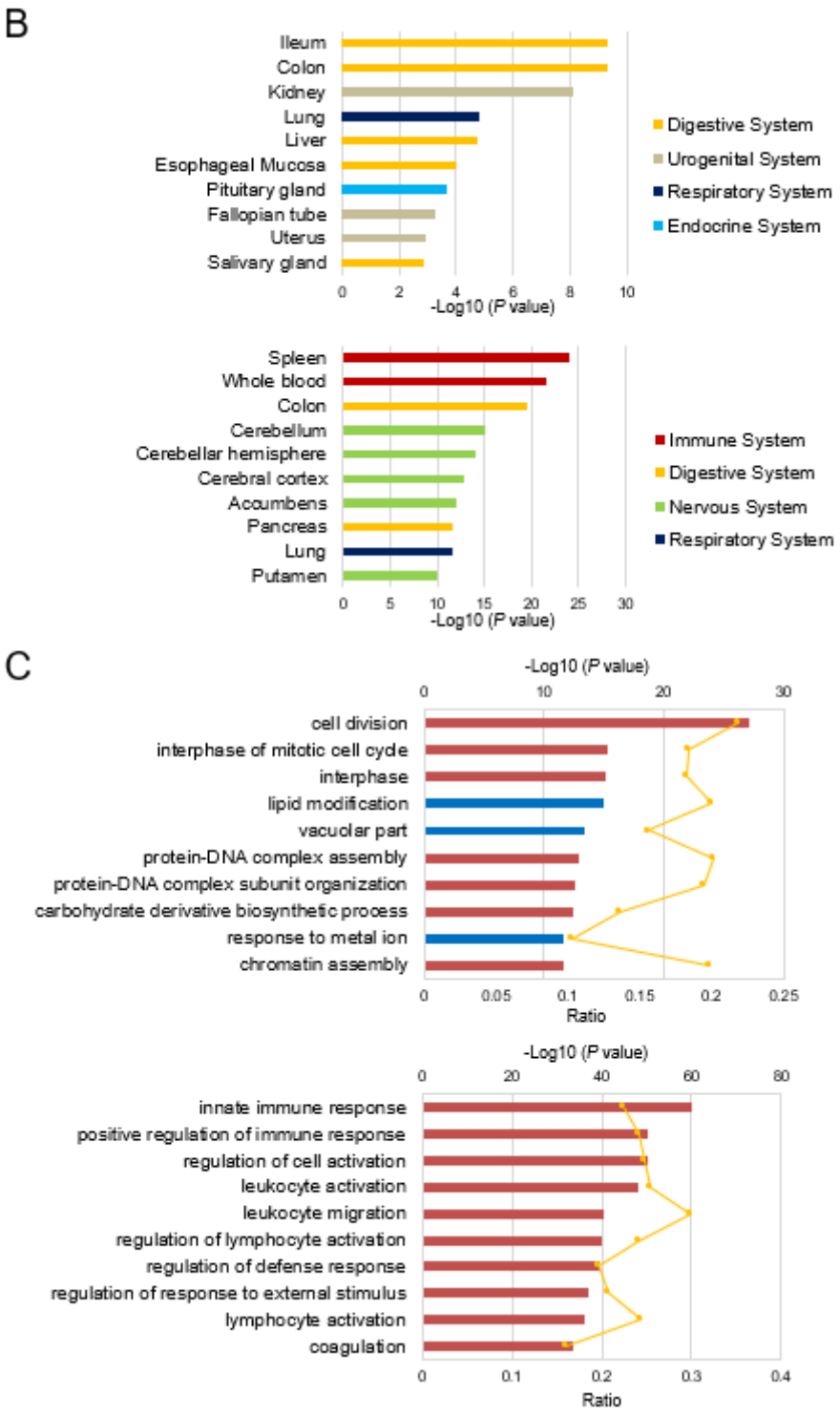

Figure 9. Residual genomic profile of CD patients

(A) PCA of colonic expression data from 19 patients with Crohn's colitis (12 responders and 7 non-responders) at the time of pre- and post-infliximab treatment and from 6 healthy controls [microarray expression data were obtained from the study by Arijs I et al. [72]]. Axis percentages

indicate variance contribution. Boxplots of PC1 distribution for each group and *P* values from control group are as indicated on the right. Abbreviations: Bf.Res, responder before treatment; Af.Res, responder after treatment; Bf.NR, non-responder before treatment; Af.NR, non-responder after treatment. (B) The top 10 enriched tissue-type in TUGs (upper) and TTGs (lower) using Nextbio body atlas application taken from the Genotype-Tissue Expression project (GTEx) are displayed. (C) The top 10 enriched GO terms in TUGs (upper) and TTGs (lower) using NextBio pathway enrichment application are displayed. Category names are presented on the Y axis. On the X axis, the significance score (negative Log of *P* value) for each pathway is indicated by the bars, and the line represents the ratio of genes in a given pathway that meets the cut-off criteria among total genes that make up that pathway. Red bars predict an overall increase in the activity of the pathway while blue bars indicate a prediction of an overall decrease in activity.

A

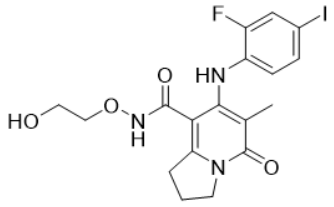

Compound A

B

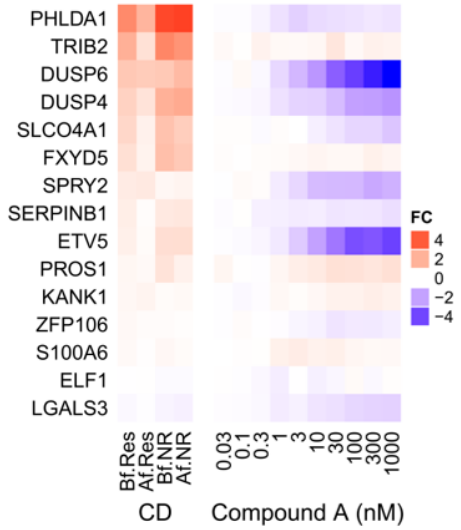

C

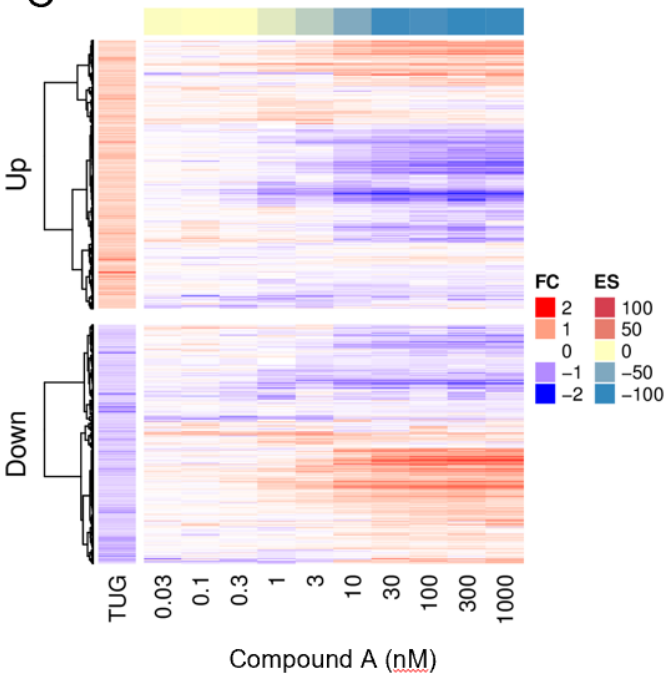

D

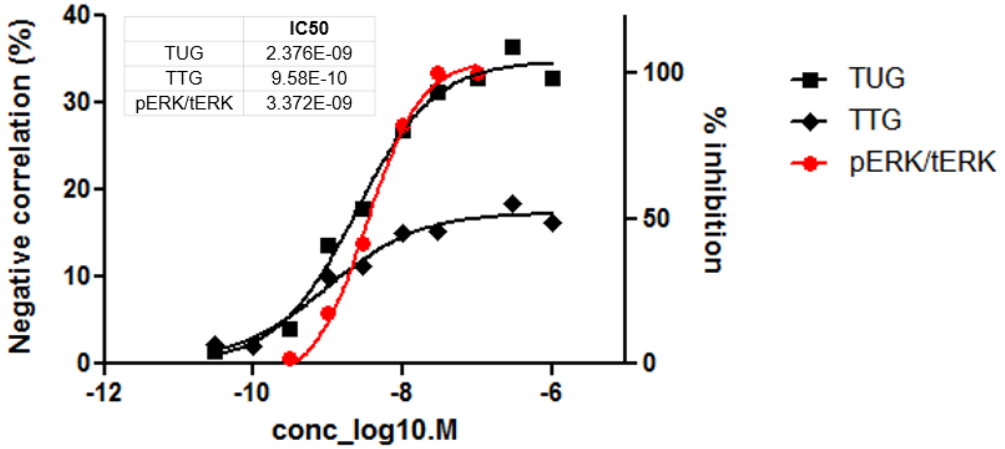

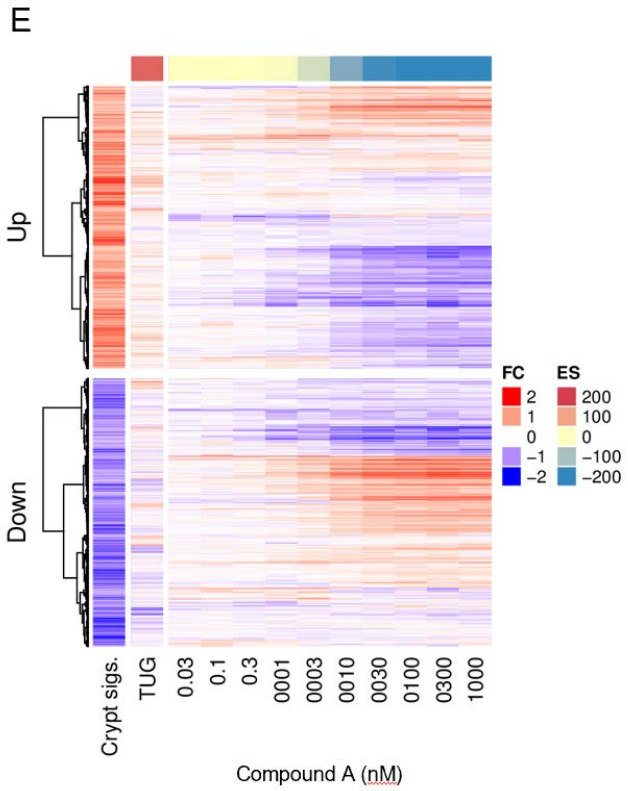

Figure 10. MEK1/2 inhibitor normalized reference CD signature in LoVo cells

(A) Chemical structure of Compound A. (B) Heatmap showing the genes from the MEK activation signature for both CD patients (left) and compared with fold change (FC) in gene expression levels in LoVo treated with Compound A across ten dose response conditions (0.03 - 1,000 nM, *n* = 3, right). (C) Heatmap of TUGs clustered into up-regulated and down-regulated genes comparing with fold change in gene expression levels in LoVo treated with Compound A across ten dose response conditions (0.03 - 1,000 nM, *n* = 3) obtained by Ampli-seq analysis. The color-coded scale for the normalized expression value is indicated at the right of the figure, which correlates with color intensity to the fold change (FC) of gene expression and enrichment score (ES). (D) IC_{50} values were calculated by plotting both negative correlation rate between Compound A DEGs of TUGs/TTGs and *in vitro* pERK inhibitory activity in LoVo cells using a nonlinear regression analysis by GraphPad Prism (GraphPad, La Jolla, CA, USA). (E) Heatmap illustrating hierarchical clustering of human immature crypt signature comparing with fold change in gene expression levels in LoVo treated with Compound A across ten dose response conditions (0.03-1,000 nM, *n* = 3). The color-coded scale for the normalized expression value is indicated at the right of the figure, which correlates with color intensity to the fold change (FC) of gene expression and enrichment score (ES).

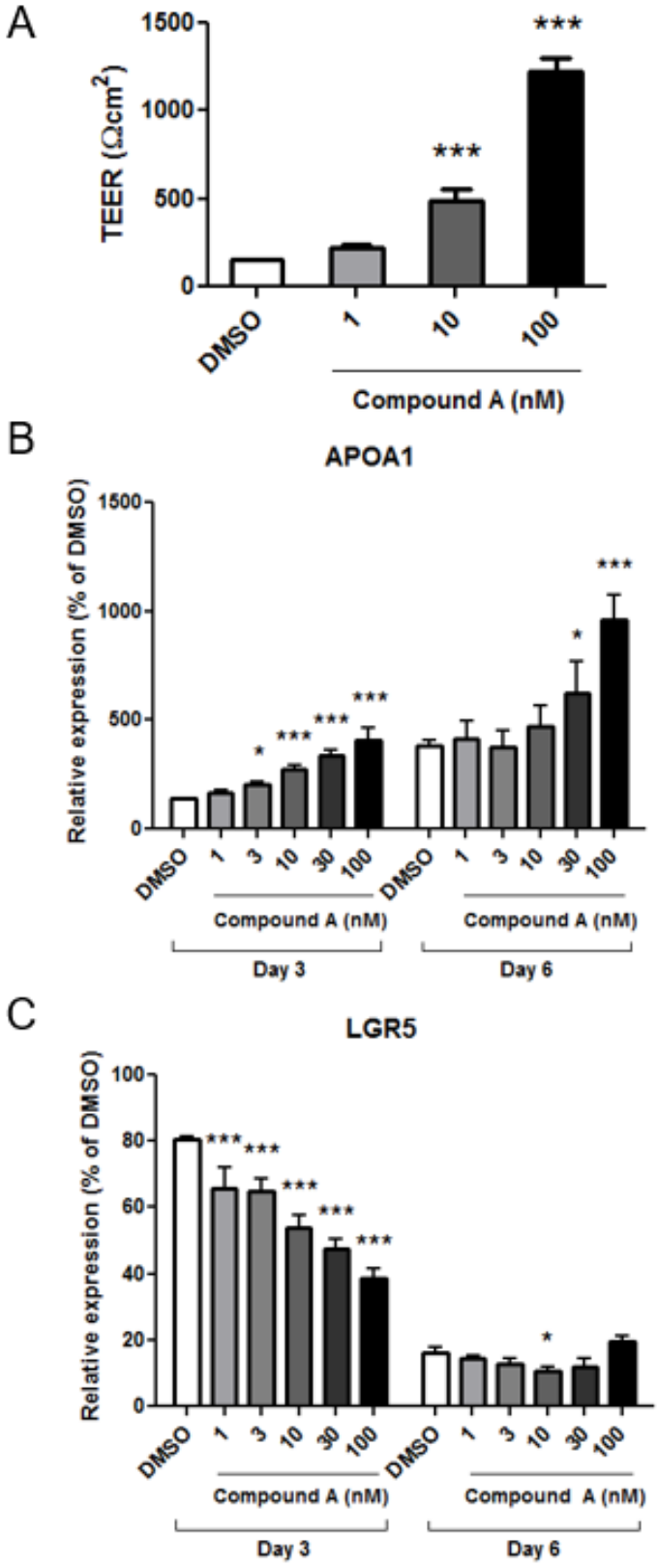
A
1500
1000
500
0
TEER (Ωcm²)
***
***
DMSO
1
10
100
Compound A (nM)
B
APOA1
Relative expression (% of DMSO)
1500
1000
500
0
*
***
***
***
*
***
DMSO
1
3
10
30
100
DMSO
1
3
10
30
100
Compound A (nM)
Compound A (nM)
Day 3
Day 6
C
LGR5
Relative expression (% of DMSO)
100
80
60
40
20
0
***
***
***
***
***
*
DMSO
1
3
10
30
100
DMSO
1
3
10
30
100
Compound A (nM)
Compound A (nM)
Day 3
Day 6

Figure 11. MEK1/2 inhibitor enhanced intestinal barrier formation by promoting differentiation of IECs

(A) TEER was measured to assay the integrity of the epithelium layer formed by differentiated Caco-2 cells. The values represent the means of $n = 4$ samples ± standard deviations (SD). Levels of statistical significance compared with DMSO control: P value < 0.0005 (***) by Williams test. Relative mRNA expression levels of *APOA1* (B) and *LGR5* (C) at day 3 and day 6 were measured by real-time RT-PCR, normalized with the expression of *GAPDH* at day 1. The values represent the means of $n = 3$ samples ± standard deviations (SD). Levels of statistical significance compared with DMSO control: P value < 0.025 (*): P value < 0.005 (**): P value < 0.0005 (***) by Williams test.

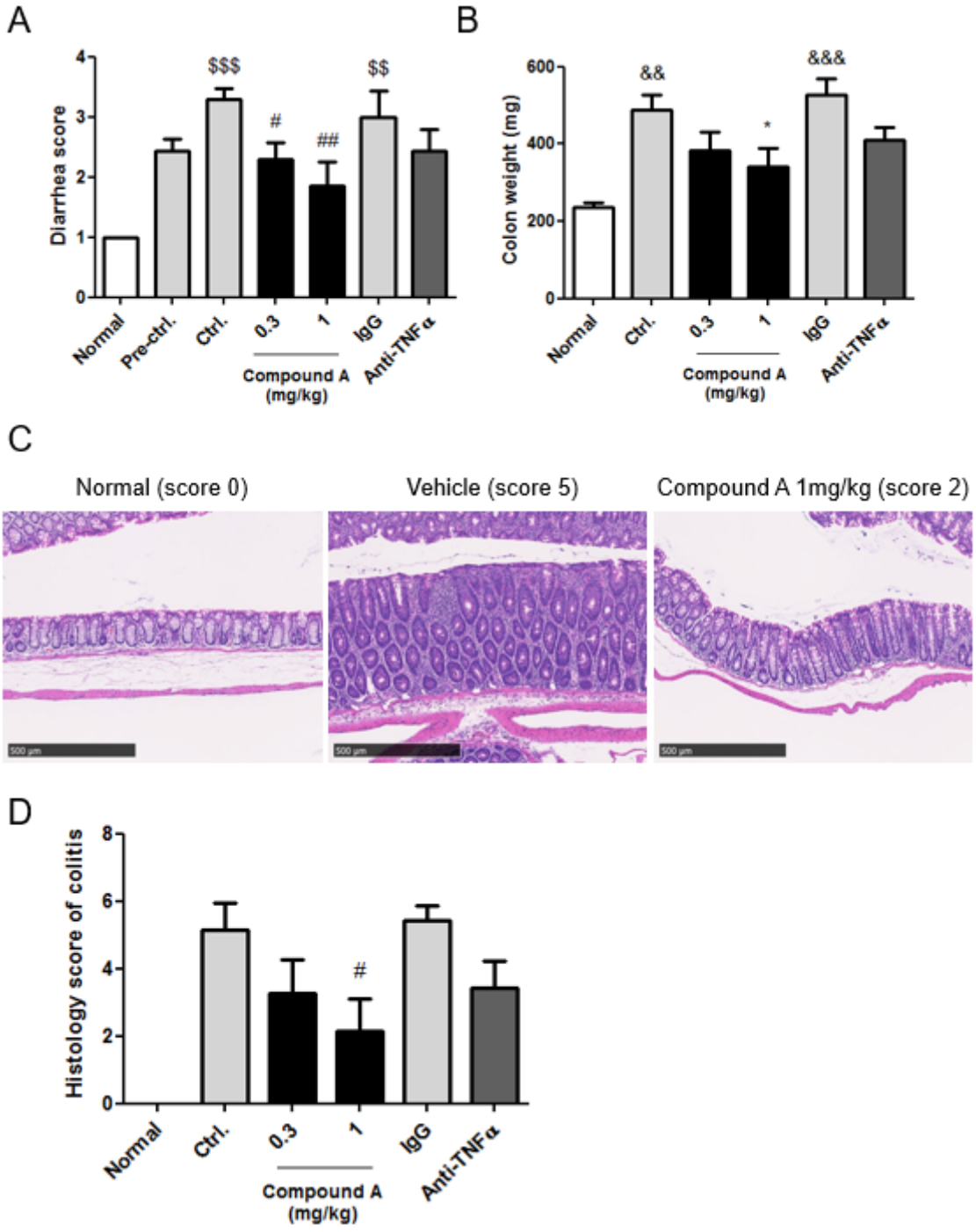

Figure 12. Therapeutic efficacy of enteric MPs of MEK1/2 inhibitor in activated T cell transfer colitis model

(A) Diarrhea score data and (B) colon weight data were analyzed in a blind fashion. (C) Representative H&E-stained colon sections of normal mice, vehicle and 1 mg/kg Compound A treated activated T cell transfer colitis mice (magnification, x200, scale bar = 500 μm). (D)

Quantitative evaluation of the histology score of colitis was analyzed. See Table 5 for the detailed data. Data are presented as the mean ± S.E. of 4 (normal) or 7 (transferred mice). $$; *P* value < 0.01, $$$; *P* value < 0.001 (Aspin-Welch test) and &&; *P* value < 0.01, &&&; *P* value < 0.001 (Student's *t*-test) vs. normal group. #; *P* value < 0.025, ##; *P* value < 0.005 (one-tailed Shirley-Williams test) and *; *P* value < 0.025 (one-tailed Williams test) vs. vehicle control group.

A

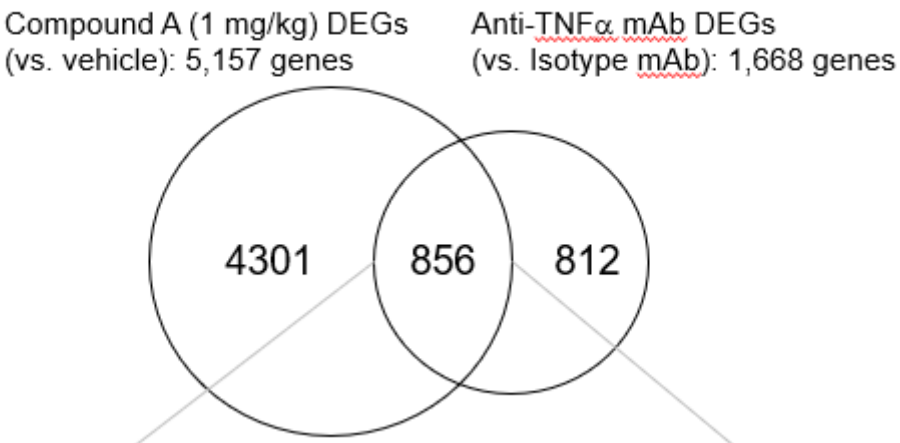
Compound A (1 mg/kg) DEGs
(vs. vehicle): 5,157 genes
Anti-TNFα mAb DEGs
(vs. Isotype mAb): 1,668 genes
4301
856
812
Overlap P value: 1.8E-212

B

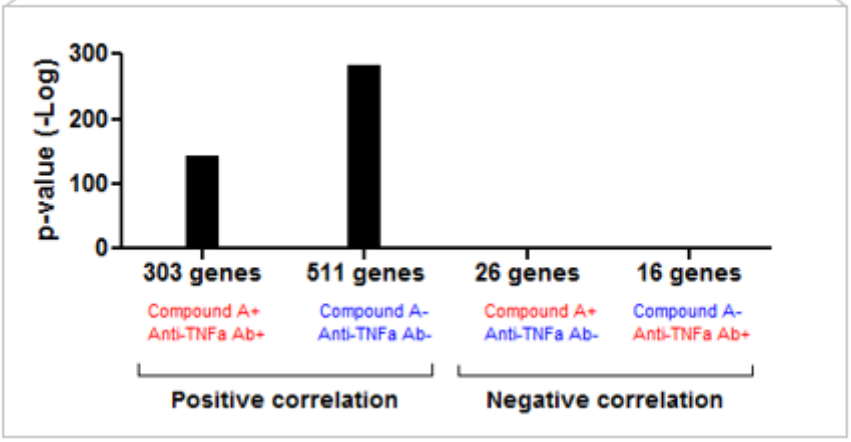
p-value (-Log)
300
200
100
0
303 genes
511 genes
26 genes
16 genes
Compound A+
Anti-TNFa Ab+
Compound A-
Anti-TNFa Ab-
Compound A+
Anti-TNFa Ab-
Compound A-
Anti-TNFa Ab+
Positive correlation
Negative correlation

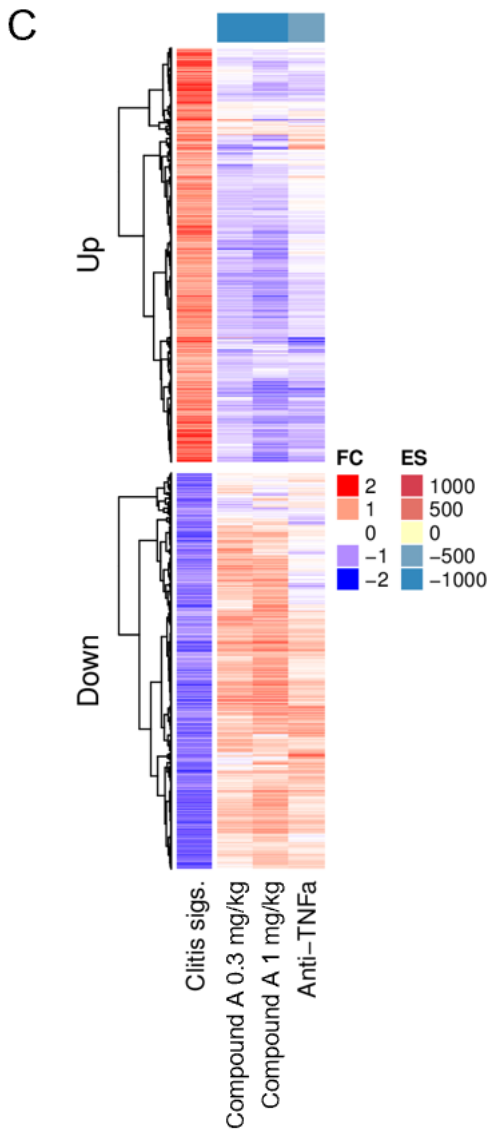

Gene subsets	Overlapped gene number	Coverage % of negative correlation
Compound A (0.3 mg/kg) DEGs vs colitis signature	2,925	30.9
Compound A (1 mg/kg) DEGs vs colitis signature	4,363	46.1
Anti-TNFα Ab DEGs vs colitis signature	1,106	11.1

D

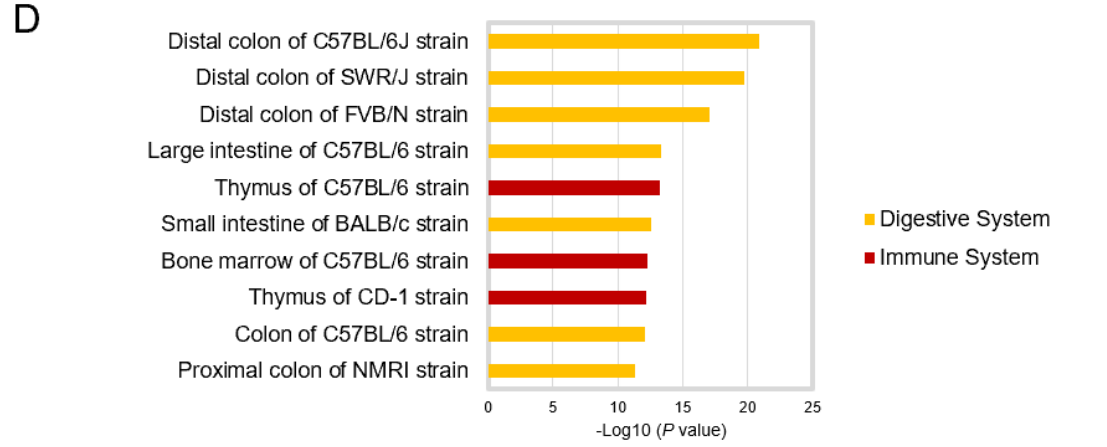
Distal colon of C57BL/6J strain
Distal colon of SWR/J strain
Distal colon of FVB/N strain
Large intestine of C57BL/6 strain
Thymus of C57BL/6 strain
Small intestine of BALB/c strain
Bone marrow of C57BL/6 strain
Thymus of CD-1 strain
Colon of C57BL/6 strain
Proximal colon of NMRI strain
0
5
10
15
20
25
-Log10 (P value)
Digestive System
Immune System

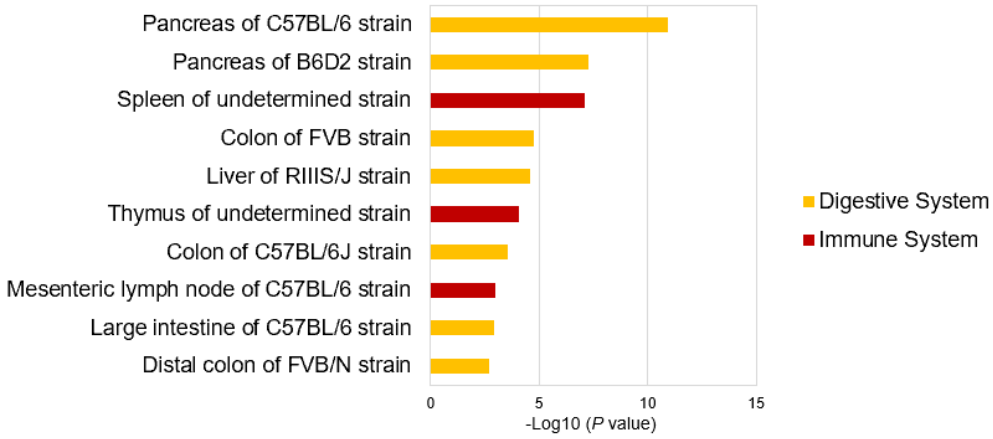
Pancreas of C57BL/6 strain
Pancreas of B6D2 strain
Spleen of undetermined strain
Colon of FVB strain
Liver of RIIIS/J strain
Thymus of undetermined strain
Colon of C57BL/6J strain
Mesenteric lymph node of C57BL/6 strain
Large intestine of C57BL/6 strain
Distal colon of FVB/N strain
0
5
10
15
-Log10 (P value)
Digestive System
Immune System

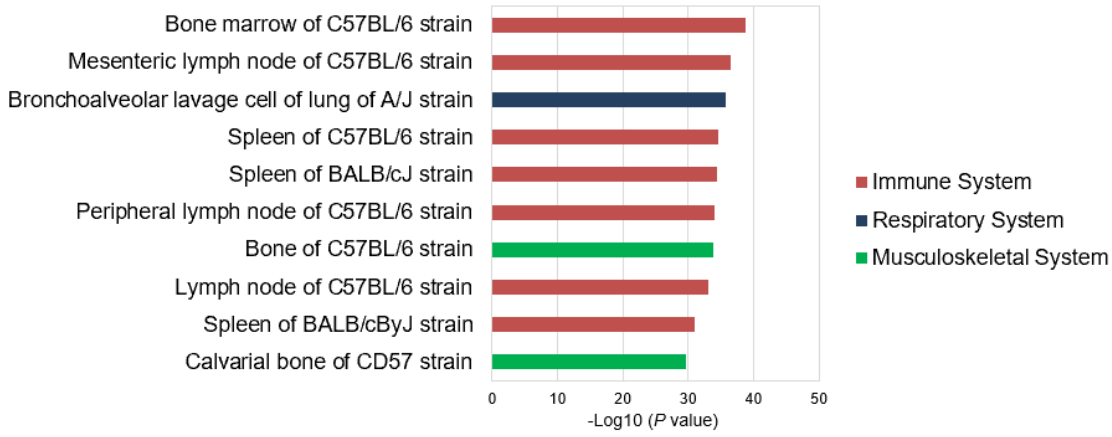
Bone marrow of C57BL/6 strain
Mesenteric lymph node of C57BL/6 strain
Bronchoalveolar lavage cell of lung of A/J strain
Spleen of C57BL/6 strain
Spleen of BALB/cJ strain
Peripheral lymph node of C57BL/6 strain
Bone of C57BL/6 strain
Lymph node of C57BL/6 strain
Spleen of BALB/cByJ strain
Calvarial bone of CD57 strain
0
10
20
30
40
50
-Log10 (P value)
Immune System
Respiratory System
Musculoskeletal System

E

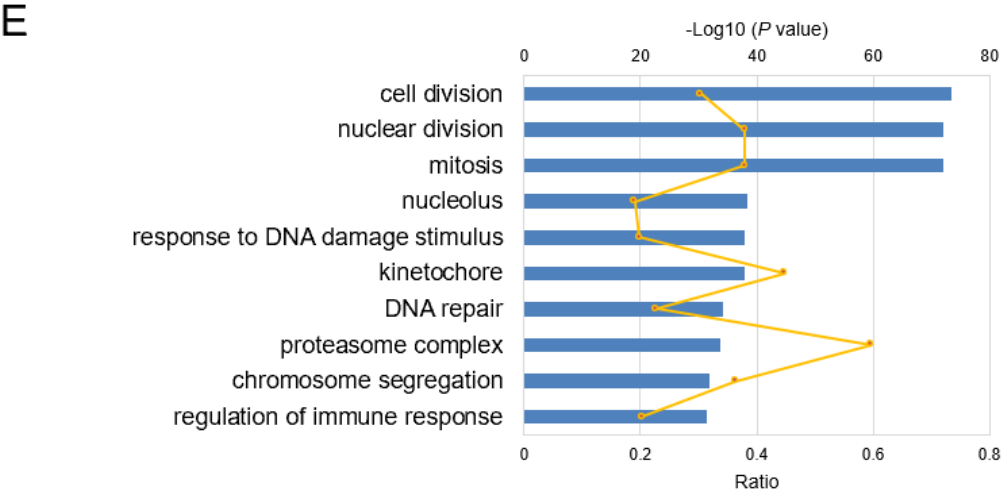
-Log10 (P value)
0
20
40
60
80
cell division
nuclear division
mitosis
nucleolus
response to DNA damage stimulus
kinetochore
DNA repair
proteasome complex
chromosome segregation
regulation of immune response
0
0.2
0.4
0.6
0.8
Ratio

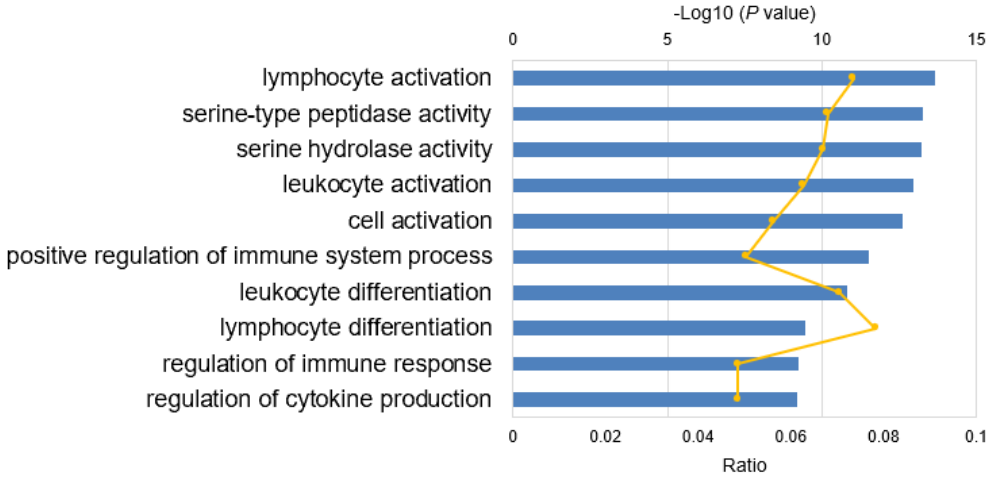
-Log10 (P value)
0
5
10
15
lymphocyte activation
serine-type peptidase activity
serine hydrolase activity
leukocyte activation
cell activation
positive regulation of immune system process
leukocyte differentiation
lymphocyte differentiation
regulation of immune response
regulation of cytokine production
0
0.02
0.04
0.06
0.08
0.1
Ratio

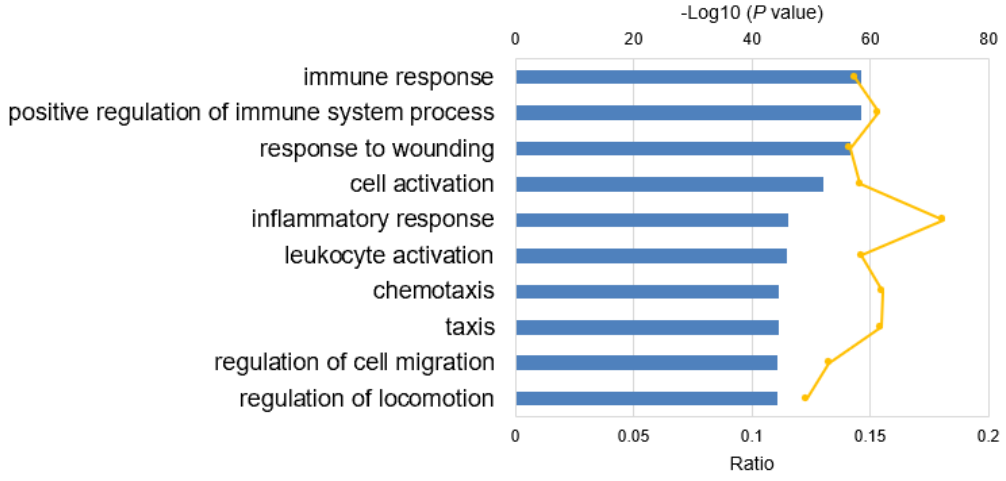
-Log10 (P value)
0
20
40
60
80
immune response
positive regulation of immune system process
response to wounding
cell activation
inflammatory response
leukocyte activation
chemotaxis
taxis
regulation of cell migration
regulation of locomotion
0
0.05
0.1
0.15
0.2
Ratio

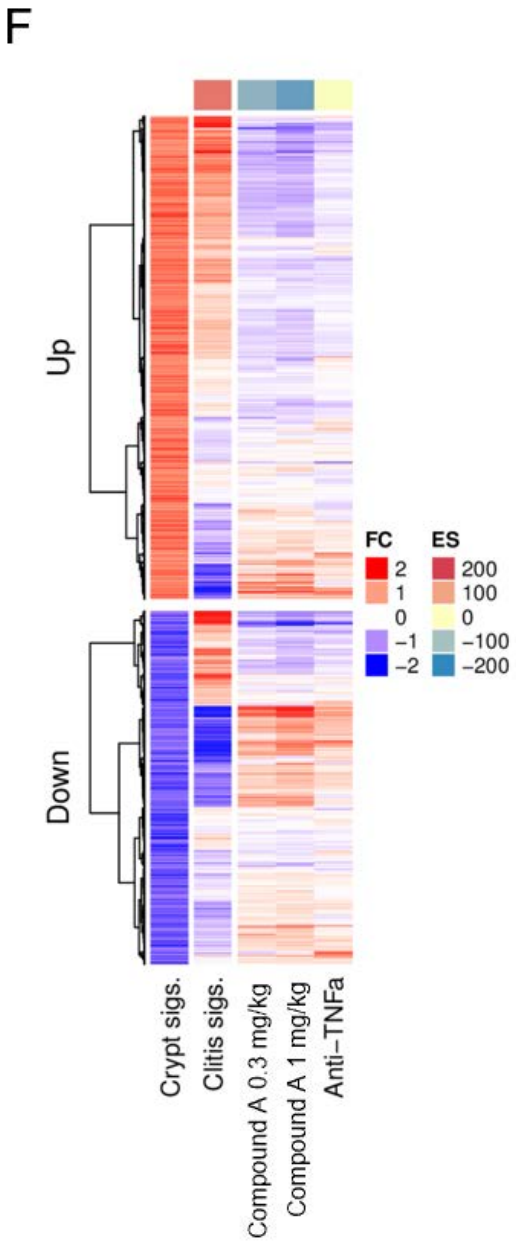

Figure 13. Therapeutic efficacy of MEK1/2 inhibitor against colonic gene expressions in activated T cell transfer colitis model

(A) Venn diagrams illustrate the numbers of significantly affected genes that were shared or were uniquely changed by 1 mg/kg Compound A or anti-TNFα mAb treatment (absolute fold change > 1.2, *P* value < 0.05). (B) Almost all genes affected by both Compound A and anti-TNFα mAb were significantly positively correlated. The X axis represents the class of each overlapping correlated genes; "+" and "−" symbols depict up-regulated and down-regulated genes, respectively, and the Y axis provides *P* value (-Log). (C) Heatmap illustrating hierarchical

clustering of colitis signature (vehicle versus normal mice) clustered into up-regulated and down-regulated genes comparing with fold change in gene expression levels in murine colitis model treated with Compound A at the dose of 0.3 and 1 mg/kg and anti-TNFα mAb. The color-coded scale for the normalized expression value is indicated at the right of the figure, which correlates with color intensity to the fold change (FC) of gene expression and enrichment score (ES). Overlapped gene number between each DEGs and colitis signature, and each coverage rate of negative correlation were indicated at the below. (D) The top 10 enriched tissue-type in each Compound A specific (upper), anti-TNFα mAb specific (middle) and common DEGs between Compound A and anti-TNFα mAb (lower) using mouse Body Atlas database. (E) The top 10 enriched GO terms in each Compound A specific (upper), anti-TNFα mAb specific (middle) and common DEGs (lower) using NextBio pathway enrichment application. Category names are presented on the Y axis. The X axis indicates the -Log10 (*P* value) of the over-representation analysis. Category names are presented on the Y axis. On the X axis, the significance score (negative Log of *P* value) for each pathway is indicated by the bars, and the line represents the ratio of genes in a given pathway that meet the cut-off criteria among total genes that make up that pathway. All blue bars predict an overall decrease in the activity of the pathway. (F) Heatmap illustrating hierarchical clustering of mouse immature crypt signature and colitis signature comparing with fold change in gene expression levels in murine colitis model treated with Compound A at the dose of 0.3 and 1 mg/kg and anti-TNFα mAb. The color-coded scale for the normalized expression value is indicated at the right of the figure, which correlates with color intensity to the fold change (FC) of gene expression and enrichment score (ES).

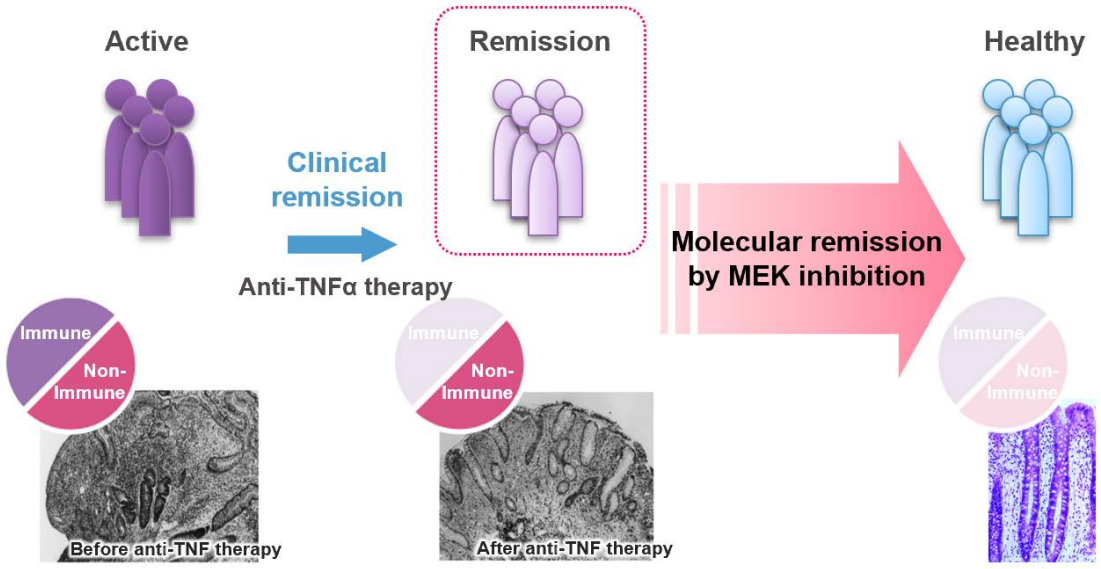

Figure 14. Schematic representation of the effect of molecular remission by MEK inhibitor that could induce a sustainable remission via normalizing molecular alterations to baseline

MEK1/2 inhibitor could be beneficial in treating CD patients by reversing TNFα-untreatable gene expression in colon, leads to accelerate restitution of dysregulated IECs and to prevent recurrence.

General Discussion

For patients, especially for multifactorial disease patients, new medicines offer fewer side effects, fewer hospitalizations, improved quality of life, and importantly, extended lives. However, the process for researching and developing new medicines is growing in difficulty and length, and the failure risks are still higher. Therefore, it is important to develop more accurate and effective way to understand disease processes and pathways and to identify appropriate target for discovering new markers for patient stratification and targeted therapies. Nowadays, it is well recognized that to access to large-scale omics data including transcriptome data to support basic research is a significant opportunity for drug discovery efficiently. Through my studies, I focused on transcriptome profiling, which is a widely used approach to dissect the genetic regulation and to expose gene expression patterns at the molecular level, to understand the molecular mechanism of heterogenous diseases.

In Chapter 1, I demonstrated that a novel irreversible LSD1 inhibitor, T-3775440, exhibited antileukemic efficacy in GFI1B-expressing AEL and AMKL cells. T-3775440 exerts anti-AML effects through a mechanism involving disruption of the LSD1-GFI1B complex, inducing transcriptional de-repression of downstream-target genes of GFI1B and consequent AML cell transdifferentiation. Because it has long been recognized that AML is a clinically heterogeneous disease with impaired myeloid differentiation, the forecast stratification and the treatment decision for patients shows difficulties and the precise molecular pathology is still incompletely understood. Given that several LSD1 inhibitors have entered clinical trials for treating patients with AML, this important finding in my study provides unique therapeutic opportunities and applications for precision medicine of AEL and AMKL specifically. Because hematopoiesis is one of the best-understood developmental pathways that individual lineage differentiation states are defined by transcriptional networks composed of combinations of transcription factors [121], several unique insights into processes that control development toward perturbed differentiation states have been reported utilized by leukemic transcription factors such as PML-RARA, MLL fusion proteins, and RUNX1-ETO [122-124]. These factors including LSD1-GFI1B complex reprogram the epigenome and thereby block the hierarchical succession of normal transcriptional networks. Considering that hematopoietic cells are defined by a certain transcriptional network, this kind of phenomenon may be of conceptual relevance not only for hematologic malignancies but also other type of heterogenous disease such as neurodegenerative

disease or tumor microenvironment in solid cancers, which affected by the state of the immune system. Therefore, dissecting the role of core transcription network in hematopoietic cells which characterizes specific segment of disease pathogenesis is a critical process to identify disease-related genes, regulators and/or biomarkers.

In Chapter 2, I presented a method for dissecting the molecular mechanism of CD patients who respond to anti-TNFα therapy by transcriptome analysis using CD patients-relevant mucosal gene signature. As a result, I found that there are certain abnormalities in CD colon that are not completely resolved by anti-TNFα therapy even after achieving clinical remission. Few studies have focused on these abnormalities regarding CD at a molecular level before. Furthermore, by conducting *in silico* computational screening to dissect the molecular pathway of these abnormalities, I demonstrated that MAPK pathway, one of the most commonly mutated oncogenic drivers in cancer, is the potential pathway that causes relapse of CD patients despite the fact that they achieved clinical remission. This signature-based screening methods using gene signatures derived from disease omics data with or without treatments can discover unknown disease mechanisms and mechanisms-of-action of molecules and drugs at a molecular level. In other words, the effectiveness of this computational drug repositioning methods offers the basis for identifying drug repositioning opportunities. Drug repositioning is a potential alternative to novel drug discovery by identifying new therapeutic applications for existing drugs, which can be re-marketed in a faster and more cost-efficient way [125, 126]. Off-label use of FDA approved drugs for cancer medical practice is one of the well-known examples [127]. Obviously, these examples were serendipitously identified, and these repositioning strategies make it hard to satisfy unmet medical needs by successfully repositioning a large number of existing drugs. To alleviate this problem, the number of drug repositioning methods, which can be classified into target-based, knowledge-based, signature-based and network-based methods, has dramatically increased with the rapid accumulation of genomics and chemical informatics data in the past decade. Especially signature-based method that I focus on in this study can be deployed to integrate available disease omics data into the drug repositioning process. One can easily access such genomics data in publicly available databases, such as NCBI-GEO (http://www.ncbi.nlm.nih.gov/geo/), SRA (http://www.ncbi.nlm.nih.gov/Traces/sra/), TCGA (https://www.cancer.gov/about-nci/organization/ccg/research/structural-genomics/tcga), GTEx (https://www.gtexportal.org/home/), CELLX (http://54.149.52.246/cgi-bin/RPPA/cellx.cgi,

[128]), CMap [70], CCLE [129] and so on. Although the multiplexity of gene expression profiling is seemingly useful, the mathematical and statistical properties still remain poorly understood [130]. To address this issue, the National Institute of Health (NIH) Library of Integrated Network-based Cellular Signatures (LINCS) project [131] has recently released the L1000 database [132], the next generation of the CMap with 1.3 million profiles from 42,080 genetic and small-molecule perturbations profiled across a large number of cell types. Once the molecular mechanisms underlying specific signatures can be dissected and extracted, it would be possible to provide more effective therapeutic options or solutions for unmet medical needs by applying these signatures for computational *in silico* screening method. This strategy could be a powerful scheme that guide to establish novel drug discovery strategies and precision medicine applications in coming years, lead to offer patients better targeted therapies.

Meanwhile, it is important to note the limitation of transcriptome analysis that captures just a snapshot in time of the total transcripts present in cells. Due to the complexity of intracellular network, no single omics analysis can independently explain fundamental pathogenesis of multifactorial diseases. To understand the biological events and acceleration of drug discovery, the dynamics of the interaction networks of wide range of biomolecules should be captured in a spatial, temporal, and quantitative manner to simulate the behavior of each molecule in the biological system. To achieve this, it would be ideal to integrate transcriptome with other omics technologies, such as SNP information, epigenetics, proteomics and metabolomics, to visualize the dynamics of molecular functions and cellular components that influence the behavior of intracellular phenomena [9]. Nowadays, techniques are still in development to analyze the phenotype of cells in a high-throughput fashion correlating changes in the gene expression to cellular phenotypes by multi-omics integration. This integration strategies should be applied to the study of multifactorial disorders to understand the genotype-phenotype relationship and also to identify biological mechanism for the prediction, prognosis, diagnosis and subtyping of patients to support therapeutic decisions more accurately.

In conclusion, my first study suggests that an irreversible LSD1 inhibitor exerts antileukemic activities in a certain subset of AML cell lines by inducing cell transdifferentiation. I found that LSD1 inhibitor caused this phenomenon by inducing the ectopic upregulation of myeloid lineage gene signature, which are normally repressed in erythroid and megakaryocytic lineage cells, based on transcriptome analysis. This finding suggests that LSD1 inhibitor could

represent a unique path to overcome the differentiation block of AML. Pharmacological inhibition of LSD1 functions has been more and more increasingly investigated as a new therapeutic approach for the treatment of patients with AML [133]. In addition, my second study provides clear evidence linking MAPK pathway to the mechanism of relapse after anti-TNFα treatment for CD which is previously unknown. I identified this novel mechanism by applying patient-derived gene signature to *in silico* computational screening method and demonstrated the effectiveness of one of the MAPK inhibitors, MEK inhibitor, in *in vitro* and *in vivo* CD model. These findings offer a robust proof-of-concept for MEK inhibitor as a promising novel therapeutic application for CD patients. Through above two approaches, hypothesis verification can be performed efficiently by extracting and predicting related molecular networks from a huge amount of transcriptome data. It is highly valuable that my studies shed light on the importance to understand multifactorial diseases as biological systems at the molecular level by considering not only the effect on a single target molecule but also the regulatory relationship of the intracellular molecular network.

Acknowledgement

I am deeply grateful to Professor Tomoki Chiba and Professors Tetsuo Hashimoto, Fuminori Tsuruta and Yuji Inagaki, University of Tsukuba, for guiding my work and valuable discussions through my doctoral program.

I also thank Dr. Yoshinori Ishikawa, Dr. Kazuhide Nakamura and Dr. Yukihiko Ebisuno, Takeda Pharmaceutical Company, for valuable suggestions, contributions and helpful supports.
I also thank all members in FIMECS, Inc. for their understanding and support on my doctoral program.

Finally, I would like to appreciate my family for supporting my life in University of Tsukuba.

References

1. Macneil LT, Walhout AJ: **Gene regulatory networks and the role of robustness and stochasticity in the control of gene expression**. *Genome Res* 2011, **21**(5):645-657.
2. Loscalzo J, Barabasi AL: **Systems biology and the future of medicine**. *Wiley Interdiscip Rev Syst Biol Med* 2011, **3**(6):619-627.
3. Amiri-Kordestani L, Basseville A, Kurdziel K, Fojo AT, Bates SE: **Targeting MDR in breast and lung cancer: discriminating its potential importance from the failure of drug resistance reversal studies**. *Drug Resist Updat* 2012, **15**(1-2):50-61.
4. Ledford H: **Translational research: 4 ways to fix the clinical trial**. *Nature* 2011, **477**(7366):526-528.
5. Jacobs JJ, Snackey C, Geldof AA, Characiejus D, Van Moorselaar RJ, Den Otter W: **Inefficacy of therapeutic cancer vaccines and proposed improvements. Casus of prostate cancer**. *Anticancer Res* 2014, **34**(6):2689-2700.
6. Kohler S: **Precision medicine –moving away from one-size-fits-all**. *Academy of Science for South Africa (ASSAf)* 2018, **14**(3):12-15.
7. Tiriveedhi V: **Impact of Precision Medicine on Drug Repositioning and Pricing: A Too Small to Thrive Crisis**. *J Pers Med* 2018, **8**(4).
8. Gjuvsland AB, Vik JO, Beard DA, Hunter PJ, Omholt SW: **Bridging the genotype-phenotype gap: what does it take?** *J Physiol* 2013, **591**(8):2055-2066.
9. Ritchie MD, Holzinger ER, Li R, Pendergrass SA, Kim D: **Methods of integrating data to uncover genotype-phenotype interactions**. *Nat Rev Genet* 2015, **16**(2):85-97.
10. Gallo Cantafio ME, Grillone K, Caracciolo D, Scionti F, Arbitrio M, Barbieri V, Pensabene L, Guzzi PH, Di Martino MT: **From Single Level Analysis to Multi-Omics Integrative Approaches: A Powerful Strategy towards the Precision Oncology**. *High Throughput* 2018, **7**(4).
11. Dudley JT, Schadt E, Sirota M, Butte AJ, Ashley E: **Drug discovery in a multidimensional world: systems, patterns, and networks**. *J Cardiovasc Transl Res* 2010, **3**(5):438-447.
12. Rattray NJW, Deziel NC, Wallach JD, Khan SA, Vasiliou V, Ioannidis JPA, Johnson CH: **Beyond genomics: understanding exposotypes through metabolomics**. *Hum Genomics* 2018, **12**(1):4.
13. Elad Noor SC, UweSauer: **Biological insights through omics data integration**. *Current Opinion in Systems Biology* 2019, **15**:39-47.
14. van Dam S, Vosa U, van der Graaf A, Franke L, de Magalhaes JP: **Gene co-expression analysis for functional classification and gene-disease predictions**. *Brief Bioinform* 2018, **19**(4):575-592.

15. Paul SM, Mytelka DS, Dunwiddie CT, Persinger CC, Munos BH, Lindborg SR, Schacht AL: **How to improve R&D productivity: the pharmaceutical industry's grand challenge**. *Nat Rev Drug Discov* 2010, **9**(3):203-214.
16. Li YY, Jones SJ: **Drug repositioning for personalized medicine**. *Genome Med* 2012, **4**(3):27.
17. Younesi E, Hofmann-Apitius M: **From integrative disease modeling to predictive, preventive, personalized and participatory (P4) medicine**. *EPMA J* 2013, **4**(1):23.
18. **https://www.cancer.org/content/dam/cancer-org/research/cancer-facts-and-statistics/annual-cancer-facts-and-figures/2017/cancer-facts-and-figures-2017.pdf**. *Cancer Facts Figures* 2017.
19. **Institute NC Surveillance, Epidemiology, and End Results (SEER) Program** 2007-2013.
20. Sandborn WJ: **The Present and Future of Inflammatory Bowel Disease Treatment**. *Gastroenterol Hepatol (N Y)* 2016, **12**(7):438-441.
21. Huang CT, Hsieh CH, Oyang YJ, Huang HC, Juan HF: **A Large-Scale Gene Expression Intensity-Based Similarity Metric for Drug Repositioning**. *iScience* 2018, **7**:40-52.
22. Kondo M, Wagers AJ, Manz MG, Prohaska SS, Scherer DC, Beilhack GF, Shizuru JA, Weissman IL: **Biology of hematopoietic stem cells and progenitors: implications for clinical application**. *Annu Rev Immunol* 2003, **21**:759-806.
23. Warner JK, Wang JC, Hope KJ, Jin L, Dick JE: **Concepts of human leukemic development**. *Oncogene* 2004, **23**(43):7164-7177.
24. Tenen DG: **Disruption of differentiation in human cancer: AML shows the way**. *Nat Rev Cancer* 2003, **3**(2):89-101.
25. Shi Y, Lan F, Matson C, Mulligan P, Whetstine JR, Cole PA, Casero RA: **Histone demethylation mediated by the nuclear amine oxidase homolog LSD1**. *Cell* 2004, **119**(7):941-953.
26. Shi YJ, Matson C, Lan F, Iwase S, Baba T, Shi Y: **Regulation of LSD1 histone demethylase activity by its associated factors**. *Mol Cell* 2005, **19**(6):857-864.
27. van der Meer LT, Jansen JH, van der Reijden BA: **Gfi1 and Gfi1b: key regulators of hematopoiesis**. *Leukemia* 2010, **24**(11):1834-1843.
28. Saleque S, Kim J, Rooke HM, Orkin SH: **Epigenetic regulation of hematopoietic differentiation by Gfi-1 and Gfi-1b is mediated by the cofactors CoREST and LSD1**. *Mol Cell* 2007, **27**(4):562-572.
29. Kerenyi MA, Shao Z, Hsu YJ, Guo G, Luc S, O'Brien K, Fujiwara Y, Peng C, Nguyen M, Orkin SH: **Histone demethylase Lsd1 represses hematopoietic stem and**

progenitor cell signatures during blood cell maturation. *Elife* 2013, **2**:e00633.

30. Sprussel A, Schulte JH, Weber S, Necke M, Handschke K, Thor T, Pajtler KW, Schramm A, Konig K, Diehl L *et al*: **Lysine-specific demethylase 1 restricts hematopoietic progenitor proliferation and is essential for terminal differentiation**. *Leukemia* 2012, **26**(9):2039-2051.
31. Harris WJ, Huang X, Lynch JT, Spencer GJ, Hitchin JR, Li Y, Ciceri F, Blaser JG, Greystoke BF, Jordan AM *et al*: **The histone demethylase KDM1A sustains the oncogenic potential of MLL-AF9 leukemia stem cells**. *Cancer Cell* 2012, **21**(4):473-487.
32. Lynch JT, Harris WJ, Somervaille TC: **LSD1 inhibition: a therapeutic strategy in cancer?** *Expert Opin Ther Targets* 2012, **16**(12):1239-1249.
33. Schenk T, Chen WC, Gollner S, Howell L, Jin L, Hebestreit K, Klein HU, Popescu AC, Burnett A, Mills K *et al*: **Inhibition of the LSD1 (KDM1A) demethylase reactivates the all-trans-retinoic acid differentiation pathway in acute myeloid leukemia**. *Nat Med* 2012, **18**(4):605-611.
34. Fiskus W, Sharma S, Shah B, Portier BP, Devaraj SG, Liu K, Iyer SP, Bearss D, Bhalla KN: **Highly effective combination of LSD1 (KDM1A) antagonist and pan-histone deacetylase inhibitor against human AML cells**. *Leukemia* 2014, **28**(11):2155-2164.
35. Subramanian A, Tamayo P, Mootha VK, Mukherjee S, Ebert BL, Gillette MA, Paulovich A, Pomeroy SL, Golub TR, Lander ES *et al*: **Gene set enrichment analysis: a knowledge-based approach for interpreting genome-wide expression profiles**. *Proc Natl Acad Sci U S A* 2005, **102**(43):15545-15550.
36. Dougherty JD, Schmidt EF, Nakajima M, Heintz N: **Analytical approaches to RNA profiling data for the identification of genes enriched in specific cells**. *Nucleic Acids Res* 2010, **38**(13):4218-4230.
37. Ueda R, Suzuki T, Mino K, Tsumoto H, Nakagawa H, Hasegawa M, Sasaki R, Mizukami T, Miyata N: **Identification of cell-active lysine specific demethylase 1-selective inhibitors**. *J Am Chem Soc* 2009, **131**(48):17536-17537.
38. Nerlov C, Graf T: **PU.1 induces myeloid lineage commitment in multipotent hematopoietic progenitors**. *Genes Dev* 1998, **12**(15):2403-2412.
39. van Bergen M, van der Reijden BA: **Targeting the GFI1/1B-CoREST Complex in Acute Myeloid Leukemia**. *Front Oncol* 2019, **9**:1027.
40. Huang DY, Kuo YY, Chang ZF: **GATA-1 mediates auto-regulation of Gfi-1B transcription in K562 cells**. *Nucleic Acids Res* 2005, **33**(16):5331-5342.
41. McGrath JP, Williamson KE, Balasubramanian S, Odate S, Arora S, Hatton C,

Edwards TM, O'Brian T, Magnuson S, Stokoe D *et al*: **Pharmacological inhibition of the histone lysine demethylase KDM1A suppresses the growth of multiple acute myeloid leukemia subtypes**. *Cancer Res* 2016.

42. Foudi A, Kramer DJ, Qin J, Ye D, Behlich AS, Mordecai S, Preffer FI, Amzallag A, Ramaswamy S, Hochedlinger K *et al*: **Distinct, strict requirements for Gfi-1b in adult bone marrow red cell and platelet generation**. *J Exp Med* 2014, **211**(5):909-927.
43. Castoldi GL, Liso V, Fenu S, Vegna ML, Mandelli F: **Reproducibility of the morphological diagnostic criteria for acute myeloid leukemia: the GIMEMA group experience**. *Ann Hematol* 1993, **66**(4):171-174.
44. Pagano L, Pulsoni A, Vignetti M, Mele L, Fianchi L, Petti MC, Mirto S, Falcucci P, Fazi P, Broccia G *et al*: **Acute megakaryoblastic leukemia: experience of GIMEMA trials**. *Leukemia* 2002, **16**(9):1622-1626.
45. Santos FP, Faderl S, Garcia-Manero G, Koller C, Beran M, O'Brien S, Pierce S, Freireich EJ, Huang X, Borthakur G *et al*: **Adult acute erythroleukemia: an analysis of 91 patients treated at a single institution**. *Leukemia* 2009, **23**(12):2275-2280.
46. Oki Y, Kantarjian HM, Zhou X, Cortes J, Faderl S, Verstovsek S, O'Brien S, Koller C, Beran M, Bekele BN *et al*: **Adult acute megakaryocytic leukemia: an analysis of 37 patients treated at M.D. Anderson Cancer Center**. *Blood* 2006, **107**(3):880-884.
47. Cervera N, Carbuccia N, Garnier S, Guille A, Adelaide J, Murati A, Vey N, Mozziconacci MJ, Chaffanet M, Birnbaum D *et al*: **Molecular characterization of acute erythroid leukemia (M6-AML) using targeted next-generation sequencing**. *Leukemia* 2015.
48. Wang ZY, Chen Z: **Acute promyelocytic leukemia: from highly fatal to highly curable**. *Blood* 2008, **111**(5):2505-2515.
49. Saleque S, Cameron S, Orkin SH: **The zinc-finger proto-oncogene Gfi-1b is essential for development of the erythroid and megakaryocytic lineages**. *Genes Dev* 2002, **16**(3):301-306.
50. Elmaagacli AH, Koldehoff M, Zakrzewski JL, Steckel NK, Ottinger H, Beelen DW: **Growth factor-independent 1B gene (GFI1B) is overexpressed in erythropoietic and megakaryocytic malignancies and increases their proliferation rate**. *Br J Haematol* 2007, **136**(2):212-219.
51. Anguita E, Gupta R, Olariu V, Valk PJ, Peterson C, Delwel R, Enver T: **A somatic mutation of GFI1B identified in leukemia alters cell fate via a SPI1 (PU.1) centered genetic regulatory network**. *Dev Biol* 2016, **411**(2):277-286.
52. Vianello P, Botrugno OA, Cappa A, Ciossani G, Dessanti P, Mai A, Mattevi A, Meroni G, Minucci S, Thaler F *et al*: **Synthesis, biological activity and mechanistic insights**

of 1-substituted cyclopropylamine derivatives: a novel class of irreversible inhibitors of histone demethylase KDM1A. *Eur J Med Chem* 2014, **86**:352-363.

53. Maes T, Mascaro C, Ortega A, Lunardi S, Ciceri F, Somervaille TC, Buesa C: **KDM1 histone lysine demethylases as targets for treatments of oncological and neurodegenerative disease**. *Epigenomics* 2015, **7**(4):609-626.

54. Zheng YC, Ma J, Wang Z, Li J, Jiang B, Zhou W, Shi X, Wang X, Zhao W, Liu HM: **A Systematic Review of Histone Lysine-Specific Demethylase 1 and Its Inhibitors**. *Med Res Rev* 2015, **35**(5):1032-1071.

55. Mohammad HP, Smitheman KN, Kamat CD, Soong D, Federowicz KE, Van Aller GS, Schneck JL, Carson JD, Liu Y, Butticello M *et al*: **A DNA Hypomethylation Signature Predicts Antitumor Activity of LSD1 Inhibitors in SCLC**. *Cancer Cell* 2015, **28**(1):57-69.

56. Randrianarison-Huetz V, Laurent B, Bardet V, Blobe GC, Huetz F, Dumenil D: **Gfi-1B controls human erythroid and megakaryocytic differentiation by regulating TGF-beta signaling at the bipotent erythro-megakaryocytic progenitor stage**. *Blood* 2010, **115**(14):2784-2795.

57. Lichtenstein GR, Abreu MT, Cohen R, Tremaine W: **American Gastroenterological Association Institute medical position statement on corticosteroids, immunomodulators, and infliximab in inflammatory bowel disease**. *Gastroenterology* 2006, **130**(3):935-939.

58. Rutgeerts P, D'Haens G, Targan S, Vasiliauskas E, Hanauer SB, Present DH, Mayer L, Van Hogezand RA, Braakman T, DeWoody KL *et al*: **Efficacy and safety of retreatment with anti-tumor necrosis factor antibody (infliximab) to maintain remission in Crohn's disease**. *Gastroenterology* 1999, **117**(4):761-769.

59. Lakatos PL, Golovics PA, David G, Pandur T, Erdelyi Z, Horvath A, Mester G, Balogh M, Szipocs I, Molnar C *et al*: **Has there been a change in the natural history of Crohn's disease? Surgical rates and medical management in a population-based inception cohort from Western Hungary between 1977-2009**. *Am J Gastroenterol* 2012, **107**(4):579-588.

60. Lazarev M, Ullman T, Schraut WH, Kip KE, Saul M, Regueiro M: **Small bowel resection rates in Crohn's disease and the indication for surgery over time: experience from a large tertiary care center**. *Inflamm Bowel Dis* 2010, **16**(5):830-835.

61. Peyrin-Biroulet L, Loftus EV, Jr., Colombel JF, Sandborn WJ: **The natural history of adult Crohn's disease in population-based cohorts**. *Am J Gastroenterol* 2010, **105**(2):289-297.

62. Gisbert JP, Marin AC, Chaparro M: **The Risk of Relapse after Anti-TNF**

Discontinuation in Inflammatory Bowel Disease: Systematic Review and Meta-Analysis. *Am J Gastroenterol* 2016, **111**(5):632-647.

63. Boyapati R, Satsangi J, Ho GT: **Pathogenesis of Crohn's disease**. *F1000Prime Rep* 2015, **7**:44.

64. Talley NJ, Abreu MT, Achkar JP, Bernstein CN, Dubinsky MC, Hanauer SB, Kane SV, Sandborn WJ, Ullman TA, Moayyedi P: **An evidence-based systematic review on medical therapies for inflammatory bowel disease**. *Am J Gastroenterol* 2011, **106 Suppl 1**:S2-25; quiz S26.

65. Zallot C, Peyrin-Biroulet L: **Deep remission in inflammatory bowel disease: looking beyond symptoms**. *Curr Gastroenterol Rep* 2013, **15**(3):315.

66. Kiesslich R, Duckworth CA, Moussata D, Gloeckner A, Lim LG, Goetz M, Pritchard DM, Galle PR, Neurath MF, Watson AJ: **Local barrier dysfunction identified by confocal laser endomicroscopy predicts relapse in inflammatory bowel disease**. *Gut* 2012, **61**(8):1146-1153.

67. D'Haens G, Van Deventer S, Van Hogezand R, Chalmers D, Kothe C, Baert F, Braakman T, Schaible T, Geboes K, Rutgeerts P: **Endoscopic and histological healing with infliximab anti-tumor necrosis factor antibodies in Crohn's disease: A European multicenter trial**. *Gastroenterology* 1999, **116**(5):1029-1034.

68. Bai JP, Alekseyenko AV, Statnikov A, Wang IM, Wong PH: **Strategic applications of gene expression: from drug discovery/development to bedside**. *Aaps J* 2013, **15**(2):427-437.

69. Chen B, Butte AJ: **Leveraging big data to transform target selection and drug discovery**. *Clin Pharmacol Ther* 2016, **99**(3):285-297.

70. Lamb J, Crawford ED, Peck D, Modell JW, Blat IC, Wrobel MJ, Lerner J, Brunet JP, Subramanian A, Ross KN *et al*: **The Connectivity Map: using gene-expression signatures to connect small molecules, genes, and disease**. *Science* 2006, **313**(5795):1929-1935.

71. Cheng J, Yang L, Kumar V, Agarwal P: **Systematic evaluation of connectivity map for disease indications**. *Genome Med* 2014, **6**(12):540.

72. Arijs I, De Hertogh G, Lemaire K, Quintens R, Van Lommel L, Van Steen K, Leemans P, Cleynen I, Van Assche G, Vermeire S *et al*: **Mucosal gene expression of antimicrobial peptides in inflammatory bowel disease before and after first infliximab treatment**. *PLoS One* 2009, **4**(11):e7984.

73. D'Haens GR, Geboes K, Peeters M, Baert F, Penninckx F, Rutgeerts P: **Early lesions of recurrent Crohn's disease caused by infusion of intestinal contents in excluded ileum**. *Gastroenterology* 1998, **114**(2):262-267.

74. Rutgeerts P, Sandborn WJ, Feagan BG, Reinisch W, Olson A, Johanns J, Travers S, Rachmilewitz D, Hanauer SB, Lichtenstein GR *et al*: **Infliximab for induction and maintenance therapy for ulcerative colitis**. *N Engl J Med* 2005, **353**(23):2462-2476.

75. Geboes K, Riddell R, Ost A, Jensfelt B, Persson T, Lofberg R: **A reproducible grading scale for histological assessment of inflammation in ulcerative colitis**. *Gut* 2000, **47**(3):404-409.

76. Jung P, Sato T, Merlos-Suarez A, Barriga FM, Iglesias M, Rossell D, Auer H, Gallardo M, Blasco MA, Sancho E *et al*: **Isolation and in vitro expansion of human colonic stem cells**. *Nat Med* 2011, **17**(10):1225-1227.

77. Merlos-Suarez A, Barriga FM, Jung P, Iglesias M, Cespedes MV, Rossell D, Sevillano M, Hernando-Momblona X, da Silva-Diz V, Munoz P *et al*: **The intestinal stem cell signature identifies colorectal cancer stem cells and predicts disease relapse**. *Cell Stem Cell* 2011, **8**(5):511-524.

78. Adams ME, Wallace MB, Kanouni T, Scorah N, O'Connell SM, Miyake H, Shi L, Halkowycz P, Zhang L, Dong Q: **Design and synthesis of orally available MEK inhibitors with potent in vivo antitumor efficacy**. *Bioorg Med Chem Lett* 2012, **22**(7):2411-2414.

79. Alhnan MA, Basit AW: **Engineering polymer blend microparticles: an investigation into the influence of polymer blend distribution and interaction**. *Eur J Pharm Sci* 2011, **42**(1-2):30-36.

80. Kendall RA, Alhnan MA, Nilkumhang S, Murdan S, Basit AW: **Fabrication and in vivo evaluation of highly pH-responsive acrylic microparticles for targeted gastrointestinal delivery**. *Eur J Pharm Sci* 2009, **37**(3-4):284-290.

81. Mele M, Ferreira PG, Reverter F, DeLuca DS, Monlong J, Sammeth M, Young TR, Goldmann JM, Pervouchine DD, Sullivan TJ *et al*: **Human genomics. The human transcriptome across tissues and individuals**. *Science* 2015, **348**(6235):660-665.

82. Dudley JT, Sirota M, Shenoy M, Pai RK, Roedder S, Chiang AP, Morgan AA, Sarwal MM, Pasricha PJ, Butte AJ: **Computational repositioning of the anticonvulsant topiramate for inflammatory bowel disease**. *Sci Transl Med* 2011, **3**(96):96ra76.

83. Dry JR, Pavey S, Pratilas CA, Harbron C, Runswick S, Hodgson D, Chresta C, McCormack R, Byrne N, Cockerill M *et al*: **Transcriptional pathway signatures predict MEK addiction and response to selumetinib (AZD6244)**. *Cancer Res* 2010, **70**(6):2264-2273.

84. Saaf AM, Halbleib JM, Chen X, Yuen ST, Leung SY, Nelson WJ, Brown PO: **Parallels between global transcriptional programs of polarizing Caco-2 intestinal epithelial cells in vitro and gene expression programs in normal colon and colon cancer**. *Mol*

Biol Cell 2007, **18**(11):4245-4260.

85. Bregenholt S, Reimann J, Claesson MH: **Proliferation and apoptosis of lamina propria CD4+ T cells from scid mice with inflammatory bowel disease**. *Eur J Immunol* 1998, **28**(11):3655-3663.

86. Zhao Y, Adjei AA: **The clinical development of MEK inhibitors**. *Nat Rev Clin Oncol* 2014, **11**(7):385-400.

87. Hua S, Marks E, Schneider JJ, Keely S: **Advances in oral nano-delivery systems for colon targeted drug delivery in inflammatory bowel disease: selective targeting to diseased versus healthy tissue**. *Nanomedicine* 2015, **11**(5):1117-1132.

88. Lapidus A, Bernell O, Hellers G, Lofberg R: **Clinical course of colorectal Crohn's disease: a 35-year follow-up study of 507 patients**. *Gastroenterology* 1998, **114**(6):1151-1160.

89. Chauvin A, Le Thuaut A, Belhassan M, Le Baleur Y, Mesli F, Bastuji-Garin S, Delchier JC, Amiot A: **Infliximab as a bridge to remission maintained by antimetabolite therapy in Crohn's disease: A retrospective study**. *Dig Liver Dis* 2014, **46**(8):695-700.

90. Coskun M: **Intestinal epithelium in inflammatory bowel disease**. *Front Med (Lausanne)* 2014, **1**:24.

91. Peterson LW, Artis D: **Intestinal epithelial cells: regulators of barrier function and immune homeostasis**. *Nat Rev Immunol* 2014, **14**(3):141-153.

92. Pastorelli L, De Salvo C, Mercado JR, Vecchi M, Pizarro TT: **Central role of the gut epithelial barrier in the pathogenesis of chronic intestinal inflammation: lessons learned from animal models and human genetics**. *Front Immunol* 2013, **4**:280.

93. Koch S, Nusrat A: **The life and death of epithelia during inflammation: lessons learned from the gut**. *Annu Rev Pathol* 2012, **7**:35-60.

94. D'Inca R, Di Leo V, Corrao G, Martines D, D'Odorico A, Mestriner C, Venturi C, Longo G, Sturniolo GC: **Intestinal permeability test as a predictor of clinical course in Crohn's disease**. *Am J Gastroenterol* 1999, **94**(10):2956-2960.

95. Arnott ID, Kingstone K, Ghosh S: **Abnormal intestinal permeability predicts relapse in inactive Crohn disease**. *Scand J Gastroenterol* 2000, **35**(11):1163-1169.

96. Vereecke L, Beyaert R, van Loo G: **Enterocyte death and intestinal barrier maintenance in homeostasis and disease**. *Trends Mol Med* 2011, **17**(10):584-593.

97. Suarez-Farinas M, Fuentes-Duculan J, Lowes MA, Krueger JG: **Resolved psoriasis lesions retain expression of a subset of disease-related genes**. *J Invest Dermatol* 2011, **131**(2):391-400.

98. Planell N, Lozano JJ, Mora-Buch R, Masamunt MC, Jimeno M, Ordas I, Esteller M,

Ricart E, Pique JM, Panes J *et al*: **Transcriptional analysis of the intestinal mucosa of patients with ulcerative colitis in remission reveals lasting epithelial cell alterations**. *Gut* 2013, **62**(7):967-976.

99. Zeissig S, Bergann T, Fromm A, Bojarski C, Heller F, Guenther U, Zeitz M, Fromm M, Schulzke JD: **Altered ENaC expression leads to impaired sodium absorption in the noninflamed intestine in Crohn's disease**. *Gastroenterology* 2008, **134**(5):1436-1447.

100. Herr R, Kohler M, Andrlova H, Weinberg F, Moller Y, Halbach S, Lutz L, Mastroianni J, Klose M, Bittermann N *et al*: **B-Raf inhibitors induce epithelial differentiation in BRAF-mutant colorectal cancer cells**. *Cancer Res* 2015, **75**(1):216-229.

101. Lemieux E, Boucher MJ, Mongrain S, Boudreau F, Asselin C, Rivard N: **Constitutive activation of the MEK/ERK pathway inhibits intestinal epithelial cell differentiation**. *Am J Physiol Gastrointest Liver Physiol* 2011, **301**(4):G719-730.

102. Coskun M: **The role of CDX2 in inflammatory bowel disease**. *Dan Med J* 2014, **61**(3):B4820.

103. Gao N, White P, Kaestner KH: **Establishment of intestinal identity and epithelial-mesenchymal signaling by Cdx2**. *Dev Cell* 2009, **16**(4):588-599.

104. Dedhia PH, Bertaux-Skeirik N, Zavros Y, Spence JR: **Organoid Models of Human Gastrointestinal Development and Disease**. *Gastroenterology* 2016, **150**(5):1098-1112.

105. Liu F, Huang J, Ning B, Liu Z, Chen S, Zhao W: **Drug Discovery via Human-Derived Stem Cell Organoids**. *Front Pharmacol* 2016, **7**:334.

106. Du SL, Yuan X, Zhan S, Tang LJ, Tong CY: **Trametinib, a novel MEK kinase inhibitor, suppresses lipopolysaccharide-induced tumor necrosis factor (TNF)-alpha production and endotoxin shock**. *Biochem Biophys Res Commun* 2015, **458**(3):667-673.

107. Sirota M, Dudley JT, Kim J, Chiang AP, Morgan AA, Sweet-Cordero A, Sage J, Butte AJ: **Discovery and preclinical validation of drug indications using compendia of public gene expression data**. *Sci Transl Med* 2011, **3**(96):96ra77.

108. Jahchan NS, Dudley JT, Mazur PK, Flores N, Yang D, Palmerton A, Zmoos AF, Vaka D, Tran KQ, Zhou M *et al*: **A drug repositioning approach identifies tricyclic antidepressants as inhibitors of small cell lung cancer and other neuroendocrine tumors**. *Cancer Discov* 2013, **3**(12):1364-1377.

109. Zerbini LF, Bhasin MK, de Vasconcellos JF, Paccez JD, Gu X, Kung AL, Libermann TA: **Computational repositioning and preclinical validation of pentamidine for renal cell cancer**. *Mol Cancer Ther* 2014, **13**(7):1929-1941.

110. Claerhout S, Lim JY, Choi W, Park YY, Kim K, Kim SB, Lee JS, Mills GB, Cho JY: **Gene expression signature analysis identifies vorinostat as a candidate therapy for**

gastric cancer. *PLoS One* 2011, **6**(9):e24662.

111. Hirose M, Okaniwa M, Hayashi Y, Takagi T: **Preparation of heterocyclic compounds as Raf inhibitors for treatment of cancer**. *Patent WO2009028629 A1* March 5, 2009.

112. Ishikawa T, Banno H, Kawakita Y, Ohashi T, Kurasawa O: **Preparation of fused heterocyclic compounds as tyrosine kinase inhibitors**. *Patent WO2008072634 A1* June 19, 2008.

113. Kawakita Y, Miwa K, Seto M, Banno H, Ohta Y, Tamura T, Yusa T, Miki H, Kamiguchi H, Ikeda Y *et al*: **Design and synthesis of pyrrolo[3,2-d]pyrimidine HER2/EGFR dual inhibitors: improvement of the physicochemical and pharmacokinetic profiles for potent in vivo anti-tumor efficacy**. *Bioorg Med Chem* 2012, **20**(20):6171-6180.

114. Hirose M, Okaniwa M, Miyazaki T, Imada T, Ohashi T, Tanaka Y, Arita T, Yabuki M, Kawamoto T, Tsutsumi S *et al*: **Design and synthesis of novel DFG-out RAF/vascular endothelial growth factor receptor 2 (VEGFR2) inhibitors: 3. Evaluation of 5-amino-linked thiazolo[5,4-d]pyrimidine and thiazolo[5,4-b]pyridine derivatives**. *Bioorg Med Chem* 2012, **20**(18):5600-5615.

115. Barrett SD, Bridges AJ, Dudley DT, Saltiel AR, Fergus JH, Flamme CM, Delaney AM, Kaufman M, LePage S, Leopold WR *et al*: **The discovery of the benzhydroxamate MEK inhibitors CI-1040 and PD 0325901**. *Bioorg Med Chem Lett* 2008, **18**(24):6501-6504.

116. Mini E, Nobili S, Caciagli B, Landini I, Mazzei T: **Cellular pharmacology of gemcitabine**. *Ann Oncol* 2006, **17 Suppl 5**:v7-12.

117. Dong Q, Feher V, Kaldor SW, Tomita N: **MEK1/2 inhibitors, methods for their synthesis, and their use in disease treatment**. *Patent US20080125437 A1* May 29, 2008.

118. Ishikawa T, Seto M, Banno H, Kawakita Y, Oorui M, Taniguchi T, Ohta Y, Tamura T, Nakayama A, Miki H *et al*: **Design and synthesis of novel human epidermal growth factor receptor 2 (HER2)/epidermal growth factor receptor (EGFR) dual inhibitors bearing a pyrrolo[3,2-d]pyrimidine scaffold**. *J Med Chem* 2011, **54**(23):8030-8050.

119. Dong Q, Dougan DR, Gong X, Halkowycz P, Jin B, Kanouni T, O'Connell SM, Scorah N, Shi L, Wallace MB *et al*: **Discovery of TAK-733, a potent and selective MEK allosteric site inhibitor for the treatment of cancer**. *Bioorg Med Chem Lett* 2011, **21**(5):1315-1319.

120. Schellhammer PF: **An evaluation of bicalutamide in the treatment of prostate cancer**. *Expert Opin Pharmacother* 2002, **3**(9):1313-1328.

121. Davidson EH: **Emerging properties of animal gene regulatory networks**. *Nature* 2010, **468**(7326):911-920.

122. Ptasinska A, Assi SA, Martinez-Soria N, Imperato MR, Piper J, Cauchy P, Pickin A, James SR, Hoogenkamp M, Williamson D *et al*: **Identification of a dynamic core transcriptional network in t(8;21) AML that regulates differentiation block and self-renewal**. *Cell Rep* 2014, **8**(6):1974-1988.

123. Saeed S, Logie C, Francoijs KJ, Frige G, Romanenghi M, Nielsen FG, Raats L, Shahhoseini M, Huynen M, Altucci L *et al*: **Chromatin accessibility, p300, and histone acetylation define PML-RARalpha and AML1-ETO binding sites in acute myeloid leukemia**. *Blood* 2012, **120**(15):3058-3068.

124. Schwieger M, Schuler A, Forster M, Engelmann A, Arnold MA, Delwel R, Valk PJ, Lohler J, Slany RK, Olson EN *et al*: **Homing and invasiveness of MLL/ENL leukemic cells is regulated by MEF2C**. *Blood* 2009, **114**(12):2476-2488.

125. Chong CR, Sullivan DJ, Jr.: **New uses for old drugs**. *Nature* 2007, **448**(7154):645-646.

126. Ashburn TT, Thor KB: **Drug repositioning: identifying and developing new uses for existing drugs**. *Nat Rev Drug Discov* 2004, **3**(8):673-683.

127. Saiyed MM, Ong PS, Chew L: **Off-label drug use in oncology: a systematic review of literature**. *J Clin Pharm Ther* 2017, **42**(3):251-258.

128. Ching KA, Wang K, Kan Z, Fernandez J, Zhong W, Kostrowicki J, Xie T, Zhu Z, Martini JF, Koehler M *et al*: **Cell Index Database (CELLX): a web tool for cancer precision medicine**. *Pac Symp Biocomput* 2015:10-19.

129. Barretina J, Caponigro G, Stransky N, Venkatesan K, Margolin AA, Kim S, Wilson CJ, Lehar J, Kryukov GV, Sonkin D *et al*: **The Cancer Cell Line Encyclopedia enables predictive modelling of anticancer drug sensitivity**. *Nature* 2012, **483**(7391):603-607.

130. Clarke R, Ressom HW, Wang A, Xuan J, Liu MC, Gehan EA, Wang Y: **The properties of high-dimensional data spaces: implications for exploring gene and protein expression data**. *Nat Rev Cancer* 2008, **8**(1):37-49.

131. Keenan AB, Jenkins SL, Jagodnik KM, Koplev S, He E, Torre D, Wang Z, Dohlman AB, Silverstein MC, Lachmann A *et al*: **The Library of Integrated Network-Based Cellular Signatures NIH Program: System-Level Cataloging of Human Cells Response to Perturbations**. *Cell Syst* 2018, **6**(1):13-24.

132. Subramanian A, Narayan R, Corsello SM, Peck DD, Natoli TE, Lu X, Gould J, Davis JF, Tubelli AA, Asiedu JK *et al*: **A Next Generation Connectivity Map: L1000 Platform and the First 1,000,000 Profiles**. *Cell* 2017, **171**(6):1437-1452 e1417.

133. Magliulo D, Bernardi R, Messina S: **Lysine-Specific Demethylase 1A as a Promising Target in Acute Myeloid Leukemia**. *Front Oncol* 2018, **8**:255.